



# **POLITECNICO**

## **MILANO 1863**

### **GUIDELINES DEFINITION FOR THE CALIBRATION OF INDIRECT CUTTING FORCE ESTIMATION SYSTEM FOR MILLING APPLICATIONS**

Supervisor : Eng. Paolo Albertelli

Cosupervisor: Prof. Yusuf Altintas

Graduation thesis of:

Manuele BURZONI, 842088

Academic Year 2016 – 2017



## ACKNOWLEDGMENT

I would like to thank Eng. Paolo Albertelli, who gave me the opportunity to carry out this thesis work allowing me to conclude a long and difficult course of study.

I would like to give special thanks to Professor Yusuf Altintas, who allowed me to realize a little dream by giving me the opportunity to live a unique professional and life experience at the MAL department at the University British of Columbia (UBC). Thank you to all members of MAL for their support and helpful advice that have given me the opportunity to complete a great job.

I want to thank Eng. Mattia Torta whose help has been fundamental for the realization of the thesis and all members of MUSP that have been close to me in last months.

Thanks to all my university friends with whom I have shared joys and sorrows during my study path.

The warmest thanks go to my girlfriend Maria, whose constant presence and support were fundamental during all this fantastic experience.

The most important thanks go to my family, to whom I want to express my most sincere and convinced feeling of gratitudine and love for having always been my fixed point of reference with their wise advice and their ability to listen and understand me, without which none of this would have been possible.

---

# Sommario

<b>TABLE LIST</b> .....	<b>V</b>
<b>FIGURE LIST</b> .....	<b>VII</b>
<b>ABSTRACT</b> .....	<b>1</b>
<b>1. INTRODUCTION</b> .....	<b>3</b>
1.1 Background and state of art on cutting force measurements .....	3
1.2 Thesis goal .....	14
<b>2 CUTTING PROCESS</b> .....	<b>19</b>
2.1 Cutting parameters .....	19
<b>3 SYSTEM PRELIMINARY CALIBRATION</b> .....	<b>23</b>
3.1 Spindle Integrated Force Sensor measurement (SIFS).....	23
3.2 Static calibration .....	28
3.2.1 <i>Static Calibration verification</i> .....	32
3.3 Low Pass Filter and Unbalanced Forces Compensation.....	34
3.4 Dynamic Calibration.....	36
<b>4 KALMAN FILTER STRATEGY</b> .....	<b>39</b>
4.1 Machine dynamic and Analytical model design .....	39
4.2 Modal Analysis fundamentals.....	41
4.2.1 <i>Experimental FRF for MDOF system</i> .....	45
4.3 State space model representattion.....	49
4.4 System numerical stability.....	54

---

4.5	Model Expansion.....	57
4.5.1	<i>State Estimation</i> .....	60
<b>5</b>	<b>EXPANDED DISTURBANCE KALMAN FILTER (EKF) .....</b>	<b>63</b>
5.1	Continuous Expanded disturbance Kalman filter Design .....	63
5.2	Extended state space model discretization .....	66
5.3	Recursive Least Square Estimator (RLSE) .....	72
5.3.1	Time Update equation.....	73
5.3.2	Optimal Gain.....	74
5.3.3	Measurement update equation.....	79
5.4	Discrete Kalman Filter Alghoritm (DKF) .....	81
<b>6</b>	<b>GUIDELINES DEFINITION FOR CUTTING PROCESS ORIENTED KALMAN TUNING.....</b>	<b>89</b>
6.1	Innovative procedure for finding.....	89
6.2	Spindle speed oriented observer tuning .....	94
6.2.1	Study of the effects of model uncertainties and on the tuning procedure 100	
6.3	Experimental Equipment and Setting.....	106
6.4	Procedure validation.....	112
6.4.1	X Axis.....	112
6.4.2	Y Axis .....	124
<b>7</b>	<b>FINAL CONSIDERATIONS, CONCLUSIONS AND FUTURE DEVELOPMENTS ....</b>	<b>131</b>
	<b>BIBLIOGRAPHY.....</b>	<b>133</b>

## Table List

Table 1 - SIFS technical data .....	26
Table 2 - SIFS characteristic .....	31
Table 3 - Dependence of calibration constants from the tool length.....	32
Table 4 - Continuous form vs Discrete form.....	71
Table 5 - Least Square Method vs Discrete Kalman Filter .....	85
Table 6 - Plant variation effect according to the logic of confidence intervals along the X-axis.....	104
Table 7 - Plant variation effect according to the logic of confidence intervals along the Y-axis.....	105
Table 8 – Experimental results along X-axis ( $R_{static} = 0.15$ $R_{dynamic} = 10$ ).....	113
Table 9 - Experimental results along X-axis ( $R_{static} = 0.15$ $R_{dynamic} = 0.15$ ) .....	118
Table 10 - Experimental results along X-axis ( $R_{static} = 10$ $R_{dynamic} = 10$ ).....	120
Table 11 - Experimental results along X-axis ( $R_{static} = 2$ $R_{dynamic} = 10$ ).....	121
Table 12 - Experimental results along Y-axis ( $R_{static} = 0.15$ $R_{dynamic} = 10$ ).....	124
Table 13 - Experimental results along Y-axis ( $R_{static} = 0.15$ $R_{dynamic} = 0.15$ ) .....	125
Table 14 - Experimental results along Y-axis ( $R_{static} = 10$ $R_{dynamic} = 10$ ).....	127
Table 15 - Experimental results along X-axis ( $R_{static} = 2$ $R_{dynamic} = 10$ ).....	128



## Figure List

Figure 1 - Rotatory and Stationary dynamometer.....	4
Figure 2 – System response formula.....	6
Figure 3 – Forcer to Force transfer function.....	7
Figure 4 - General work system overview .....	13
Figure 5 - Compensation process scheme.....	17
Figure 6 - Geometry model of milling operation.....	19
Figure 7 - Signal processing path.....	23
Figure 12 - Static calibration equipment.....	29
Figure 13 - Comparison between measured and applied force in static calibration .	30
Figure 14 - Dynamic calibration equipment .....	33
Figure 15 - Verification of the dynamic calibration.....	34
Figure 16 - Unbalanced forces subtraction .....	35
Figure 17 - Dynamic calibration sequence .....	37
Figure 18 – MDOF dynamic model of the Spindle structure .....	40
Figure 19 - Modal Analysis fundamentals .....	42
Figure 20 - Continuous Expanded disturbance Kalman filter.....	64
Figure 21 - Comparison between TF, measured and fitted FRF in X and Y direction .....	68
Figure 22 - Discrete System.....	72
Figure 23 - Block diagram of a discrete time Kalman filter applied on a discret system according to Greval & Andrew 2008 (pag.138).....	85
Figure 24 - Comparison between reference force and compensated force spectrums in	

---

cutting test .....	91
Figure 25 - Comparison between reference force and compensated force spectrums in Tap Test.....	92
Figure 26 - Flow chart algorithm.....	93
Figure 27 - Relation between Q and R parameters for X axis.....	96
Figure 28 - Relation between Q and R parameters for Y axis.....	97
Figure 29 - Dependence of parameter Q on Spindle speed .....	98
Figure 30 - Plant Variation Overview .....	99
Figure 31 - X-axis Confidence Intervals .....	102
Figure 32 - Y-axis Confidence Intervals.....	103
Figure 33 - a Quaser UX600 Multit Face 5 Axes Machine Center .....	106
Figure 34 - four-fluted carbide end mill SH40750 from DATA FLUTE.....	107
Figure 35 - Table dynamometer of the type KISTLER 9257B .....	108
Figure 36 - Measurement Chain Overview .....	111
Figure 37 - Experimental Operating logic.....	112
Figure 38 - RMSE comparison between static and dynamic test along X-axis ( $R_{static} = 0.15$ $R_{dynamic} = 10$ ).....	113
Figure 39 - Compensation results for X-direction measurement with dynamometer of a cutting operation with 9000 rpm spindle speed in time domain ( $R_{static} = 0.15$ $R_{dynamic} = 10$ ).....	114
Figure 40 - Compensation results for X-direction measurement with dynamometer of a cutting operation with 4500 rpm spindle speed in time domain ( $R_{static} = 0.15$ $R_{dynamic} = 10$ ).....	115
Figure 41 - Compensation results for X-direction measurement with dynamometer of a cutting operation with 8400 rpm spindle speed in time domain ( $R_{static} = 0.15$	

<i>Rdynamic</i> = 10).....	115
Figure 42 - Compensation results for X-direction measurement with dynamometer of a cutting operation with 11600 rpm spindle speed in time domain ( <i>Rstatic</i> = 0.15 <i>Rdynamic</i> = 10).....	116
Figure 43 - Dynamic test optimal curves comparisons for X-axis ( <i>Rdynamic</i> = 0.15 <i>Rdynamic</i> = 10).....	117
Figure 44 - Comparison between RMSE values calculated using optimal Q values during Cutting test along X-axis ( <i>Rdynamic</i> = 0.15 <i>Rdynamic</i> = 10).....	117
Figure 45 - RMSE comparison between static and dynamic test along X-axis ( <i>Rstatic</i> = 0.15 <i>Rdynamic</i> = 0.15) .....	118
Figure 46 - Compensation results for X-direction measurement with dynamometer of a cutting operation with 9000 rpm spindle speed in time domain (lower graph) and frequency domain (lupper plot).....	119
Figure 47 - RMSE comparison between static and dynamic test along x axis ( <i>Rstatic</i> = 10 <i>Rdynamic</i> = 10) .....	120
Figure 48 - RMSE comparison between static and dynamic test along X-axis ( <i>Rstatic</i> = 2 <i>Rdynamic</i> = 10) .....	122
Figure 49 - General Overview of experimental results for X-axis .....	123
Figure 50 - RMSE comparison between static and dynamic test along Y-axis ( <i>Rstatic</i> = 0.15 <i>Rdynamic</i> = 10) .....	124
Figure 51 - Dynamic test optimal curves comparisons fo Y-axis ( <i>Rdynamic</i> = 0.15 <i>Rdynamic</i> = 10).....	125
Figure 52 - Comparison between RMSE values calculated using optimal Q values during Cutting test along Y-axis ( <i>Rdynamic</i> = 0.15 <i>Rdynamic</i> = 10) .....	126
Figure 53 - RMSE comparison between static and dynamic test along Y-axis	

---

<i>(Rstatic = 0.15 Rdynamic = 10)</i> .....	126
Figure 54 - RMSE comparison between static and dynamic test along Y-axis	
<i>(Rstatic = 10 Rdynamic = 10)</i> .....	127
Figure 55 - RMSE comparison between static and dynamic test along y axis	
<i>(Rstatic = 2 Rdynamic = 10)</i> .....	128
Figure 56 - General Overview of experimental results for Y-axis.....	129
Figure 57 - Comparison between compensation results for Y-direction with different <i>Rdynamic</i> of a cutting operation with 17600 rpm spindle speed in time domain	130

## Abstract

Although the milling process monitoring technology has been well consolidated in recent years, the reliability of decision-making process through monitoring systems still represents a significant challenge.

Keeping the cutting forces exerted on the tool tip under control increase the tool service life and avoids premature breakage, thus reducing costs and production time. Nowadays, there are various measuring instruments that allow to estimate in real time the forces during the machining process, but some of these, as the dynamometer, have severe industrial limitations, while others may require very onerous investments.

The goal of this work is to propose and validate an approach able to estimate in real time the machine tools cutting forces during a milling operation through a SIFS (Spindle Integrated Force Sensors) system.

In this thesis, a Kalman filter observer has been developed based on the real system dynamic behaviour identified through an experimental modal analysis (EMA).

The state observer has been tested and designed on a machining centre during milling tests and relies on piezoelectric sensors that can be easily integrated into a commercial electrospindle.

The algorithm developed in this work is able to perform an optimal and automatic calibration of the filter which guarantees a good force estimation as the spindle speed varies, without preliminary cutting operations.

---

***Key words:*** Milling process, Machine dynamic, cutting force indirect measurements, Kalman filter tuning strategies, System dynamics compensation.

## 1. Introduction

In the first part of this Chapter, a brief Background about the different methods used to predict the cutting forces is presented.

In the second part, we analyze more in detail the real purpose of this thesis.

### 1.1 Background and state of art on cutting force measurements

The process reliability and tool status monitoring are essential for safe automation in machining, e.g. milling or drilling.

For the force measurement during milling operations, different approaches have been developed.

Exist two different methods to measure cutting forces:

**DIRECT METHODS:** the force value is obtained by directly reading the Magnitude value [N] from the instrument.

**INDIRECT METHODS:** the instrument measurement is linked to the force value but is not homogeneous with it, so to use this method is necessary to know in advance the relationships between these quantities.

## Direct methods

The most common direct method for the cutting forces monitoring is using *fixed piezoelectric quartz dynamometers* and *rotating dynamometers*.

The stationary dynamometers are mounted on the work table and the workpiece is attached to the dynamometer, while rotary dynamometers are connected to the spindle head as tool holders for cutting force and torque measurement.

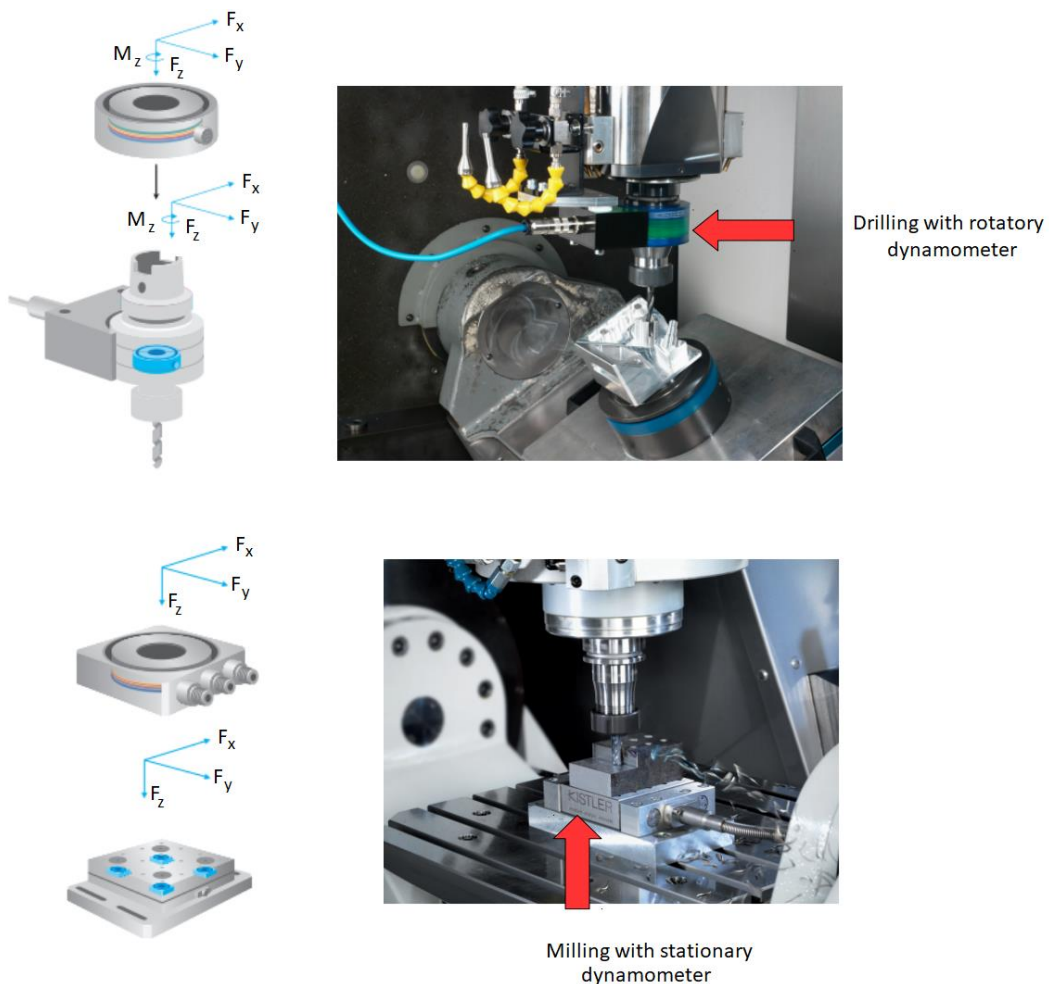


Figure 1 - Rotatory and Stationary dynamometer

## Indirect Methods

Beside the use of table dynamometer, there are other indirect technics that can be used for this task.

### *SIFS (Spindle Integrated Force Sensors)*

The SIFS system can be easily implemented in existing machines by retrofitting the spindle system. The measurement of cutting forces performed by the SIFS has several advantages if compared to the measurement carried out through a dynamometer [JUN ET AL. 2002, p. 742].

- The machine space around the table is not reduced.
- The size of a workpiece is not limited by the dynamometer dimensions.
- The SIFS is not directly exposed to cutting fluids, chips and crashes during machining.
- The spindle related parameters, (bearing wear and misalignments) can be also measured.

Different studies [BYRNE ET AL. 1995]. [JUN ET AL. 2002] and [PARK 2003] evaluated the effect of the implementation of SIFS to the overall dynamics and thermal behavior of the machine and spindle. They concluded that the dynamic of the overall machine was not significantly affected. Furthermore, thermal effects can be neglected for most cases, since the spindle cooling is generally set outside the spindle system.

## *DRIVE CURRENT*

Another method to predict the cutting forces is to use the current drawn by the feed drives.

The motor current reflects the inertial loads of all active drives during velocity changes along the tool path, the effects of servo control system and structural dynamics of the drive chain, friction in the guides and cutting loads during machining. The accuracy of predicting the cutting forces is dependent on the precision of the mathematical model that describes the transmission of forces from the tool tip to servo motor as the required current.

The motor current command, position and velocity of each drive are sampled from the CNC system at discrete time intervals directly.

### *Cutting force estimation problem in indirect methods*

Generally, a system can be seen as a black-box with unknown properties.

$$\boxed{\text{Response}} = \boxed{\text{Properties}} * \boxed{\text{Input}}$$

Figure 2 – System response formula

In the case of mechanical systems, the input is constituted by a generic force of excitement while the output is the dynamic response of the system that may be detected in one or more points.

In order to characterize the input-output relationships of components or systems in control theory, are commonly used functions called transfer functions (TF).

In this thesis to characterize the input-output relationships *Force to Force* transfer function is used.

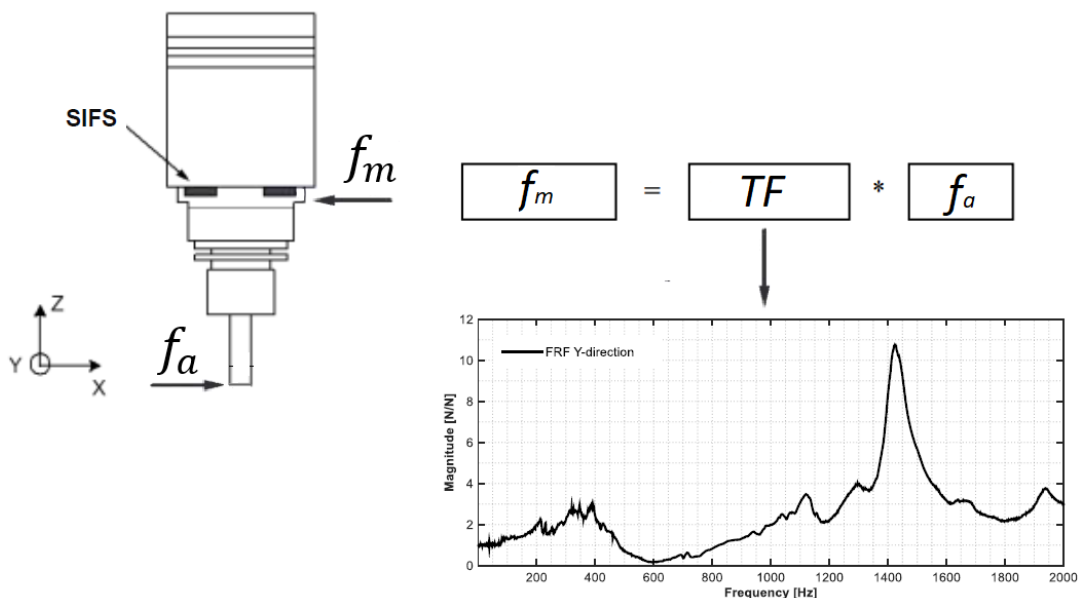


Figure 3 – Forcr to Force transfer function

However, if we use the Indirect methods the possible match between the of periodicity of the milling forces multiple of the spindle frequency (SF) and the natural

eigenmodes of machine in which the SIFS is intergrated, can lead to a distortion of the measurement.

From a practical point of view it means that when we are close to the natural frequency of the system the output  $f_m$  doesn't correspond to the real one. In order to estimate milling forces accurately at high rotational Spindle Speeds, the bandwidth of a sensor must be greater than at least the third harmonic of a tooth passing frequency [PARK 2003], but any force sensing system which is far away from the force application point has a limited bandwidth, caused by structural dynamics of the mechanical elements between those two points.

Several methods able to compensate the effects structural dynamics on the force estimation have been conceived over the years

The simplest method to compensate the dynamics would be through the inversion of the transfer function.

The inverse of the transfer function in Laplace domain  $G(s)^{-1}$  can be calculated by swapping the numerator and denominator which leads to the following equation (see formula 4.29 in Chapter 4.3).

$$\frac{1}{TF} = G(s)^{-1} = \frac{U(s)}{Y(s)} = \frac{f_a}{f_m} = \frac{s^k + a_1s^{k-1} + \dots + a_{k-1}s + a_k}{b_0s^m + b_1s^{m-1} + \dots + b_{m-1}s + b_m} \quad (1-1)$$

Where

$k$  = number of selected modes

$f_a$  =  $f_{input}$

$$f_m = f_{output}$$

$$U(s) = G(s)^{-1} \cdot Y(s) \quad (1-2)$$

Nevertheless, this approach has some drawback.

- The order of the denominator  $m$  has to be equal or higher than the order of the numerator  $k$  to ensure the stability of the procedure [LOHMANN 2012].

Since this criterion cannot be fulfilled for all transfer functions, the application of this methodology is quite heavily limited [CHUNG ET AL. 1994].

*Today the limitation of the number of eigenmodes considered for a fitted FRF is still one of the main limitations for the compensation accuracy.*

If the number of eigenmodes wasn't being limited, a perfect fitting of the *measured FRF* would be possible, therefore a good force compensation result would be guaranteed, but since more eigenmodes are considered this could lead to polynomials of higher order and the linked, numerical stability is not assured.

- Furthermore [PARK 2003, p. 13–15] shows that issues related to the noise amplification (especially at high frequencies) can occur when an inverse filter methodology is used. This means that the approach leads to a bad noise to signal ratio.

## *Kalman filter*

In order to increase the bandwidth of the proposed sensors system, in this paper, has been developed an observer of cutting forces that it was designed and tested on a machine centre. The observer is generally used to estimate physical quantities not directly measurable.

In this work the observer is based on Kalman filtering model, it built on using the machine tool dynamic identifies by means of an Experimental Modal Analysis (See Chapter 4.2).

The transfer function is a mathematical description of the system dynamic properties, which can be described by linear equations invariant over time; in control problems these equations are used in the state space form (see Chapter 4.3).

Figure 4 is an extreme compensation process simplification that wants to show how from a theoretical point of view the spindle system TF can be represented through the state space model.

$A_e$  = System Dynamics Matrix

$C_e$  = Output Matrix

$f_a(t)$  = Input or excitation force

$f_m(t)$  = Measured Output force

$x_e(t)$  = State vector of the system

$\hat{f}_a$  = compensated force

The signal measured by the SIFS will be compensated by the Kalman filter, which is modelled starting from a simplification of the real plant.

The compensated force is strongly correlated to the use of Kalman's gain; in particular an increment of the K parameter value it means to attribute more confidence to the measurement and less to the predictive model and vice versa (see Chapter 5.4).

The correct force estimation starts from a correct use of the gain that derives from a correct initialization of the filter (see Chapter 5.3.2).

The state of a dynamic system is the smallest set of variables (called state variables) such that knowledge of these variables at  $t = t_0$ , together with knowledge of the input for  $t \geq t_0$ , completely determines the behavior of the system for any time  $t \geq t_0$  (See Chapter 4.3).

Generally, the Kalman filter is an estimator used to estimate the state of a linear dynamic system perturbed by Gaussian white noise measurements.

However, in this thesis the main goal is to evaluate the input force applied on the Tool tip, then the modelled spindle system dynamics can be expanded to include the input force  $f_a$  as one of the unknown state and generate the Expanded Kalman filter (See Chapter 5).

[PARK ET AL. 2004] designed a *continuous disturbance Expanded Kalman filter* to compensate the distorted forces and estimate the real applied forces at the tool tip. Another similar work was developed by [ALBERTELLI 2015] in (2015-FORCE-VIB-KALMAN), the Kalman filter exploits the real-time data coming not only from a single sensor (as done in PARK & ALTINTAS 2005) but it relies on signals coming

from a triaxial accelerometer mounted in the spindle housing and on inner inductive sensors that measure the relative spindle housing-shaft radial displacements.

In this way, the observer compensates, for both forces and vibrations, the effects of the machine structure low frequency dynamics and the spindle high frequency dynamics.

The observer, fusing the data coming from the sensors, assures the extension of the frequency bandwidth of the performed estimations. In this manner, the developed system can be used over a vast range of machining operations.

The introduced enhancement allows extending the observer compensating properties and makes it suitable for different milling scenarios.

These compensation approaches don't consider *cross talk influences* between the different machine directions which lead to an additional distortion of the measurement, this part has been integrated in [THOMAS 2015].

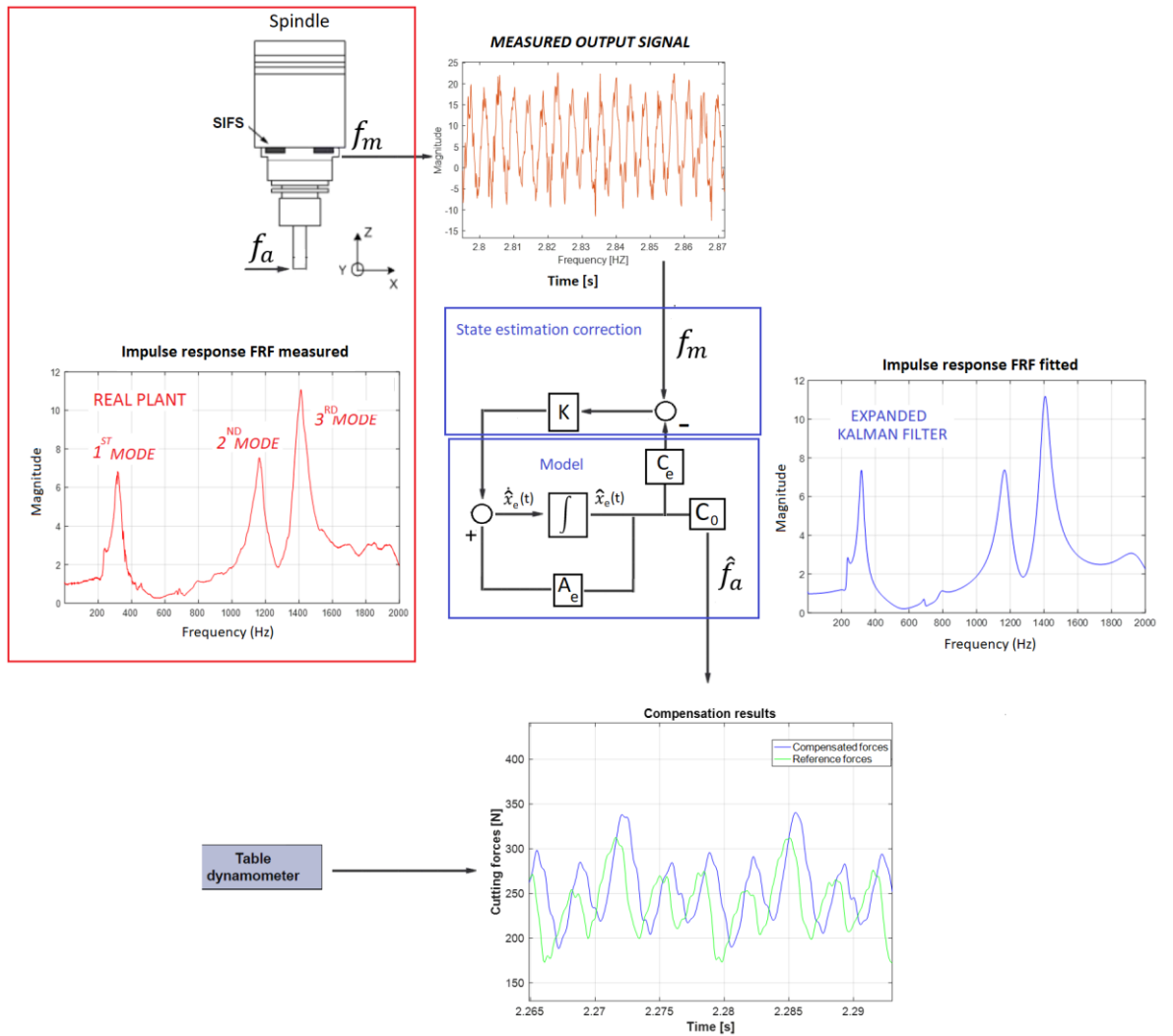


Figure 4 - General work system overview

## 1.2 Thesis goal

The entire force compensation process consists in a series of complex operations that must be carried out according to well-defined rules; every single inaccuracy introduced makes the overall percentage error increasing.

In the following elaboration, every single operation involved in the force compensation project will be presented in detail "step by step", trying to highlight all the limitations.

The goal of the thesis is to understand whether it is possible to perform an optimal calibration of the entire compensation process that can guarantee a good estimate of force as the spindle speed varies.

Particular attention has been paid to the choice of the noise parameters in the *single input/ output (SISO) Kalman filter* calibration, which are often responsible for a suboptimal prediction and that still today we aren't able to obtain automatically.

- 1) The parameter  $\mathbf{R}$  involved in the computation of the measurement noise matrix  $\mathbf{R}$  (responsible to define the measurement uncertainty)

$$\mathbf{R}_{m \times m} \quad m = \text{number of inputs}$$

In our case with a *single input/single output (SISO) Kalman filter*

$$\mathbf{R} = R$$

- 2) The parameter  $Q$  involved in the computation of the process noise covariance matrix  $Q$  (responsible to define the uncertainty on the estimation of the process)

$$Q_{n \times n} \quad n = \text{number of states}$$

$$Q = \text{lti\_disc}(A_e, \Gamma, Q_c, Ts\_filt)$$

Where:

- $A_e$  = (EKF) Feedback Matrix
- $\Gamma$  = Process Noise coupling matrix
- $Ts\_filt$  = filter sampling time
- $Q_{c(1 \times 1)} = \begin{bmatrix} Q & \dots & 0 \\ \vdots & \ddots & \vdots \\ 0 & \dots & Q \end{bmatrix} = \text{Continuous time process noise Covariance}$

This Matlab command allows to discretize the Expanded State Space Model

Expanded State Space Model [See Chapter 4.5]

$$\dot{x}_e = A_{e(n \times n)} x_e + \Gamma_{(n \times 1)} w \quad w \sim N(0, Q_c) = \text{process noise}$$

$$f_m = C_e x_e + v$$

Discrete Expanded State Space Model (See Chapter 5.2)

$$\begin{aligned}x_{k+1} &= F_k x_k + w_k & w_k &\sim N(0, \mathbf{Q}) = \text{process noise} \\f_{m,k} &= H_k x_k + v_k\end{aligned}$$

Nowadays the filter calibration is a manual operation carried out thanks to the use of expensive software that allows numerical simulation of the periodic milling machining at different rotational speeds, this allows to generate specific calibration tables depending on the machine tool and cutting parameters used.

From a practical point of view, we spend a lot of time simulating and evaluating the collected data to find an optimal calibration.

The noise matrices construction is one of the most difficult aspects of Kalman filter design.

The simple Tap Test operation excites all frequencies within the selected Bandwidth, so selecting the appropriate Spindle frequency (SF) and the associated multiple frequencies it is possible to simulate a real milling operation and make an automatic tuning of the filter in a very simple and fast way for all rotational velocities.

However, due to changes of machine dynamics during operation, those predictions can be inaccurate under high-speed conditions, because prior to machining it is in general unknown how the tool-tip FRF of a given tool-holder combination will change, see [Martin Hermann Postel 2015]

The study about the effects of model uncertainties and on the filter tuning procedure is presented in section 6.2.1

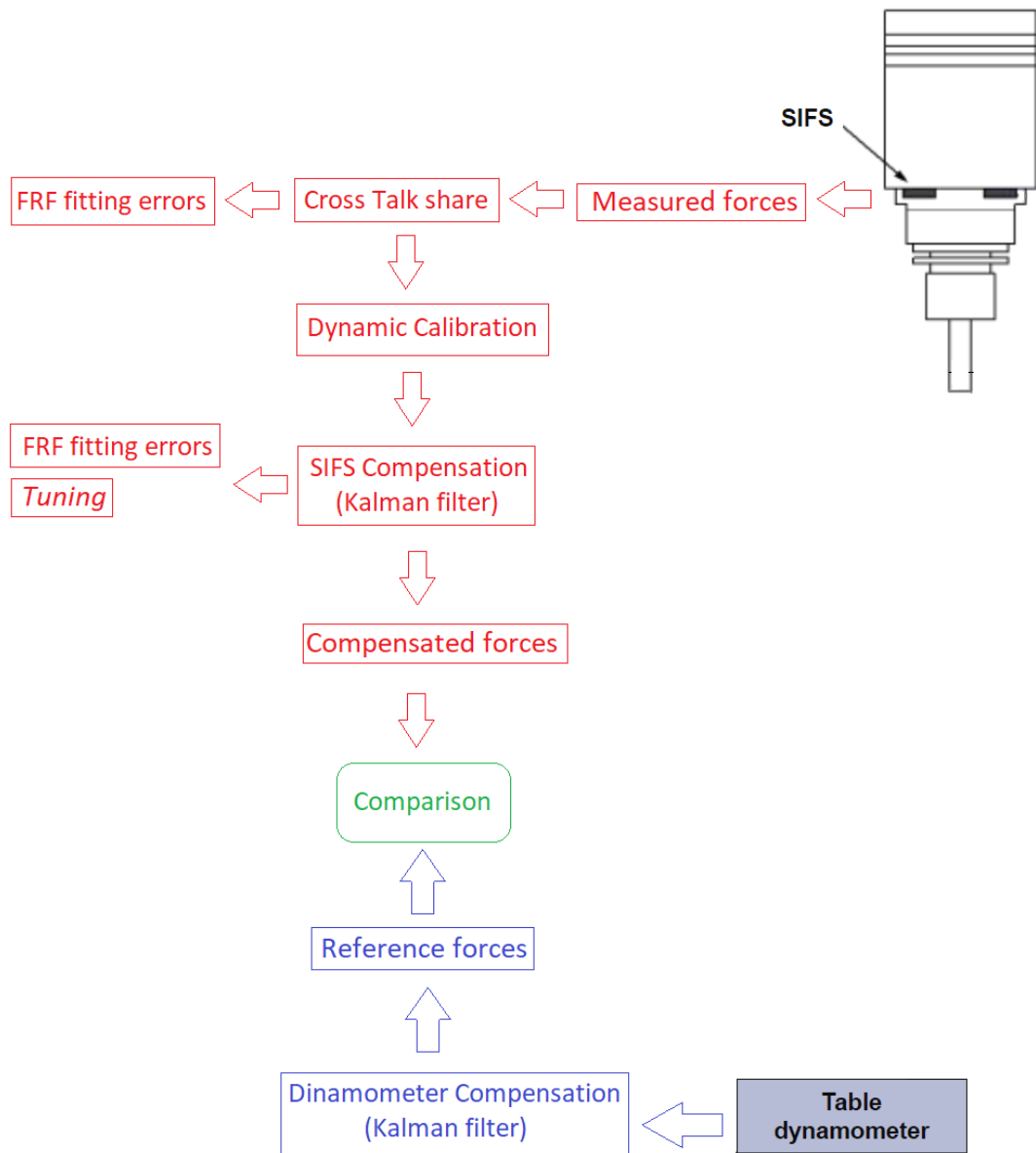


Figure 5 - Compensation process scheme



## 2 Cutting Process

This Chapter provides the necessary theoretical background for the following parts of the thesis.

Since this thesis deals with the measurement of cutting forces, basic cutting parameters and equations are introduced on the basis of [ALTINTAS 2012].

### 2.1 Cutting parameters

Let's see now what are the main parameters affecting the milling operation.

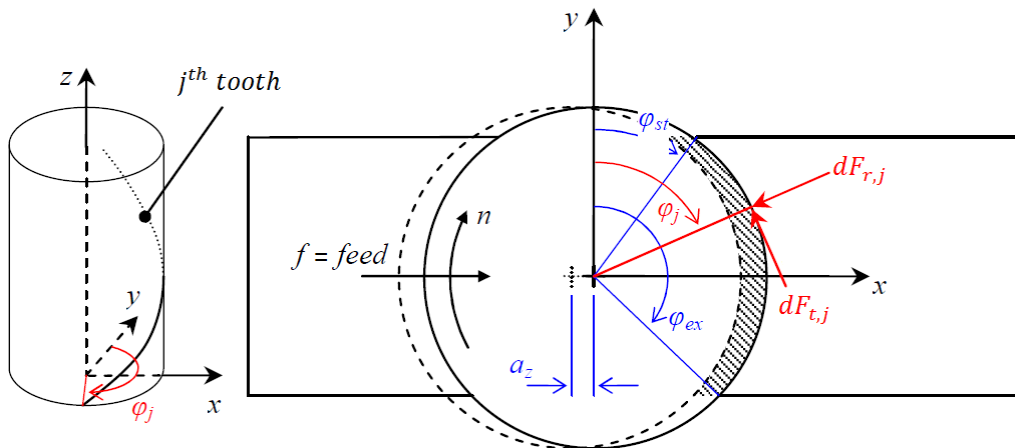


Figure 6 - Geometry model of milling operation

Where:

$\varphi_j$  is the instantaneous angle of immersion of the  $j^{th}$  tooth [rad] ( $j = 1, \dots, Z$ )

$Z$  is the number of teeth of the tool

$\varphi_{st}$  is the cutting entry angle [rad]

$\varphi_{ex}$  is the cutting exit angle [rad]

$f$  is the feed [ $mm/round$ ]

$n$  is the rotational speed of the spindle [rpm]

$$n = \frac{\omega_T}{Z} \cdot 60 \quad (2-1)$$

$\omega_T$  is the Tooth Passing Frequency [Hz]

$a_z$  is the feed rate [ $\frac{mm}{tooth \cdot round}$ ]

$$a_z = \frac{f}{Z} \quad (2-2)$$

$dF_{r,j}$  is the radial force of the  $j^{th}$  tooth [N]

$dF_{t,j}$  is the tangential force of the  $j^{th}$  tooth [N]

$dF_{a,j}$  is the axial force of the  $j^{th}$  tooth [N] normal to the plane xy

The three forces acting during the milling machining are

$$\begin{cases} dF_{t,j} = dF_{t,j}(\varphi) = [K_{tc} \cdot h_j(\varphi) + K_{te}] \cdot dz \\ dF_{r,j} = dF_{r,j}(\varphi) = [K_{rc} \cdot h_j(\varphi) + K_{re}] \cdot dz \\ dF_{a,j} = dF_{a,j}(\varphi) = [K_{ac} \cdot h_j(\varphi) + K_{ae}] \cdot dz \end{cases} \quad (2-3)$$

N.B. The subscript "c" stands for cut and the subscript "e" stands for edge.

In summary the coefficients of the previous formulas are

$K_{tc}$  : cutting coefficient in tangential direction

$K_{rc}$  : cutting coefficient in radial direction

$K_{ac}$  : cutting coefficient in axial direction

$K_{te}$  : edge coefficient in tangential direction

$K_{re}$  : edge coefficient in radial direction

$K_{ae}$  : edge coefficient in axial direction

The first three are linked to the cutting process, the last three are linked to the friction.

Both the radial and tangential force is function of the chip section which has the following expression

$$\text{chip section} : A(t) = a_p \cdot h_j(t) \quad (2-4)$$

being  $h_j(t)$  the chip width [mm] and  $a_p$  the depth of cut [mm].

As we can notice from the previous formula the chip section depends on  $h_j(t)$  which is not constant but depends on  $\varphi_j(t)$ , a function of time, as shown in the following formula

$$h_j(t) = a_z \cdot \sin \varphi_j(t) \rightarrow h_j = h_j(\varphi(t)) \quad (2-5)$$

So, in general the expression of the chip section is

$$A(t) = a_p \cdot h(t) = a_p \cdot (a_z \cdot \sin \varphi_j(t)) = a_p \cdot a_z \cdot \sin \varphi_j(t) \quad (2-6)$$

After some mathematical passages presented in [ALTINTAS 2012] ( p.43-47) we are able to express the average cutting force in X-Y and Z direction as follow

$$\left\{ \begin{array}{l} \bar{F}_x = \left\{ \frac{Na_p a_z}{8\pi} [K_{tc} \cdot \cos(2\varphi) - K_{rc} \cdot (2\varphi - \sin(2\varphi))] + \frac{Na_p}{2\pi} [-K_{te} \cdot \sin(\varphi) + K_{re} \cdot \cos(2\varphi)] \right\}_{\varphi_{st}}^{\varphi_{ex}} \\ \bar{F}_y = \left\{ \frac{Na_p a_z}{8\pi} [K_{tc} \cdot (2\varphi - \sin(2\varphi)) + K_{rc} \cdot \cos(2\varphi)] - \frac{Na_p}{2\pi} [+K_{te} \cdot \cos(\varphi) + K_{re} \cdot \sin(2\varphi)] \right\}_{\varphi_{st}}^{\varphi_{ex}} \\ \bar{F}_z = \left\{ \frac{Na_p}{2\pi} [-K_{ac} \cdot a_z \cdot \cos(\varphi) + K_{ae} \cdot \varphi] \right\}_{\varphi_{st}}^{\varphi_{ex}} \end{array} \right. \quad (2-7)$$

The before described cutting forces can lead to a dynamic excitation of the machine structure.

### 3 System preliminary calibration

In this chapter, the SIFS measurements system is presented.

The measure signal before to be compensate by the Kalman filter is treated through different operations as presented in the following figure

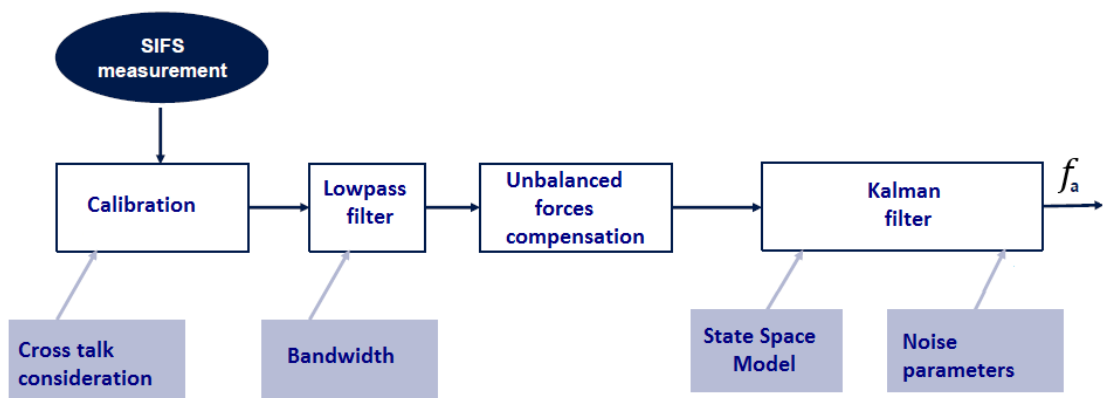


Figure 7 - Signal processing path

#### 3.1 Spindle Integrated Force Sensor measurement (SIFS)

The system consists of three pairs of piezoelectric sensors of the type *Kistler SlimLine 9135B29* to measure forces in three main directions.

The six piezoelectric force sensors are embedded in a ring, which is positioned

inside the spindle housing, as shown in the following figure

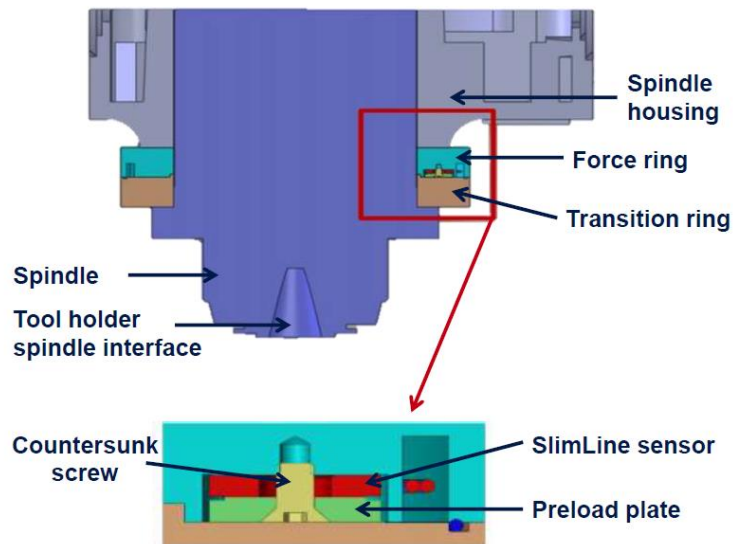


Figure 8 - Section view of the mounted force ring system with detailed preloaded

The forces are lead from the tool holder spindle interface over the spindle to the transition ring and the force ring with its six preloaded force sensors and finally to the spindle housing.

If the sensor must measure very large forces, or it cannot be positioned directly in the path of the force (as in our case), it is often mounted in a force shunt.

This arrangement allows the SlimLine sensor to be used to solve a wide variety of measurement problems. According to [KISTLER 2009A], sensors mounted in force shunt *always have to be calibrated after their mounting*. The six sensors are distributed in a  $60^\circ$  angle around the circle like presented in the Figure .

According to [PARK 2003 p. 21–22], this arrangement is ideal to compensate unequal deformations and improve the sensitivity of the force measurements.

The Y-sensors are located along the machines Y-axis, whereas a line through the X-sensors and the machines Y-direction draws an angle of  $60^\circ$ . The position of the Z-sensors is again shifted by  $60^\circ$  clockwise towards the Y-sensors.

The signal measured by each channel of the SIFS in every direction is amplified by a charge amplifier to transform the electrical signal in a Force reference.

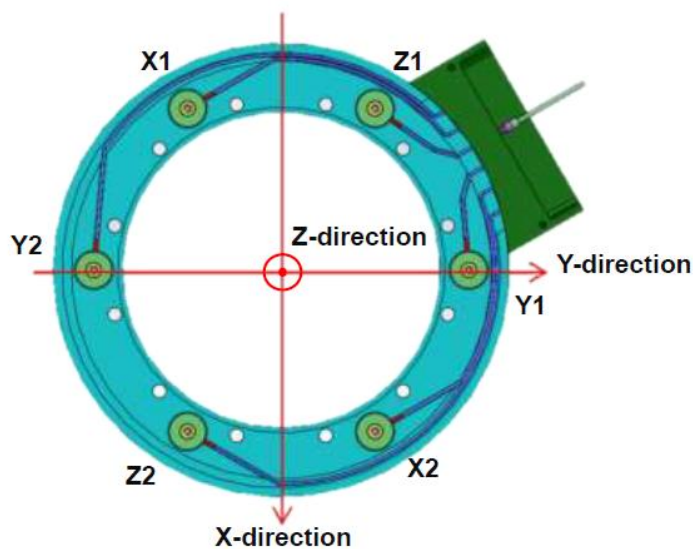


Figure 9 - Force ring with six SlimLine sensors distributed in a  $60^\circ$  angle

A SlimLine sensor consists of two crystal ring washers, an electrode and a housing with connector. The force to be measured must be evenly distributed over the ring surface. The mechanical compressive stress results in an electric charge being generated in the quartz crystal. This charge is proportional to the applied force and does not depend on the dimensions of the quartz washers (longitudinal piezoelectric effect).

The polarity is chosen so that a compression force generates a negative charge, which is then converted into a positive voltage in the charge amplifier. The housing serves

as ground connection. However, this principle of operation leads to the ability of measuring compressive stresses, whereas tensile stresses cannot be measured.

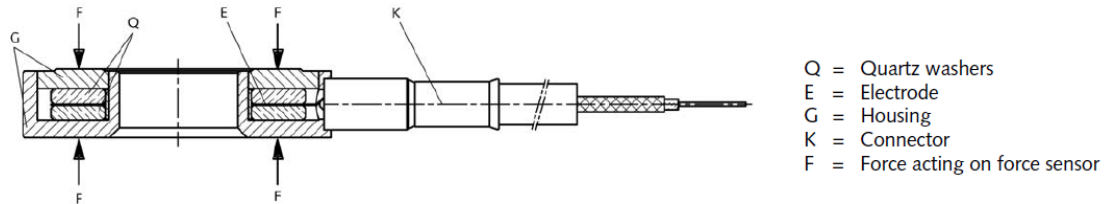


Figure 10 - Kistler SlimLine 9135B29

To overcome this problem the SlimLine sensors are used preloaded, in our case each of the sensors is preloaded in this way (preload force for sensor Z1: 6035 N, Y2: 6050 N, X3: 6050 N, X4: 6040 N Y5:6045 N, Z6: 6034 N).

Kistler preloading disk of the Type 9410A are used to ensure a uniform force distribution over the ring surface. The most important technical data of the used sensor are summarized in following table:

<i>Kistler SlimLine 9135B29</i>			
Measuring range $F_z$ [kN]	[0...36]	Range Limit Value B [kN]	36
Overload $F_z$ [kN]	42	Linearity (preloaded) [%/FSO]	$\leq \pm 1$
Sensitivity [pC/N]	3.8	Hysteresis(preloaded)	<1
Rigidity [kN/ $\mu\text{m}$ ]	7	Response threshold[N]	<0,01
Max. Possible	62	Maximum tolerable	150
Bending Moment [Nm]		Surface pressure [N/ $\text{mm}^2$ ]	

Table 1 - SIFS technical data

The resultant stress on the sensor is the sum of three contributors:

- The bending stresses caused by the lateral force  $F_s$
- direct stresses caused by  $F_z$
- preload stresses caused by  $F_v$

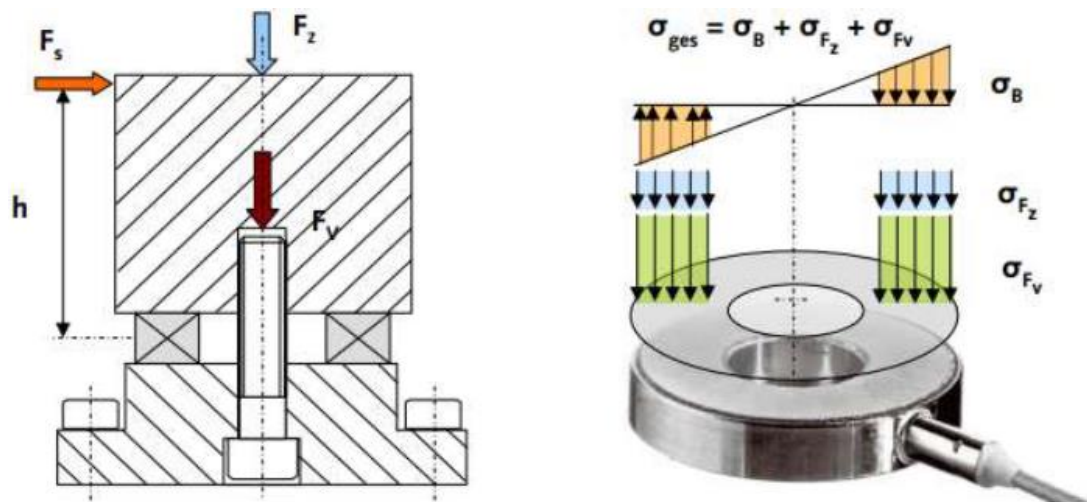


Figure 11 - Forces acting on the sensor

The lateral forces are measured only indirectly through the bending of the spindle, generating tensile and compressive stresses in Z-direction of the sensor.

To prevent any tensile stresses on the sensors is necessary that the axial compressive stresses caused using preload and axial force must be higher than the tensile stresses caused by any lateral forces.

To measure the stresses, the application point of the force must be considered.

*The longer the tool, the more distance is between force application point and sensor and therefore the greater is the momentum which is causing the bending of the spindle.*

The calibration in Z-direction is not affected by the distance of the force application point since Z-direction corresponds to the real measurement direction of the sensors.

*The occurrence of a drift of the measured signal is caused by a lack of charge due to the piezoelectric effect, therefore this phenomenon has to be considered*

## 3.2 Static calibration

In order to acquire sensitivity factors (calibration constants) of the integrated sensor, the *static calibration procedure* was carried out and below describe.

The sensor system is statically calibrated by applying a gradually increasing load at the tool tip of dummy tool.

The dummy tool is a simple round beam mounted into a tool holder. For every calibration test seven weights are suspended to the dummy tool successively, each individual weight has the mass of 10 *lbs* which corresponds to 4.54 *kg* or 44.50 *N*.

In particular for the calibration in Z-direction, the weight is hung on the dummy tool since Z-direction corresponds to the gravity direction, whereas for X- and Y-direction a pulley system is used to deflect the gravity forces as depicted in the Figure 8

OBS→During the static calibration a significant drift component of the measured SIFS signal occur (up to 5 N/min) that it must be removed, for more details see [Park 2003]. The measured force in each direction is calculated like the absolute mean value of the sum of the forces measured from two sensors.

$$f_{static\_calib,y} = -0.5 \cdot (f_{meas,y1} - f_{meas,y2}) \quad (3-1)$$

$$f_{static\_calib,x} = 0.5 \cdot (f_{meas,x1} - f_{meas,x2})$$

$$f_{static\_calib,z} = 0.5 \cdot (f_{meas,z1} + f_{meas,z2})$$

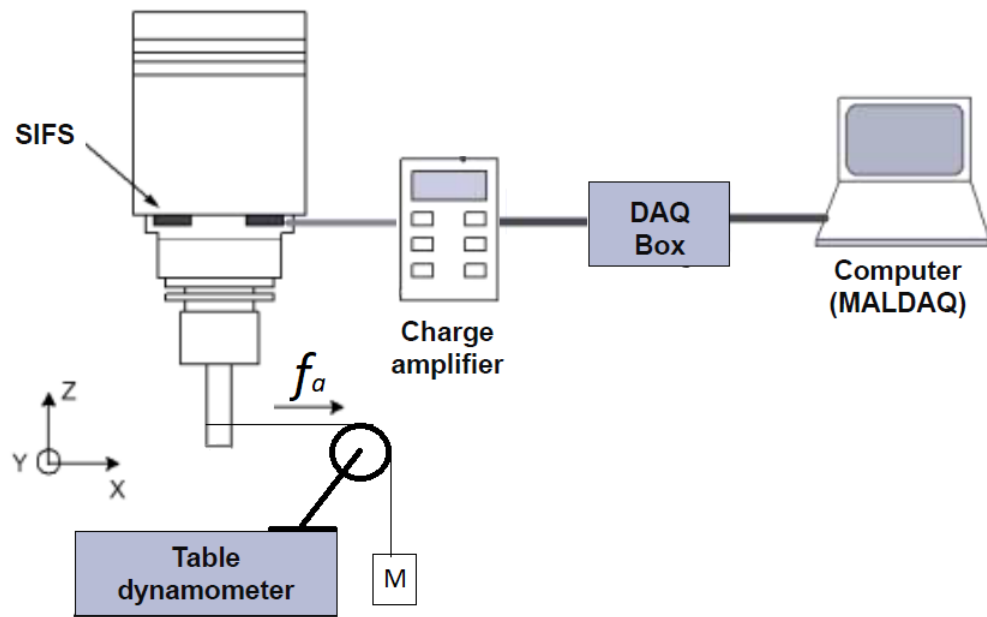


Figure 8 - Static calibration equipment

Finally, once  $f_{static\_calib,i}$  has been reconstructed from piezo sensors signals for each different weight, the calibration constant is the mean between the calibration constants computed for each different casuistry using the following formula

$$c_i = \frac{f_{a,i}}{f_{static\_calib,i}} \quad (3-2)$$

Where:

$f_{a,i}$  = real applied force  $i = X, Y, Z$  direction

$f_{static\_calib,i}$  = mean static force

The sensitivity of the sensor can be compute like the ratio between the charge amplifier sensitivity and the calibration costant

$$S_i = \frac{Sens_{charge\ Ampl.}}{c_i} \quad (3-3)$$

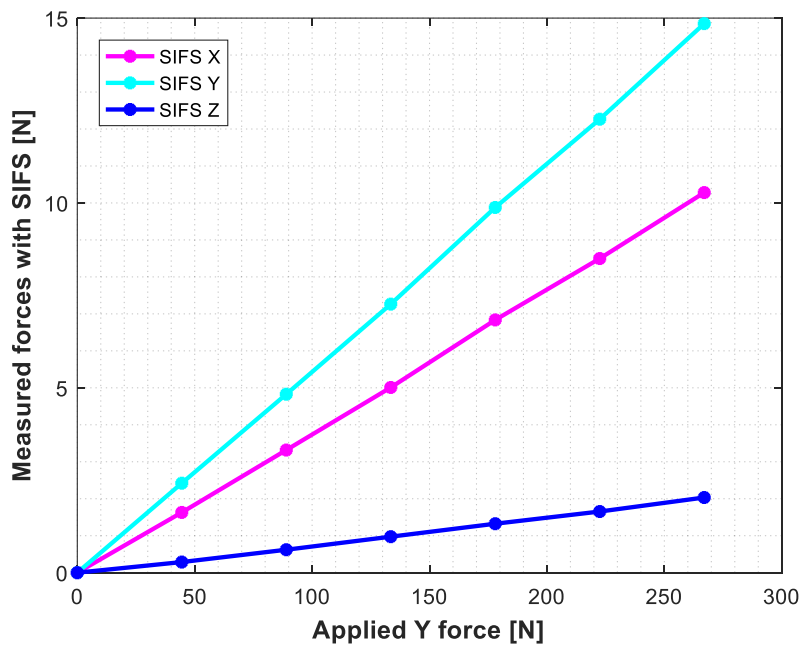


Figure 9 - Comparison between measured and applied force in static calibration

In the Table 2, the SIFS sensitivities in the main directions and all calibration constants (include the Crosstalk components) are summarized.

Exist a linear relation between calibration constant and the tool length since the moment is directly linear dependent from the arm of lever and the applied force.

The following equation describes the length dependence of the calibration constant

$$c_i = c_{i,1} \cdot L + c_{i,offset} \quad (3-4)$$

Where:

$c_{i,1}$  = calibration factor

$L$  = length of the tool plus tool holder combination

$c_{i,offset}$  = offset value

For the computation of these factors see [THOMAS 2015].

In this way we can express the calibration constants in a new form directly dependent from the Tool length as shown in Table 3

<i>direction</i>	<i>Sensitivity</i>	<i>Calibration costant</i>	<i>Calibration costant Cross talk components</i>
X	$s_x = 0.209 \frac{pC}{N}$	$c_x = 18$	
Y	$s_y = 0.217 \frac{pC}{N}$	$c_y = 18.2$	$c_{Y,x} = 26,5$ $c_{Y,z} = 139,3$
Z	$s_z = 0.061 \frac{pC}{N}$	$c_z = 62$	$c_{X,z} = -341$

Table 2 - SIFS characteristic

Direction	Length Dependence L(mm)
X	$c_X = -0.059 \cdot L + 26.203$
Y	$c_Y = -0.063 \cdot L + 26.718$
Z	$c_Z = 62,46$ (length independent)
Cross talk in X, caused by Y-load	$c_{Y,x} = -0.121 \cdot L + 44.545$
Cross talk in Z, caused by Y-load	$c_{Y,z} = -0.398 \cdot L + 186.16$
Cross talk in Z, caused by X-load	$c_{X,z} = 1.840 \cdot L - 597.73$

Table 3 - Dependence of calibration constants from the tool length

### 3.2.1 Static Calibration verification

For the verification of the calibration a dummy tool is used to apply static load to a workpiece which is clamped on a table dynamometer. The experimental setup is depicted in the figure 14. For the calibration, the tool is displaced with small steps against the workpiece on the dynamometer to increase the interaction forces.

The calibration was considered adequate when the load measured by the SIFS ( $f_{mean\_static,i}$ ) correspond to the real applied forces on the tool tip ( $f_{a,i}$ ) measured by the reference dynamometer with a variation of less than 5%.

*In this case for a greater precision the static Cross-Talk contributions are considered*

$$\begin{aligned}
 f_{static\_calib,y} &= -0.5 \cdot (f_{meas,y1} - f_{meas,y2}) \cdot c_y \\
 f_{static\_calib,x} &= \left( 0.5 \cdot (f_{meas,x1} - f_{meas,x2}) - \frac{f_{static\_calib,y}}{c_{yx}} \right) \cdot c_x
 \end{aligned} \tag{3-5}$$

$$f_{static\_calib,z} = \left( \left( 0.5 \cdot (f_{meas,z1} - f_{meas,z2}) \right) - \frac{f_{static\_calib,y}}{c_{yz}} - \frac{f_{static\_calib,x}}{c_{xz}} \right) \cdot c_z$$

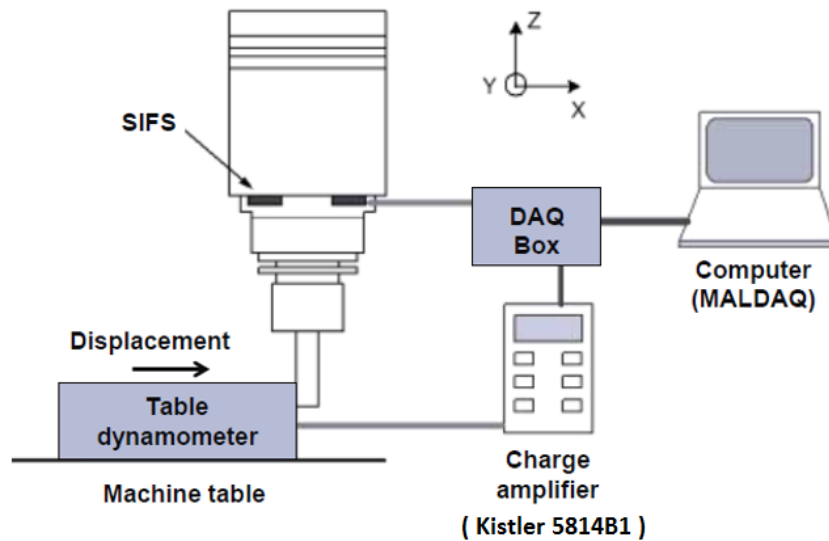


Figure 10 - Dynamic calibration equipment

A verification example is depicted in the figure 15 for applied X-forces.

As it can be seen, the experimental results match very well the reference force measurement.

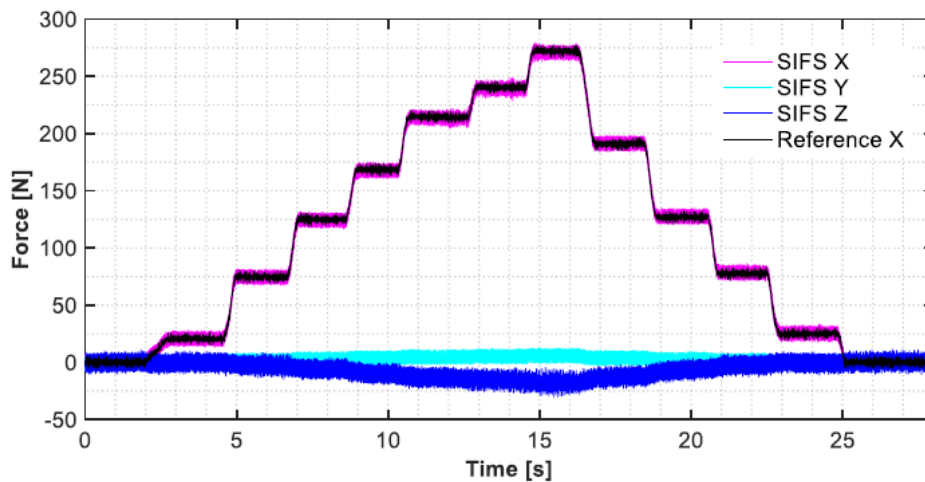


Figure 11 - Verification of the dynamic calibration

### 3.3 Low Pass Filter and Unbalanced Forces Compensation

The task of the low pass filter within the cutting force compensation process is to remove signal contents above the Kalman filter bandwidth obtained thanks to the Westemier algorithm (see [Westermier 2010] - Compensation of Cutting Force Measurements)

Generally, usual lowpass filters cause an additional phase lag, which is undesirable for cutting force compensations. In this work a zero-phase filtering technique, is used.

Nevertheless, the simple filtering does not lead to acceptable results since the frequencies of the unbalanced forces are multiples of the spindle frequency.

Therefore, the signal still contains noise components resulting from the eccentricity

of the rotating spindle that generates unbalanced forces.

The unbalanced forces are square functions of the rotational speeds.

$$f_u = m_0 \cdot e \cdot \left(\frac{n}{60}\right)^2 \cdot \sin\left(\frac{n}{60} \cdot t\right) \quad (3-6)$$

For example, the comparison of unbalanced vibration occurring at 1000 rpm and 10000 rpm would be 100 times.

The appropriate way to compensate these disturbance is to subtract the unbalanced forces  $f_u$  from the dynamically calibrated measured force  $f_{dynamic\_calib,i}$ .

The time before the real cutting when the spindle is already rotating at the normal speed but the tool is not yet engaged in the workpiece is called air cutting phase.

Theoretically, the measured forces during the air cutting phase should be equal to zero because there are no proper forces acting on the tool tip, so the mean value of the measured forces correspond to the unbalanced force.

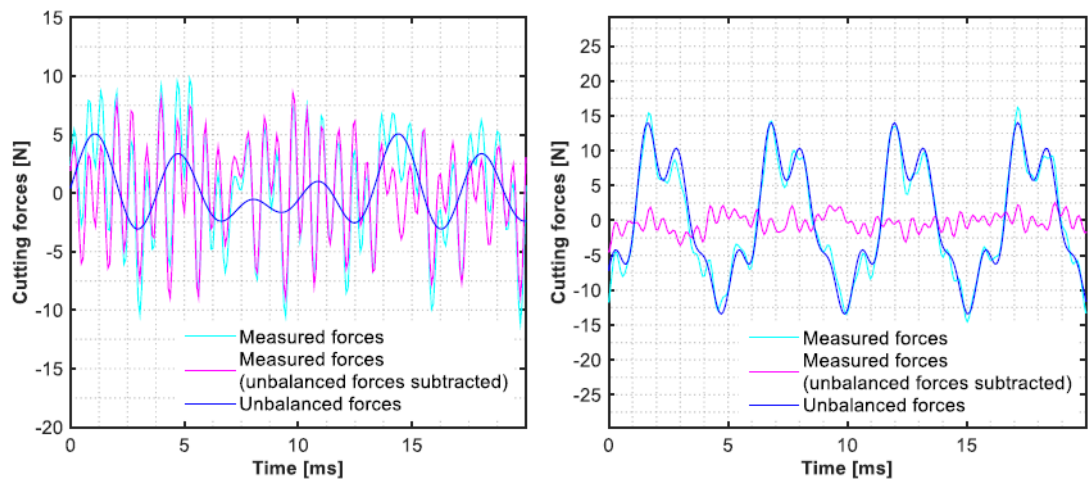


Figure 12 - Unbalanced forces subtraction

As visible in the left plot, the measurement noise is dominating for lower spindle speeds like 4500 *rpm* compared to the unbalanced forces.

For higher spindle speeds, the unbalanced forces dominate as visible in the right plot. The unbalanced forces need to be identified as a separate signal without measurement noise to subtract them from the actual measurement.

For more details about the unbalanced forces and their influence on covariance matrix and the white Gaussian noise distribution see [THOMA SEMM 2015].

### 3.4 Dynamic Calibration

In the Static calibration, the forces caused by Cross Talk contributions don't consider the system dynamic but only the geometric disposition of the sensors [THOMAS 2015].

Since the amount of cross talk forces is not constant for every frequency, the simple subtraction of the static cross talk forces does not lead to accurate dynamically calibrated measurements. In order to discover the real dynamic contribution that the force in one direction cause in another direction is necessary to study the structure dynamic of the spindle and built an accurate analytical model of it in its all directions. Once Computed the Cross-TF of the system in all directions is possible to compute the dynamic cross talk forces  $(f_{x,cross} \ f_{y,cross})$  using the Matlab command “lsim” which simulates the dynamic system time response to arbitrary inputs.

Remembering that the measures are calibrated by the static calibration constant  $c_i$  (Obtained in the static calibration phase) to get the correct proportion between

excitation force and cross talk measurement. At first, in a similar way to the static calibration a possible drift of the signal is compensated and secondly, the measurements are dynamically calibrated by the following equations

$$\begin{aligned}
 f_{dynamic\_calib,y} &= -0.5 \cdot (f_{meas,y1} - f_{meas,y2}) \cdot c_y \\
 f_{dynamic\_calib,x} &= (0.5 \cdot (f_{meas,x1} - f_{meas,x2}) - f_{y,cross}) \cdot c_x \\
 f_{dynamic\_calib,z} &= \left( (0.5 \cdot (f_{meas,z1} - f_{meas,z2})) - f_{y,cross} - f_{x,cross} \right) \cdot c_z
 \end{aligned}
 \tag{3-7}$$

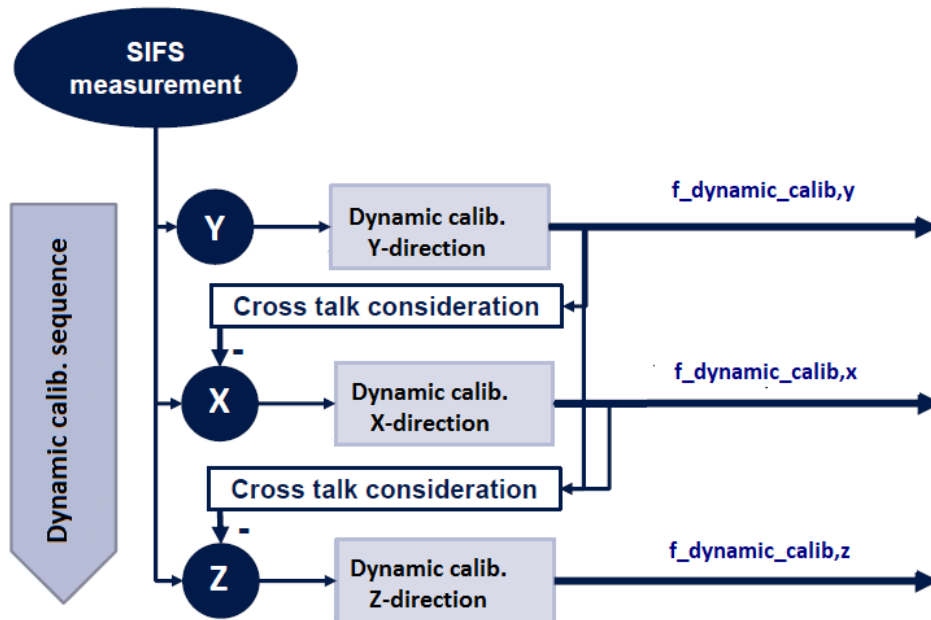


Figure 13 - Dynamic calibration sequence



## 4 Kalman filter strategy

In this paragraph, we are going to talk about the last step of the whole signal compensation process, the Kalman filtering.

It is important to underline like the  $TF = \frac{f_m}{f_a}$  doesn't consider the eigenmodes of the system so when we are close to the natural frequency of it the output  $f_m$  doesn't correspond to the real one.

In order to obtain the real force in output we need to Compensate the machine dynamic and the noise of the system through the Kalman filter strategy.

Firstly, we must be able to model mechanical systems in mathematical terms and analyse their dynamic characteristics.

### 4.1 Machine dynamic and Analytical model design

A mathematical model of a dynamic system is defined as a set of equations that represents the dynamics of the system accurately, or at least fairly well.

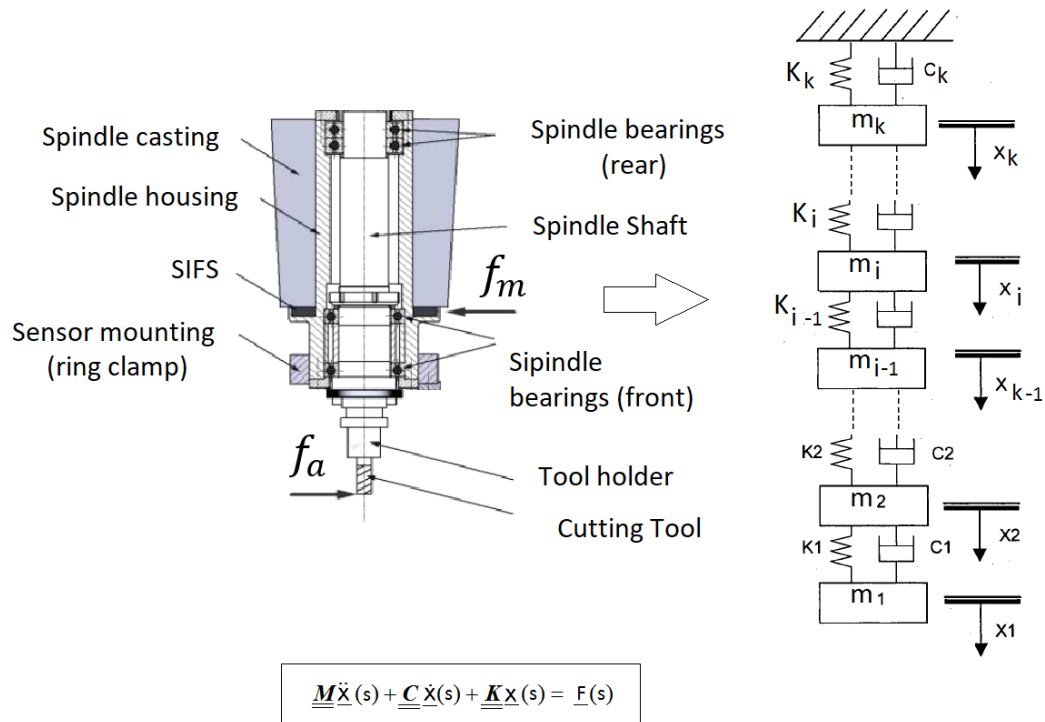
For mechanical systems, such differential equations may be obtained by using Newton's physical laws. The first step consists into create an equivalent Mass-Spring-Damper model of the Spindle structure, as shown in the Figure 13.

Where:

*The subscript  $k$  represent number of modes*

$f_m$  = measured force from the Spindle Integrated Force Sensor (SIFS)

$f_a$  = is the applied force at the tool tip.



Where:

$$\underline{\underline{M}} = \begin{bmatrix} m_1 & & & & \\ & m_2 & & & \\ & & \ddots & & \\ & & & & m_k \end{bmatrix} \quad \underline{\underline{C}} = \begin{bmatrix} c_1 + c_2 & -c_2 & \dots & 0 \\ -c_2 & c_2 + c_3 & \dots & 0 \\ \dots & \dots & \dots & \dots \\ 0 & \dots & \dots & c_k \end{bmatrix} \quad \underline{\underline{K}} = \begin{bmatrix} k_1 + k_2 & -k_2 & \dots & 0 \\ -k_2 & k_2 + k_3 & \dots & 0 \\ \dots & \dots & \dots & \dots \\ 0 & 0 & \dots & k_k \end{bmatrix}$$

$$\underline{x}(s) = \begin{Bmatrix} x_1(s) \\ x_2(s) \\ \vdots \\ x_k(s) \end{Bmatrix} \quad \underline{F}(s) = \begin{Bmatrix} 0 \\ 0 \\ \vdots \\ f_a(s) \end{Bmatrix}$$

Figure 14 – MDOF dynamic model of the Spindle structure

The mathematical model is the result derived from a compromise between the simplicity of the model and the accuracy of the analysis results.

An important assumption regards the linearity of the system that permit the superposition principle application. The principle of superposition states that the response produced by the simultaneous application of two different forcing functions is the sum of the two individual responses, so for the linear system, the response to several inputs can be calculated by treating one input at a time and adding the results. From a physical point of view, thanks to the assumption of system linearity we are trying to see the initial behaviour of the system like the sum of independent simple oscillators, each of which is characterized from a single DOF independent from the others but who contributes to the total displacement of the system. In this thesis in order to characterize the input-output relationships a *Force to Force TF* is used.

## 4.2 Modal Analysis fundamentals

The dynamic structure of the system can be described by means of modal parameters. A particularity of the N DOF system consist into using the eigenvectors (modal shapes of the system) for the diagonalization of the differential equations system that describes the physical model; in this way, we can consider the dynamic response of our system as the sum of  $k$  different modes. We analyse the problem from an analytically point of view. Firstly, to find the eigenvectors we have to compute the natural frequencies of the system, so we consider

- Negligible process damping

- No external Forces apply to the system

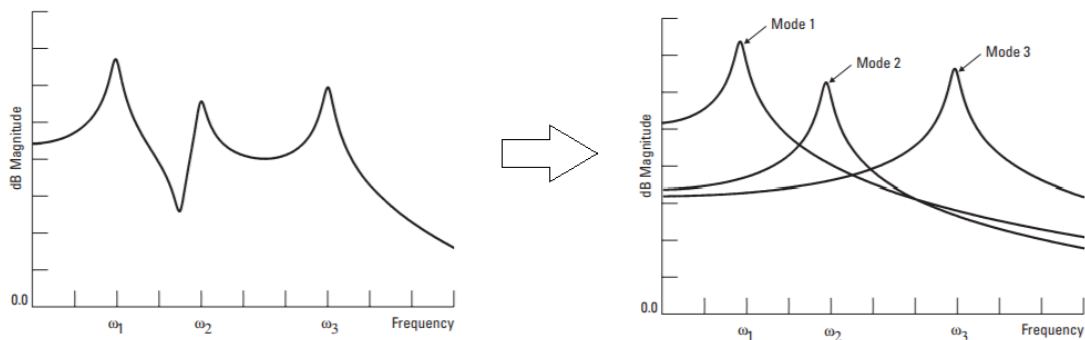


Figure 15 - Modal Analysis fundamentals

The equation of motion becomes

$$[M]\ddot{\underline{x}} + [K]\underline{x} = 0 \quad (4-1)$$

This is a typical eigenvalues problem expressed as

$$[K]\underline{v} = \omega_n[M]\underline{v} \quad (4-2)$$

$\underline{v}$  = eigenvectors of the system or modal shapes

$\omega_n$  = eigenvalue or natural frequency of the system

$$([K] - \omega_n[M])\underline{v} = 0 \quad (4-3)$$

The not trivial solution of the characteristic equation is

$$\det([K] - \omega_n[M]) = 0 \quad (4-4)$$

Whence we can find the eigenvalues grouped in the diagonal matrix  $\Lambda$

$$[\Lambda] = \begin{bmatrix} \omega_{n,1} & \cdots & 0 \\ \vdots & \ddots & \vdots \\ 0 & \cdots & \omega_{n,k} \end{bmatrix} \quad (4-5)$$

$$\omega_{n,1} \geq \omega_{n,2} \geq \cdots \geq \omega_{n,k} \quad (4-6)$$

The last step is to compute the eigenvectors

$$\underline{v}_1, \underline{v}_2, \dots, \underline{v}_k \quad (4-7)$$

Where  $[\Phi]$  is equal to

$$[\Phi]_{k \times k} = [\underline{v}_1 \ \underline{v}_2 \ \cdots \ \underline{v}_k] \quad (4-8)$$

Once that the modal matrix is define we can pass in modal coordinates

$$\underline{x}(s) = [\Phi] \cdot \underline{q}(s) \quad (4-9)$$

Substituting in the equation of motion and premultiplying for  $[\phi]^T$  we obtain the diagonalization of the matrices

$$\underbrace{[\phi]^T[M][\phi]}_{[\hat{M}]} \ddot{q}(s) + \underbrace{[\phi]^T[C][\phi]}_{[\hat{C}]} \dot{q}(s) + \underbrace{[\phi]^T[K][\phi]}_{[\hat{K}]} q(s) = \underbrace{[\phi]^T F}_{\hat{F}} \quad (4-10)$$

$$[\hat{M}] \ddot{q}(s) + [\hat{C}] \dot{q}(s) + [\hat{K}] q(s) = \hat{F} \quad (4-11)$$

The new system is composed by K differential equations independents from each other.

We normalize the system against the mass.

$$\begin{aligned} \begin{bmatrix} 1 & \cdots & 0 \\ \vdots & \ddots & \vdots \\ 0 & \cdots & 1 \end{bmatrix} \begin{bmatrix} \ddot{q}_1 \\ \vdots \\ \ddot{q}_k \end{bmatrix} + \begin{bmatrix} 2\zeta_1\omega_{n,1} & \cdots & 0 \\ \vdots & \ddots & \vdots \\ 0 & \cdots & 2\zeta_k\omega_{n,k} \end{bmatrix} \begin{bmatrix} \dot{q}_1 \\ \vdots \\ \dot{q}_n \end{bmatrix} + \\ + \begin{bmatrix} \omega_{n,1} & \cdots & 0 \\ \vdots & \ddots & \vdots \\ 0 & \cdots & \omega_{n,k} \end{bmatrix} \begin{bmatrix} q_1 \\ \vdots \\ q_k \end{bmatrix} = \phi^T \begin{bmatrix} 0 \\ \vdots \\ f_a \end{bmatrix} \end{aligned} \quad (4-12)$$

- Modal coordinates don't have any physical meaning

For more complex real structures, it is not possible to derive the equations just theoretically.

In order to identify the values of  $\omega_i \zeta_i$  Experimental Modal Analysis (EMA) is conducted.

Similarly, EMA uses the impact hammers to acquire the FRF; the input is the impact

force applied to the tool tip  $f_a$ , and the output is the force from SIFS  $f_m$  derived by averaging the frequency response curves obtained from several successive impact tests to increase robustness of the measurements.

### 4.2.1 Experimental FRF for MDOF system

To understand how the experimentally TF for MDOF system is build, we need to explain the dynamic of a simple structure with a single-degree of freedom.

A (SDOF) system can be modelled by a combination of mass ( $m$ ), spring ( $k$ ), and damping ( $c$ ) elements.

When an external force  $F(t)$  is exerted on the structure, its motion is described by the following differential equation:

$$m\ddot{x} + c\dot{x} + kx = f(t) \quad (4-13)$$

If the system is in a rest condition and receives a hammer hit for a very short duration it tends to statically deviates from its equilibrium and it experiences free vibrations.

The amplitude of vibrations decays with time as a function of the system's damping constant. The frequency of the vibrations is mainly dominated by the stiffness and the mass and is lightly influenced by the viscous damping constant, which is very small in mechanical structures.

When the damping constant is zero ( $c = 0$ ), the system oscillates at its natural frequency as follows:

$$\omega_n = \sqrt{\frac{k}{m}} \rightarrow \omega_n^2 = \frac{k}{m} \quad (4-14)$$

The damped natural frequency of the structure is defined by

$$\omega_d = \omega_n \sqrt{1 - \zeta^2} \quad (4-15)$$

A damping ratio  $\zeta$  is always less than one in mechanical structures. In most metal structures  $\zeta < 0.05$  or even less and is defined as

$$\zeta = \frac{c}{c^*} \quad (4-16)$$

Where:

$$c^* = 2\sqrt{km} \rightarrow \frac{c}{m} = \frac{2\sqrt{km}}{m} \zeta = 2\zeta\omega_n \quad (4-17)$$

If divide all equation of motion terms for  $m$  we get

$$\ddot{x} + 2\zeta\omega_n\dot{x} + \omega_n^2x = \frac{\omega_n^2}{k}f(t) \quad (4-18)$$

When an external force  $f(t)$  is present, the system experiences forced vibrations.

The general response of the structure can be evaluated by solving the differential equation of the motion. The Laplace transform of the equation of motion with initial displacement  $x(0)$  and vibration velocity  $x'(0)$  under externally applied force

$F(t)$  is expressed as

$$\mathcal{L}(\ddot{x} + 2\zeta\omega_n\dot{x} + \omega_n^2x) = \mathcal{L}\left(\frac{\omega_n^2}{k}f(t)\right) \quad (4-19)$$

$$s^2x(s) - sx(0) - x'(0) + 2\zeta\omega_n sx(s) + 2\zeta\omega_n x(0) + \omega_n^2x(s) = \frac{\omega_n^2x}{k}f \quad (4-20)$$

The SDOF system's general response, can be expressed as follow:

$$x(s) = \frac{\omega_n^2}{k} \frac{1}{s^2 + 2\zeta\omega_n s + \omega_n^2} f(s) + \frac{(s + 2\zeta\omega_n)x(0) - x'(0)}{s^2 + 2\zeta\omega_n s + \omega_n^2} \quad (4-21)$$

The transfer function of the system is represented by neglecting the effect of initial conditions that will eventually disappear as transient vibrations.

$$\phi(s) = \frac{x(s)}{f(s)} = \frac{\omega_n^2}{k} \frac{1}{s^2 + 2\zeta\omega_n s + \omega_n^2} \quad (4-22)$$

In this work, force to force FRF is used to identify the transfer function of the spindle.

Knowing that

$$f_o(s) = k_o x(s) \quad (4-23)$$

Where:

$k_o = \text{stiffness measurement device}$

$$\alpha^{-1} = \frac{k_o}{k} \quad (4-24)$$

Substituting we get

$$G(s) = \frac{f_o(s)}{f(s)} = \frac{\omega_n^2 \alpha^{-1}}{s^2 + 2\zeta \omega_n s + \omega_n^2} \quad (4-25)$$

$(s^2 + 2\zeta_k \omega_n s + \omega_n^2) =$  characteristic equation of the system

The characteristic equation has two complex conjugated roots:

$$\begin{aligned} s_1 &= -\zeta \omega_n + j \omega_d \\ s^*_1 &= -\zeta \omega_n - j \omega_d \end{aligned} \quad (4-26)$$

The previous  $G(s)$  equation is not used to evaluate the FRF from measurements because of the presence of noise in the sensor signals.

The FRF cannot be calculated directly in the frequency domain, that ratio must pass through the estimators (Altintas 2000, pag 93)

For K DOF system we get

$$G(s) = \frac{f_m}{f_a} = \sum_{i=1}^k \frac{\omega_{n,i}^2 \alpha_i^{-1}}{(s^2 + 2\zeta_i \omega_{n,i} s + \omega_{n,i}^2)} \quad (4-27)$$

The result of an experimental FRF measurement is usually a table providing the

magnitude  $M$  and phase  $\Phi$  values for each frequency  $\omega$  within the examined frequency range.

If the peaks of resonance are enough far for not affecting each other, exist algorithms that permit to compute the modal parameters  $\omega_{n,i}$ ,  $\zeta_i$ ,  $\alpha_i^{-1}$  of the transfer function for each mode [EWINS 2000].

In order to obtain a continuous transfer function from these measurement values, a nonlinear curve fitting method is used in this thesis. Since FRF measurements are conducted by means of the software CUTPRO® by MAL Inc., which also provides an advanced curve fitting tool for FRF measurement data, the background of curve fitting techniques is not covered in this thesis (Altintas 2000).

### 4.3 State space model representattion

Since the transfer function is a mathematical description of the dynamic system properties, it can be also described by a polynomial of  $k^{th}$  order; where  $k$  is the number of mass dampers using for the construction of the physical model and the number of eigenfrequencies.

Firstly, consider the differential equation system that involves derivatives of the forcing function, such as

$$y^k + a_1 y^{k-1} + \dots + a_{k-1} \dot{y} + a_k y = b_0 u^m + b_1 u^{m-1} + \dots + b_{m-1} \dot{u} + b_m u \quad (4-28)$$

Where:

$u = f_a =$  input Force

$y = f_m =$  output Force

The TF in Laplace domain in polynomial form

$$G(s) = \frac{Y(s)}{U(s)} = \frac{f_m}{f_a} = \frac{b_0 s^m + b_1 s^{m-1} + \dots + b_{m-1} s + b_m}{s^k + a_1 s^{k-1} + \dots + a_{k-1} s + a_k} \quad (4-29)$$

In optimal control problems is advantageous to use state-space representations.

The state of a dynamic system is the smallest set of variables (called state variables) such that knowledge of these variables at  $t = t_0$ , together with knowledge of the input for  $t \geq t_0$ , completely determines the behavior of the system for any time  $t \geq t_0$ .

least  $n$  variables  $x_1, x_2, \dots, x_k$  are needed to completely describe the behaviour of a dynamic system.

The main problem in defining the state variables for this case lies in the derivative terms of the input  $u$ . The state variables must be such that they will eliminate the derivatives of  $u$  in the state equation.

One way to obtain a state equation and output equation for this case is to define the following  $n$  variables as a set of  $n$  state variable

$$\begin{aligned}x_1 &= y - \beta_0 u \\x_2 &= \dot{y} - \beta_0 \dot{u} - \beta_1 u_1 = \dot{x}_1 - \beta_1 u \\x_3 &= \dot{x}_2 - \beta_2 u \\&\vdots \\x_k &= \dot{x}_{k-1} - \beta_{k-1} u\end{aligned}\tag{4-30}$$

Where  $\beta_0, \beta_1, \dots, \beta_{n-1}$  are determined from

$$\begin{aligned}\beta_0 &= b_0 \\ \beta_1 &= b_1 - a_1 \beta_0 \\ \beta_2 &= b_2 - a_1 \beta_1 - a_2 \beta_0 \\ \beta_3 &= b_3 - a_1 \beta_2 - a_2 \beta_1 - a_3 \beta_0 \\ &\vdots \\ \beta_k &= b_k - a_1 \beta_{k-1} - \dots - a_{k-1} \beta_1 - a_{k-1} \beta_0\end{aligned}\tag{4-31}$$

With this choice of state variables, the existence and uniqueness of the solution of the state equation is guaranteed. (Note that this is not the only choice of a set of state variables.) With the present choice of state variables, we obtain

$$\begin{aligned}
 \dot{x}_1 &= x_2 + \beta_1 u \\
 \dot{x}_2 &= x_3 + \beta_2 u \\
 &\vdots \\
 \dot{x}_{k-1} &= x_k + \beta_{k-1} u \\
 \dot{x}_k &= -a_k x_1 - a_{k-1} x_2 - \dots - a_1 x_k + \beta_k u
 \end{aligned} \tag{4-32}$$

In our case

$$y = f_m \wedge u = f_a$$

$$\begin{bmatrix} \dot{x}_1 \\ \dot{x}_2 \\ \vdots \\ \dot{x}_k \end{bmatrix} = \begin{bmatrix} 0 & 1 & 0 & \dots & 0 \\ 0 & 0 & 1 & \dots & 0 \\ \dots & \dots & \dots & \dots & \dots \\ 0 & 0 & 0 & \dots & 1 \\ -a_k & -a_{k-1} & -a_{k-2} & \dots & -a_1 \end{bmatrix} \begin{bmatrix} x_1 \\ x_2 \\ \vdots \\ x_k \end{bmatrix} + \begin{bmatrix} \beta_1 \\ \beta_2 \\ \vdots \\ \beta_k \end{bmatrix} f_a \tag{4-33}$$

$$f_m = [1 \quad 0 \quad \dots \quad 0] \begin{bmatrix} x_1 \\ x_2 \\ \vdots \\ x_k \end{bmatrix} + \beta_0 f_a \tag{4-34}$$

It becomes

$$\begin{aligned}
 \dot{x} &= A_{s(kxk)} x + B_{s(kx1)} f_a \\
 f_m &= C_{s(1xk)} x + D_s f_a
 \end{aligned} \tag{4-35}$$

Where:

$A_s$  = Dynamics matrix of the system

$B_s$  = Input Matrix

$C_s$  = Output Matrix

$D_s$  = Input-output direct link matrix

If there is no direct link between Input-Output, then D matrix is equal to 0

## 4.4 System numerical stability

$$\begin{aligned}\dot{x} &= A_s x + B_s f_a \\ f_m &= C_s x\end{aligned}\tag{4-36}$$

Care must be taken on the numerical stability; in fact, if the system becomes unstable the computation of the Kalman gain (see Eq 5.38 in Chapter 5.3.2) is not correct.

for a generic  $A$  matrix the stability condition is respects only if

$$\kappa(A)^{-1} > \text{machine precision}\tag{4-37}$$

Where:

$$\kappa(A) = \text{condition number} = \|A\|_{\infty} \|A^{-1}\|_{\infty}\tag{4-38}$$

$$\|\cdot\|_{\infty} = \text{infinite norm}$$

The condition number depends by number of considered modes, higher is the number of modes, bigger is condition number and poorer is stability of the system.

The machine precision which is calculated with the Matlab command `eps` and returns the machine precision as  $2.22045 \cdot 10^{-16}$ .

In our case the matrices  $A_s, C_s$  contain both very large and very small numbers which result in poorly conditioned matrices with respect to the inversion of matrices and eigenvalue analysis.

Remember that a small perturbation of an ill conditioned matrix elements might produce a big variation in the linear system solution. Good or bad condition can be defined after [GREWAL ET AL. 2008, p. 230–232] as follows: “One might, for example, describe a matrix  $A$  as being ‘ill-conditioned with respect to inversion’ if  $A$  is ‘close’ to being singular”. Important is to underline that none singular matrix is invertible; in this case we need to transform the system matrices into equivalent system by applying a transformation matrix  $T$  ( $x_n = Tx$ ) where the index  $n$  represents the new transformed and better conditioned matrices.

$$\dot{x}_n = A_{n(kxk)}x_n + B_{n(kx1)}f_a \quad (4-39)$$

$$f_m = C_{n(1xk)}x_n$$

Where:

$$A_n = TAT^{-1}$$

$$B_n = \frac{TB}{\lambda}$$

$$C_n = \lambda CT^{-1}$$

$\lambda = \text{scale factor} = 1$        $T = \text{transormation matrix}$

Another important criterion for the state-space matrices is its observability.

The observability matrix  $O$  is thereby defined as follows

$$O = [C^T A^T C^T \quad (A^T)^2 C^T \quad \dots \quad (A^T)^{k-1} C_T] \quad (4-40)$$

A system is called observable when its observability matrix  $O$  has full rank.

In this case the rank of the observability matrix (compared to the  $A$  matrix dimensions  $k$ ) must to be

$$\text{rank}(O) = 2k + 1 \quad (4-41)$$

From a controlling point of view “Observability is the issue of whether the state of a dynamic system with a known model is uniquely determinable from its inputs and outputs” [GREWAL ET AL. 2008, p. 55–56]. Therefore, observability describes the ability to recover all states of a deterministic system if there is no noise.

The second observability condition is

$$\kappa(O)^{-1} > \text{machine precision} \quad (4-42)$$

The condition of the observability matrix is chosen close to machine precision to consider as many modes as possible and on the same time not violate the observability criterion.

Finally, is important to underline as the choose of very high and small eigenmodes damping values might lead to not full ranked observability matrixes which are therefore not observable.

To compensate this trade-off between observability and accuracy of the fitting, the number of modes should be kept as little as possible and their damping values should be chosen in the same range. These three proofs are repeated in each step for the construction of the discrete Kalman filter.

## 4.5 Model Expansion

Remember that the main goal is to evaluate the force applied on the Tool tip, then the modelled spindle system dynamics can be expanded to include the input force  $f_a$  as one of the unknown state.

The input force can be divided into two main components

$$f_a = f_{ha} + f_c \quad (4-43)$$

Where:

$f_{ha} = \cos\omega_t t \cdot w_{ac} = \text{harmonic force component}$

$w_{ac} = \text{periodic disturb}$

$\dot{f}_c = 0 + w_{dc} = \text{constant force component} \quad w_{dc} = \text{noise}$

Consider only the harmonic component and define the TF function in Laplace domain.

$$G(t) = \frac{f_{ha}(t)}{w_{ac}(t)} = \cos\omega_t t \rightarrow G(s) = \frac{s}{s^2 + \omega_t^2} = \frac{f_{ha}(s)x_{2f}}{w_{ac}(s)x_{2f}} \quad (4-44)$$

Where:

$\omega_t = \text{Tooth passing frequency}$

Through several mathematical steps

$$\frac{x_{2f}}{w_{ac}} = \frac{1}{s^2 + \omega_t^2} \quad (4-45)$$

$$\frac{f_{ha}}{x_{2f}} = s \quad (4-46)$$

Antitrusting and defining  $\dot{x}_{2f} = x_{1f}$

$$\begin{aligned} \dot{x}_{1f} &= 0 - \omega_t^2 x_{2f} + w_{ac} \\ \dot{x}_{2f} &= x_{1f} \\ f_{ha} &= x_{1f} \end{aligned} \quad (4-47)$$

We get

$$A_f = \begin{bmatrix} 0 & -\omega_t^2 \\ 1 & 0 \end{bmatrix} \quad B_f = \begin{bmatrix} 1 \\ 0 \end{bmatrix} \quad C_f = [1 \quad 0] \quad x_f = \begin{bmatrix} x_{1f} \\ x_{2f} \end{bmatrix}$$

The state space equivalent

$$\begin{aligned} \dot{x}_f &= A_f x_f + B_f w_{ac} \\ f_{ha} &= C_f x_f \end{aligned} \quad (4-48)$$

Substituting in (4-39) we get

$$\dot{x}_n = A_n x_n + B_n (f_c + C_f x_f) \quad (4-49)$$

$$f_m = C_n x_n$$

If we consider the constant component of the input force as an unknown, so we can rewrite the state space model in this way

$$\begin{bmatrix} \dot{x}_n \\ f_m \end{bmatrix} = \begin{bmatrix} A_n & B_n & B_n C_f \\ 0 & 0 & 0 \\ 0 & 0 & A_f \end{bmatrix} \begin{bmatrix} x_n \\ f_c \\ x_f \end{bmatrix} + \begin{bmatrix} 0 \\ \theta_{ac} \\ \theta_{dc} \end{bmatrix} w \quad (4-50)$$

$$f_m = [C_n \quad 0 \quad 0] \begin{bmatrix} x_n \\ f_c \\ x_f \end{bmatrix}$$

Where:

$$\theta_{dc} = \frac{w_{dc}}{w} \quad \wedge \quad \theta_{ac} = \frac{w_{ac}}{w}$$

It becomes

$$\dot{x}_e = A_{e(n \times n)} x_{e(n \times 1)} + \Gamma w \quad w \sim N(0, Q_c) = \text{process noise} \quad (4-51)$$

$$f_m = C_{e(1 \times n)} x_e + v \quad v = \text{measurement noise}$$

### 4.5.1 State Estimation

The measurements are affected by noise, in order to obtain the best results, we have to minimize the residuals between the measurement and the prediction.

The residual is defined as

$$\varepsilon_f = f_m - C_e \hat{x}_e \quad (4-52)$$

According to [GAUSS 2004], the most fitting value for  $x_e$  is the vector  $\hat{x}_e$  that minimizes the sum of squares of the measurement residuals, so by performing z tests, we can define the following objective function like the sum of the residuals square.

$$J = \varepsilon_{f1}^2 + \varepsilon_{f2}^2 + \dots + \varepsilon_{fz}^2 = \underline{\varepsilon}_{fz} \cdot \underline{\varepsilon}_{fz}^T \quad (4-53)$$

In order to find the minimum of the objective function, let's put the derivative equal to 0

$$\frac{\partial J}{\partial \hat{x}_e} = 0 \quad (4-54)$$

From which the best state estimate is equal to

$$\hat{x}_e = (C_e C_e^T)^{-1} C_e^T f_m \quad (4-55)$$

Where:

$$(C_e C_e^T)^{-1} = C^\dagger = \text{pseudoinverse matrix}$$

The pseudoinverse matrix exist only if

- $z \geq n$  , the number of measures must be greater or equal to the number of states variables
- $C_e$  must to be full rank

Being the  $C_e$  matrix  $z \times n$  dimension, for each new estimation, it increases its size, so compute the state estimates at every new measurement it becomes computationally onerous.

To solve this problem the expanded state vector can be estimated through the expanded disturbance Kalman filter of SIFS



## 5 Expanded disturbance Kalman filter (EKF)

The cutting forces measure is performed by the most accurate transducer for this goal; the dynamometer.

However, as we explained in the introduction chapter the dynamometers are restricted to the laboratory use rather than to practical applications because of the limited size, mounting constraints and the high costs, etc.

In order to overcome some of the mentioned problems, in this thesis, an observer of cutting forces has been developed. The observer was designed and tested on a machine centre.

The observer is based on Kalman filtering model built on using the machine tool dynamic identifies by means of an experimental modal analysis.

The observer was also tested during milling tests and relies on a piezoelectric sensors that can be easily integrated, in a commercial electro spindle, thus assuring an easy industrial diffusion.

### 5.1 Continuous Expanded disturbance Kalman filter Design

To overcome the computational problem linked to the state estimation, the Expanded disturbance Kalman filter for the SIFS is used.

In particular we can write the dynamic model of the system in a recursive form using the Kalman gain.

$$\dot{\hat{x}}_e = A_e \hat{x}_e + k(f_m - \hat{f}_m) = A_e \hat{x}_e + k(f_m - C_e \hat{x}_e) = (A_e - kC_e) \hat{x}_e + kf_m \quad (5-1)$$

Where:

$k = \text{continuous Kalman filter gain}$  which is assumed to be constant

$(f_m - C_e \hat{x}_e) = \text{correction term}$

[PARK ET AL. 2004] applied the continuous Kalman filter for all three directions on the force signal measured of the spindle integrated force sensors.

Graphically

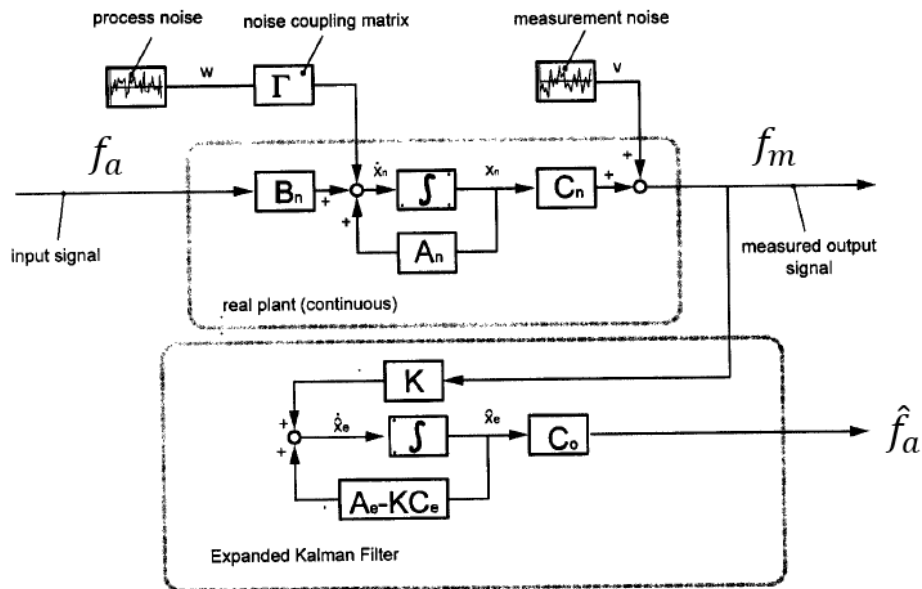


Figure 16 - Continuous Expanded disturbance Kalman filter

How to compute  $\hat{f}_a$ ?

$$\hat{x}_e = (A_e - kC_e)\hat{x}_e + kf_m \quad (5-2)$$

In Laplace domain

$$[sI - (A_e - kC_e)]\hat{x}_e = kf_m \quad (5-3)$$

Where:

$I = Identity\ matrix$

Knowing that

$$\hat{x}_e = \frac{\hat{f}_a}{C_o} \quad (5-4)$$

The input force is then (ALTINTAS 2000 pag.100)

$$\hat{f}_a = \frac{C_o adj[sI - (A_e - kC_e)]}{det[sI - (A_e - kC_e)]} \cdot k \cdot f_m \quad (5-5)$$

## 5.2 Extended state space model discretization

In this thesis, the actual force applied at the tool tip were compute by the discrete time domain recursive filter, see [WESTERMEIER 2010] and [DUNWOODY 2010].

Suppose the plant to be controlled is described by

$$\dot{x}_e(t) = A_e x_e(t) + \Gamma w(t) \quad w \sim N(0, Q_c) = \text{process noise} \quad (5-6)$$

With measurements

$$f_m = C_e x_e + v \quad v = \text{measurement noise} \quad (5-7)$$

In order to control the plant using state feedback, we would first need to estimate its state  $x(t)$ .

We can apply the discrete Kalman filter to the continuous plant by first discretizing it.

To do this, we begin with the solution to Equation (5-6)

$$x_e(t) = e^{A_e(t-t_0)} x_e(t_0) + \int_{t_0}^t e^{A_e(t-\tau)} \Gamma w(\tau) d\tau \quad (5-8)$$

Choosing  $t_0 = kT$  like a generic initial state and  $t = kT + T$  the next sampling state

$$x_e(kT + T) = e^{A_e(T)} x_e(kT) + \int_{kT}^{kT+T} e^{A_e(kT+T-\tau)} \Gamma w(\tau) d\tau \quad (5-9)$$

The second term is a smoothed (i.e., low-pass filtered) version of the continuous white process noise  $w(t)$  weighted by the state transition matrix and the noise input matrix  $\Gamma$ .

It is not difficult to show that this term describes a discrete white noise sequence.

Hence, define

$$w_k = \left[ \int_{kT}^{kT+T} e^{A_e(kT+T-\tau)} \Gamma w(\tau) d\tau \right] \quad w_k \sim N(0, \mathbf{Q}) \quad (5-10)$$

Defining

$$\begin{aligned} x_e(kT) &= x_k \quad \wedge \quad x_e(kT + T) = x_{k+1} \\ F_k &= e^{A_e(T)} \end{aligned} \quad (5-11)$$

From equation (5-9) we get

$$x_{k+1} = F_k + w_k \quad (5-12)$$

Discretizing the measurement equation is easy since it has no dynamics.

$$H_k = C_e \quad (5-13)$$

For more information see [Lewis, Xie et al 2007].

Finally, the discretized dynamic system results to be

$$\begin{aligned} x_{k+1} &= F_k x_k + w_k & w_k &\sim N(0, Q) \\ f_{m,k} &= H_k x_k + v_k \end{aligned} \quad (5-14)$$

The discretization is a trade-off between the accuracy of the obtained discrete time model and its numerical stability.

The shorter the sampling time the closer is the discrete time model to the continuous time model, but the smaller is its numerical stability.

Thus, the numerical properties of the discrete time model has to be investigated.

An analysis of the observability and the condition numbers of  $F_k$  for different sampling times lead to an optimal sampling time of  $1 \cdot 10^{-4} s$  for this application

Besides the numerical properties of the derived discrete time system, this sampling time also provides satisfying approximations of the continuous time system. This is proven in following figure, where the transfer behavior of a continuous time and a discrete time model are compared

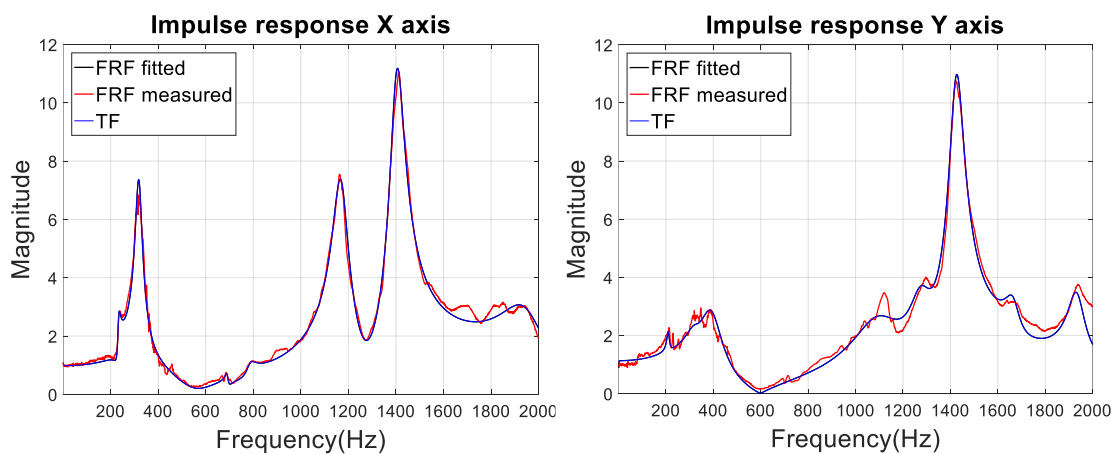


Figure 17 - Comparison between TF, measured and fitted FRF in X and Y direction

If the expected value  $\hat{x}$  after  $k - 1$  measurements is known and there is a new measurement  $f_{mk}$ , the expanded state vector can be estimated through the expanded discrete state space model that can be represented in the following form

$$\begin{aligned} x_k &= F_{k-1}x_{k-1} + w_{k-1} && \text{System dynamic model} && (5-15) \\ f_{m,k} &= H_k x_k + v_k && \text{Measurement model} \end{aligned}$$

Remembering that for a continuous system, the matrix  $A$  relates the state between the first derivative of the state and the state itself. For a discrete system,  $F$  relates the states between the previous time step  $k - 1$  and the current time step  $k$ .

Both  $F$  and  $H$  are assumed to be constant over time as the regarded system is a LTI system. The variables  $w_k$  and  $v_k$  represent the process and measurement noise, which both are assumed to be white Gaussian distribution with the known covariance matrix  $\mathbf{Q}$  and  $\mathbf{R}$ .

Since the Kalman filter demands the measurement noise to be a white noise with Gaussian distribution, is important to verify this condition to obtain correct results during the forces experimental compensation [THOMAS 2015].

In this context, a Gaussian distribution means the probability density function has the shape of a Gaussian curvature.

The equivalent mathematical description can be written as follows

$$p(x) = \frac{1}{\sigma\sqrt{2\pi}} e^{\left(\frac{-1}{2\sigma^2}(x-\bar{x})^2\right)} \quad (5-16)$$

Changes of the mean value  $\bar{x}$  would shift the curve to the left or right.

An increased or decreased variance  $\sigma$  would lead to either a spread or squeeze of the curve.

For more details about the Noisy Dynamic Model see (GREAWL & ANDREWS 2008) [PARK 2006, CHAPTER 2].

The kurtosis value of a Gaussian distribution is three [DECARLO 1997]

$$k = \frac{E(x - \bar{x})^4}{\sigma^4} \quad (5-17)$$

It is further assumed that  $w_k$  and  $v_k$  are uncorrelated and constant over every time step.

$$E[w_k w_j^T] = \text{measurement noise covariance matrix} = \begin{cases} \mathbf{Q}, & k = j \\ 0, & \text{otherwise} \end{cases}$$

$$E[v_k v_j^T] = \text{system noise covariance matrix} = \begin{cases} \mathbf{R}, & k = j \\ 0, & \text{otherwise} \end{cases}$$

$$E[v_k w_j^T] = 0 \quad \text{for all } k, j$$

CONTINUOUS FORM	DISCRETE FORM
<p>System dynamic model</p> $\dot{x}_e = A_e x_e + \Gamma w \quad \rightarrow$ <p>Measurement model</p> $f_m = C_e x_e + v \quad \rightarrow$	$x_k = F_{k-1} x_{k-1} + w_{k-1}$ $f_{m,k} = H_k x_k + v_k$
<p><math>k = \text{number of state variables}</math>  <math>z = \text{number of proofs}</math></p>	<p><math>k = \text{measurement numbers}</math>  <math>n = \text{number of state variables}</math></p>

Table 4 - Continuous form vs Discrete form

### 5.3 Recursive Least Square Estimator (RLSE)

The Kalman filter estimates the status of the process at a certain moment and obtains feedback in the form of noisy measurements.

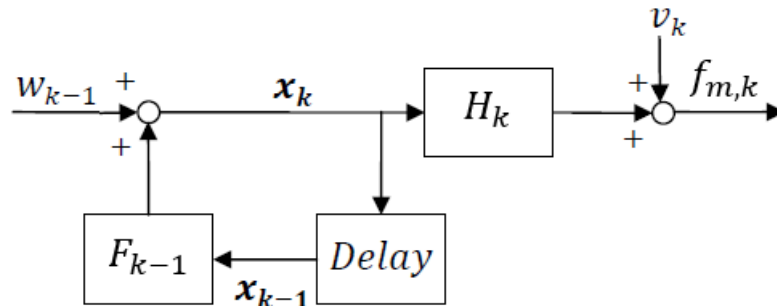


Figure 18 - Discrete System

As we have already seen for the continuous form to update the measurements avoiding computational problems is necessary to use the recursive least square estimator (RLSE).

$$\hat{x}_k = \hat{x}_{k-1} + k_k(f_{m,k} - H_k \hat{x}_{k-1}) \quad (5-18)$$

$$f_{m,k} = H_k x_k + v_k$$

The RLSE builds the basis for the derivation of an optimal state estimator like the discrete Kalman filter.

### 5.3.1 Time Update equation

The Kalman filter operates by propagating the mean and covariance of the state through time.

*How does the mean of the state  $\bar{x}_k$  change with time?*

The expected value  $\hat{x}_k$  is defined as its average value over a large number of experiments, so we can write

$$\bar{x}_k = E(x_k) = \hat{x}_k = F_{k-1}\hat{x}_{k-1} \quad (5-19)$$

*How does the covariance of  $x_k$  change with time?*

Per definition of covariance matrix

$$P_k = E [(x_k - \hat{x}_k) \cdot (x_k - \hat{x}_k)^T] \quad (5-20)$$

Knowing that  $x_k$  value is equal to

$$x_k = F_{k-1}x_{k-1} + w_{k-1} \quad (5-21)$$

Substituting (5-19) and (5-21) in (5-20) we get

$$(x_k - \hat{x}_k) \cdot (x_k - \hat{x}_k)^T = F_{k-1}(x_{k-1} - \hat{x}_{k-1})(x_{k-1} - \hat{x}_{k-1})^T F_{k-1}^T + \quad (5-22)$$

$$w_{k-1}w_{k-1}^T + F_{k-1}(x_{k-1} - \hat{x}_{k-1})w_{k-1}^T + w_{k-1}(x_{k-1} - \hat{x}_{k-1})^T F_{k-1}^T$$

Remembering that

- $w_k$  and  $v_k$  are uncorrelated and constant over every time the last two terms are equal to 0.
- $P_{k-1} = (x_{k-1} - \hat{x}_{k-1})(x_{k-1} - \hat{x}_{k-1})^T$
- $Q_{k-1} = w_{k-1}w_{k-1}^T$

Finally, we get

$$P_k = F_{k-1}P_{k-1}F_{k-1}^T + Q_{k-1} \quad (5-23)$$

This is called a discrete time Lyapunov equation, and it is fundamental in the derivation of the Kalman filter.

### 5.3.2 Optimal Gain

To optimize the Kalman gain, create a new objective function like the sum of the mean value of the square residuals calculated in  $k$  proofs between the  $i^{th}$  state variable and its estimation for each  $n^{th}$  variables

$$J_k = E[(x_1 - \hat{x}_1)^2] + \dots E[(x_i - \hat{x}_i)^2] + \dots + E[(x_n - \hat{x}_n)^2] \quad (5-24)$$

$n = \text{number of state variables}$

$k = \text{number of measurements}$

The mean is done to delete the noise component.

The objective function can be rewrite as

$$J_k = E(\varepsilon_{x1,k}^2 + \varepsilon_{x2,k}^2 + \dots + \varepsilon_{xn,k}^2) = E(\varepsilon_{x,k} \cdot \varepsilon_{x,k}^T) \quad (5-25)$$

Remembering that per definition of covariance matrix

$$P_k = E[(x_k - \hat{x}_k) \cdot (x_k - \hat{x}_k)^T] = E(\varepsilon_{x,k} \cdot \varepsilon_{x,k}^T) = TrP_k \quad (5-26)$$

Where trace stands for residues, i. e. the covariance matrix indicates the correlation between state residues.

Finally, we get

$$J_k = TrP_k \quad (5-27)$$

Before to compute the optimal gain matrix  $K_k$  let us think about the RLSE mean error estimation. The mean error estimation can be computed as

$$E(\varepsilon_{x,k}) = E(x_k - \hat{x}_k) = E[x_k - \hat{x}_{k-1} - k_k(f_{m,k} - H_k \hat{x}_{k-1})] \quad (5-28)$$

Substituting  $f_{mk}$  we get

$$E(\varepsilon_{x,k}) = E[x_k - \hat{x}_{k-1} - k_k(H_k x_k + v_k - H_k \hat{x}_{k-1})] \quad (5-29)$$

Collecting the error vector and knowing that  $\varepsilon_{xk,k-1} = x_k - \hat{x}_{k-1}$  we get

$$\begin{aligned} E(\varepsilon_{x,k}) &= E[\varepsilon_{xk,k-1} - k_k H_k (x_k - \hat{x}_{k-1}) - k_k v_k] \\ &= (I - k_k H_k) E(\varepsilon_{xk,k-1}) - k_k E(v_k) \end{aligned} \quad (5-30)$$

Substituting in (5-26)

$$\begin{aligned} P_k &= E(\varepsilon_{x,k} \cdot \varepsilon_{x,k}^T) = \{[(I - k_k H_k) E(\varepsilon_{xk,k-1}) - k_k E(v_k)] \cdot [\dots]^T\} \\ &= (I - k_k H_k) E(\varepsilon_{xk,k-1} \cdot \varepsilon_{xk,k-1}^T) (I - k_k H_k)^T \\ &\quad - k_k E(v_k \varepsilon_{xk,k-1}^T) (I - k_k H_k)^T \\ &\quad - (I - k_k H_k) E(v_k^T \varepsilon_{xk,k-1}) k_k^T + k_k E(v_k v_k^T) k_k^T \end{aligned} \quad (5-31)$$

Now note that the estimation error at time  $(k - 1)$  is independent of the measurement noise at time  $k$ , therefore

$$(v_k^T \varepsilon_{xk,k-1}) = E(v_k \varepsilon_{xk,k-1}^T) = 0 \quad (5-32)$$

And knowing that

$$P_{k-1} = E(\varepsilon_{xk,k-1} \cdot \varepsilon_{xk,k-1}^T) \quad (5-33)$$

$$R_k = E(v_k v_k^T)$$

We get the expanded formula for a posteriori error covariance

$$P_k = (I - k_k H_k) P_{k-1} (I - k_k H_k)^T + k_k R_k k_k^T \quad (5-34)$$

This is consistent with intuition in the sense that as the measurement noise ( $R_k$ ) increases the uncertainty in our estimate ( $P_k$ ) also increases.

Note that ( $P_k$ ) should be define positive and symmetric since it is a covariance matrix, and the form of Equation (5-34) guarantees that ( $P_k$ ) will be define positive, if ( $P_{k-1}$ ) and ( $R_k$ ) are define positive and symmetric.

Returning to the objective of this paragraph, namely the calculation of optimal Kalman's gain, we find the value of  $K_k$  that minimizes the cost function  $J_k$

Remembering that  $\frac{\partial \text{Tr}[ABA^T]}{\partial A} = 2AB$  if B is symmetric [See SIMON 2006 Pag 15]

In our case the (5-34) becomes

$$\frac{\partial J_k}{\partial k} = \frac{\partial [P_k]}{\partial k} = 2(I - k_k H_k) P_{k-1} (-H^T) + 2K_k R_k \quad (5-35)$$

To find the value of the gain that minimizes the cost function, we set the above

derivative equal to zero and then solve for  $k_k$  as follows:

$$\frac{\partial J_k}{\partial k} = 0 = 2(I - k_k H_k) P_{k-1} (-H^T) + 2K_k R_k \quad (5-36)$$

$$k_k = P_{k-1} H^T (H_k P_{k-1} H_k^T + R_k)^{-1} \quad (5-37)$$

For a more intuitive comprehension of the Kalman gain formula, it need to premultiply the right side by  $P_k P_k^{-1}$ , which is equal to the identity matrix

$$k_k = P_k P_k^{-1} P_{k-1} H^T (H_k P_{k-1} H_k^T + R_k)^{-1} \quad (5-38)$$

If we substitute in (5-34) equation, the equation (5-38) and expand terms, after some mathematical steps [See SIMON 2006 Pag 87] we obtain

$$P_k^{-1} = P_{k-1}^{-1} H_k^T R_k^{-1} H_k \quad (5-39)$$

So, continuing with the demonstration we get

$$\begin{aligned} k_k &= P_k (P_{k-1}^{-1} H_k^T R_k^{-1} H_k) P_{k-1} H^T (H_k P_{k-1} H_k^T + R_k)^{-1} \quad (5-40) \\ &= P_k (H_k^T + H_k^T R_k^{-1} H_k P_{k-1} H_k^T) (H_k P_{k-1} H_k^T + R_k)^{-1} \end{aligned}$$

Now we bring  $H_k^T$  out to the left side of the parentheses and premultiply the first parentheses expression by  $R_k^{-1}$ , and multiply on the inside of the parenthesis by  $R_k$

$$k_k = P_k H_k^T R_k^{-1} (R_k + H_k P_{k-1} H_k^T) (H_k P_{k-1} H_k^T + R_k)^{-1} \quad (5-41)$$

$$k_k = P_k H_k^T R_k^{-1} \quad (5-42)$$

To provide an intuitive interpretation, consider  $H_k = I$ , i. e. all states are measurable. In this case,  $P_k$  and  $R_k$  are matrixes of the same size. Assuming moreover that  $R$  is diagonal (there is no correlation between the different measurement noises) it is observed how the gain  $k_k$  is diagonal and represents the ratio between two statistical quantities, the uncertainty on the estimation of the process ( $\mathbf{Q}$ ) and the uncertainty on the measurement ( $\mathbf{R}$ ).

Precisely, the gain is proportional to the uncertainty on the estimation of the process and inversely proportional to the uncertainty on the measurement.

A small uncertainty in the estimation of the process and a great uncertainty on the measurements suggest to the gain not to update much the current estimation, on the contrary, a great uncertainty on the estimation of the process and a small uncertainty on the measurements suggest that the current data contain a great amount of information to be used for updating the estimation.

### 5.3.3 Measurement update equation

To calculate the covariance matrix during the measurement update phase, it is necessary to replace the optimum gain value in a *posteriori error covariance* extended formula.

This step is necessary to relate the covariance matrix at  $k$  step and the covariance matrix at step  $k - 1$  in this way

$$P_k = [I - k_k H_k] P_{k-1} \quad (5-43)$$

Where:

$$k_k = P_{k-1} H^T (H_k P_{k-1} H_k^T + R_k)^{-1}$$

So

$$P_k = P_{k-1} - P_{k-1} H^T (H_k P_{k-1} H_k^T + R_k)^{-1} H_k P_{k-1} \quad (5-44)$$

Secondly to obtain a new measurement as we have already seen for the continuous form exist a similar linear recursive form as follow

$$\hat{x}_k = \hat{x}_{k-1} + k_k (f_{m,k} - H_k \hat{x}_{k-1}) \quad (5-45)$$

$$f_{m,k} = H_k x_k + v_k$$

## 5.4 Discrete Kalman Filter Algorithm (DKF)

The notation of the recursive least squares method (RLS) and the discrete Kalman filter (DKF) differ.

The DKF distinguishes between a *posteriori estimate*  $\hat{x}_k^+$  and a *priori estimate*  $\hat{x}_k^-$  of  $x_k$ .

A posteriori case is displayed by the superscript " + " and utilizes all measurements, up to and including time  $t_k$ :

$$\hat{x}_k^+ = E[x_k | f_{m,1}, f_{m,2} \dots f_{m,k}] = \text{a posteriori estimate}$$

On the other hand, a priori case is displayed by the superscript " - ". It denotes that only measurements before the time step  $t_k$  are considered:

$$\hat{x}_k^- = E[x_k | f_{m,1}, f_{m,2} \dots f_{m,k-1}] = \text{a priori estimate}$$

It is important to note that  $\hat{x}_k^-$  and  $\hat{x}_k^+$  are both estimates of the same quantity; they are both estimates of  $x_k$ .

The difference is the instant of time when the estimation takes place;  $\hat{x}_k^-$  is calculated before the current measurement  $f_{m,k}$  so is less accurate than  $\hat{x}_k^+$  which instead takes the measurement into account.

The equations for the discrete Kalman filter fall into two main groups already described in the previous chapter,

- The *time update equations* are responsible for projecting forward (in time) the current state and error covariance estimates to obtain the a priori estimates for the next time step.
- The *measurement update equations* are responsible for the feedback i.e. for incorporating a new measurement into the a priori estimate to obtain an improved a posteriori estimate.

After each time step and measurement update pair, the process is repeated with the previous a posteriori estimates used to project or predict the new a priori estimates.

The formulas found in the previous chapter are presented in the table below.

The left column represents the notation of the recursive least squares method, whereas the right column shows the notation used for the Kalman filter

### *Dynamic System*

$$x_k = F_{k-1}x_{k-1} + w_{k-1}$$

$$f_{m,k} = H_k x_k + v_k$$

$$E [w_k w_j^T] = \begin{cases} Q_k, & k = j \\ 0, & \text{otherwise} \end{cases}$$

$$E [v_k v_j^T] = \begin{cases} R_k, & k = j \\ 0, & \text{otherwise} \end{cases}$$

$$E [v_k w_j^T] = 0 \quad \text{for all } k, j$$

LEAST SQUARE ESTIMATION	DISCRETE KALMAN FILTER
<p><b>INITIALIZATION</b></p> <p><b>Initial State</b></p> $\hat{x}_0 = E(x_0) \quad \rightarrow$ <p><b>Initial Covariance</b></p> $P_0 = E [(x_0 - \hat{x}_0) \cdot (x_0 - \hat{x}_0)^T] \quad \rightarrow$ <p>The initial value for the covariance matrix <math>P_0</math> and state vector <math>x_0</math> is chosen to be the zero.</p>	$\hat{x}_0^+ = E(x_0)$ $P_0^+ = E [(x_0 - \hat{x}_0^+) \cdot (x_0 - \hat{x}_0^+)^T]$

<p><b>TIME UPDATE</b></p> <p>Estimate state vector</p> $E(x_k) = \hat{x}_k = F_{k-1}\hat{x}_{k-1} \quad \rightarrow$ <p>Error Covariance P</p> $P_k = F_{k-1}P_{k-1}F_{k-1}^T + Q_{k-1} \quad \rightarrow$	$\hat{x}_k^- = F_{k-1}x_{k-1}^+$ $P_k^- = F_{k-1}P_{k-1}^+F_{k-1}^T + Q_{k-1}$
<p><b>KALMAN GAIN</b></p> $k_k = P_{k-1}H^T(H_kP_{k-1}H_k^T + R_k)^{-1} \quad \rightarrow$	$k_k = P_k^-H^T(H_kP_k^-H_k^T + R_k)^{-1}$
<p><b>MEASUREMENT UPDATE</b></p> <p>Estimate state vector</p> $\hat{x}_k = \hat{x}_{k-1} + k_k(f_{m,k} - H_k\hat{x}_{k-1}) \quad \rightarrow$ <p>Error Covariance P</p> $P_k = [I - k_kH_k]P_{k-1} \quad \rightarrow$	$\hat{x}_k^+ = \hat{x}_k^- + k_k(f_{m,k} - H_k\hat{x}_k^-)$ $P_k^+ = [I - k_kH_k]P_k^-$

Table 5 - Least Square Method vs Discrete Kalman Filter

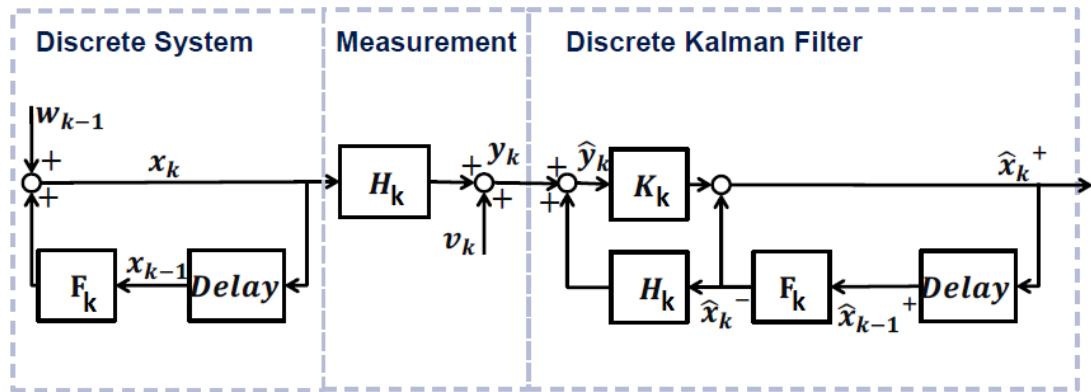


Figure 19 - Block diagram of a discrete time Kalman filter applied on a discrete system according to Greval & Andrew 2008 (pag.138)

First of all, the Kalman filter is characterized by a variable gain over time  $K$  so it is interesting to study its characteristics.

A closer look at the Kalman gain equation shows that this step is not affected by the measurement  $f_{m,k}$  but only by the system parameters  $F_k$ ,  $H_k$ ,  $Q_k$  and  $R_k$ .

This means that if the system is time-invariant and the process and measurement noise covariances ( $Q$ ,  $R$ ) are time-invariant, under the hypothesis of linearity, stationariness, observability and controllability of the system, the gain tends to a constant value due to the achievement of the  $P$  matrix regime to a finite value.

$$\lim_{k \rightarrow \infty} k_k = k_{\infty} \quad (5-46)$$

In this case we can talk of steadystate Kalman filter.

Using a steadystate filter has the advantage that we do not have to compute the estimation-error covariance or Kalman gain in real time.

Note that a steady-state Kalman filter is still a dynamic system.

The term “steady-state” Kalman filtering means that the Kalman filter is time-invariant;

and the Kalman's gain can be calculated and saved before the algorithm computation therefore, the filter performance can be analyzed without an actual experimental measurement.

This saves calculation time, because only the measurement update phase has to be calculate

$$\hat{x}_k = \hat{x}_{k-1} + k_k(f_{m,k} - H_k \hat{x}_{k-1}) \quad (5-47)$$

Once the filter has been initialized, the three main formulas of the recursive algorithm involved in the gain computation are

$$P_k^- = F_{k-1} P_{k-1}^+ F_{k-1}^T + Q_{k-1} \quad \textit{Time update} \quad (5-48)$$

$$k_k = P_k^- H_k^T (H_k P_k^- H_k^T + R_k)^{-1} \quad \textit{Optimal gain} \quad (5-49)$$

$$P_k^+ = [I - k_k H_k] P_k^- \quad \textit{Measurement update} \quad (5-50)$$

Now we will see how a priori and a posteriori Kalman filter equations can be combined into a single equation to provide an intuitive explanation about the Q and

R matrix role in the Kalman gain computation.

At a step “k+1” from eq. (5-48) we obtain

$$P_{k+1}^- = F_k P_k^+ F_k^T + Q_k \quad (5-51)$$

Replacing the eq. (5-50) in the previous formula we get

$$\begin{aligned} P_{k+1}^- &= F_k (P_k^- - k_k H_k P_k^-) F_k^T + Q_k \\ &= F_k P_k^- F_k^T - F_k k_k H_k P_k^- F_k^T + Q_k \end{aligned} \quad (5-52)$$

Substituting the Optimal gain in the previous formula we get

$$P_{k+1}^- = F_k P_k^- F_k^T - F_k P_k^- H_k^T (H_k P_k^- H_k^T + R_k)^{-1} H_k P_k^- F_k^T + Q_k \quad (5-53)$$

This equation, called a discrete Riccati equation, shows how  $P_{k+1}^-$  can be computed on the basis of  $P_k^-$ ; without an intermediate calculation of  $P_k^+$ .

In the hypothesis of a steadystate kalman filter

$$P_k^- = P_{k+1}^- = P_\infty \quad (5-54)$$

So, it is possible to write

$$k_{\infty} = P_{\infty}^{-1} H_k^T (H_k P_{\infty}^{-1} H_k^T + R)^{-1} = P_{\infty}^{-1} H_k^T R^{-1} \quad (5-55)$$

In particular we can observe like a decrement of the R matrix responsible for defining the uncertainty on the measurement leads two different effects

Primary effect: In eq. (5-55) a  $R_k$  decrement leads to an increment of the Kalman filter gain

Secondary effect: In eq. (5-53) a  $R_k$  decrement leads to a  $P_{k+1}^{-1}$  decrement so consequently to a decrement of the Kalman filter gain

The Primary effect is predominant respect of the secondary effect so in general an increment on the measurement uncertainty R leads to decrement of the gain.

On the other hand, an increase of the Q matrix responsible for defining process uncertainty leads to an increase of the P matrix and consequently of the gain k.

Remembering that a small uncertainty in the estimation of the process and a great uncertainty about the measurements suggest that the gain does not update much of the current estimation; on the contrary, a great uncertainty about the estimation of the process and a small uncertainty about the measurements suggest that the current data contain a large amount of information to be used to update the estimation.

## 6 Guidelines definition for cutting process oriented Kalman tuning

In this chapter we will demonstrate the close connection between static (natural response of the system) and dynamic (Cutting test system response), thanks to which we are able to understand the real functioning of the filter during cutting tests already in the dynamic identification phase of the model.

The goal of this Section is to demonstrate how a simple TapTest can be used to set correctly the Q and R parameters.

From a practical point of view this means that the filter can be calibrated very easily without to carry out additional cutting tests, thus obtaining a considerable saving in terms not only of cost but also of time.

### 6.1 Innovative procedure for finding

In order to quantify the difference between two signals, the RMSE is a common measure error.

The squaring of the error results in emphasizing large deviations of the signals, more than small ones.

This index will be calculated respectively between the spectra of two signals in the frequency domain to not consider the phase delay component in time domain that would lead to an incorrect use of this index.

$$RMSE = \sqrt{\frac{1}{N_{samples}} \cdot \sum_{k=1}^{N_{samples}} (signal\ spectrum_1 - signal\ spectrum_2)} \quad (6-1)$$

In our specific case *signal spectrum 1* is the one computed on the Kalman filter output, while *signal spectrum 2* is the one calculated on the reference force.

The algorithm is divided into two parts:

- **Cutting Tests**

The portions of the acquired signal, relative to the input and output phase of the tool from the workpiece, are not considered in the analysis.

For each cutting test the algorithm identifies all the maximums relative of the spectrum, i. e. the Spindle Frequency (SF) and all the fundamental multiple frequencies within the selected bandwidth.

The values related to the fundamental multiple frequencies are not punctual values, so the algorithm only considers those samples that fall within a

frequency range calculated considering a variation of  $\pm 1$  on the maximum magnitude value of each fundamental multiple frequency in the cutting test. Secondly, the algorithm calculates the RMSE between Kalman's filter prediction and dynamometric measurement, varying the value of parameter  $q$  according with the following formula

$$q_n = 2^n \quad n = 1, \dots, 30 \quad (6-2)$$

In this way we are able to build the dynamic curves that show the RMSE index variation in function of  $Q$  parameter during the Cutting Test.

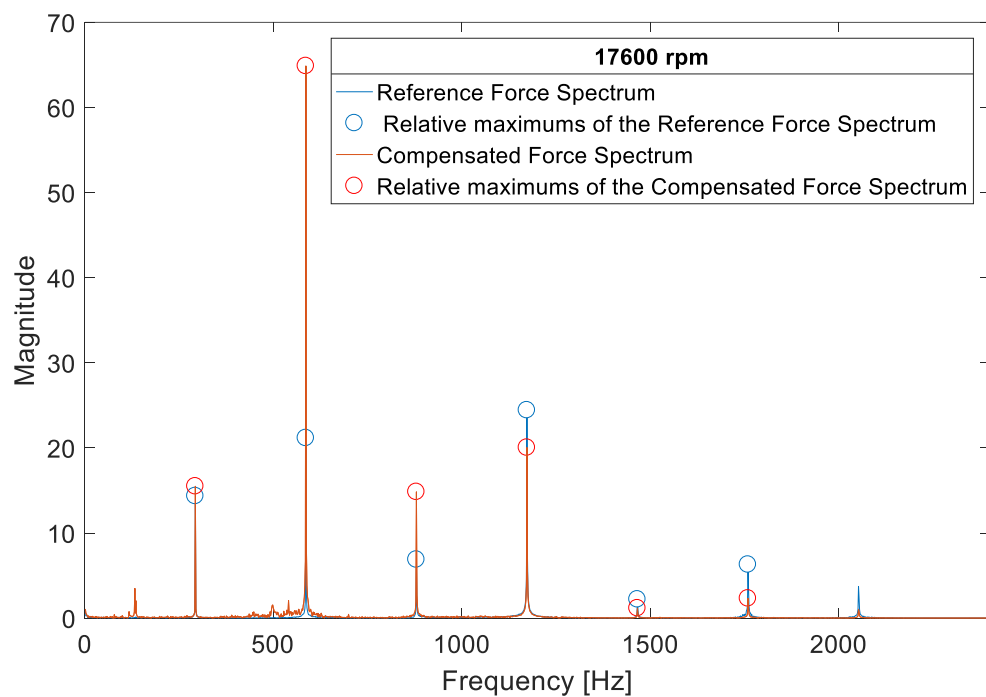


Figure 20 - Comparison between reference force and compensated force spectrums in cutting test

- Tap Test

Following the same logic, so using the same samples of the Cutting Tests but simulating a higher number of Spindle speeds, the algorithm generates a surface that extends over all frequencies and highlights the minimum zones.

The last step consists into place the minimum points resulting from the Cutting tests on the coloured map and see if there is a correspondence between the results from the TapTest and the dynamic results.

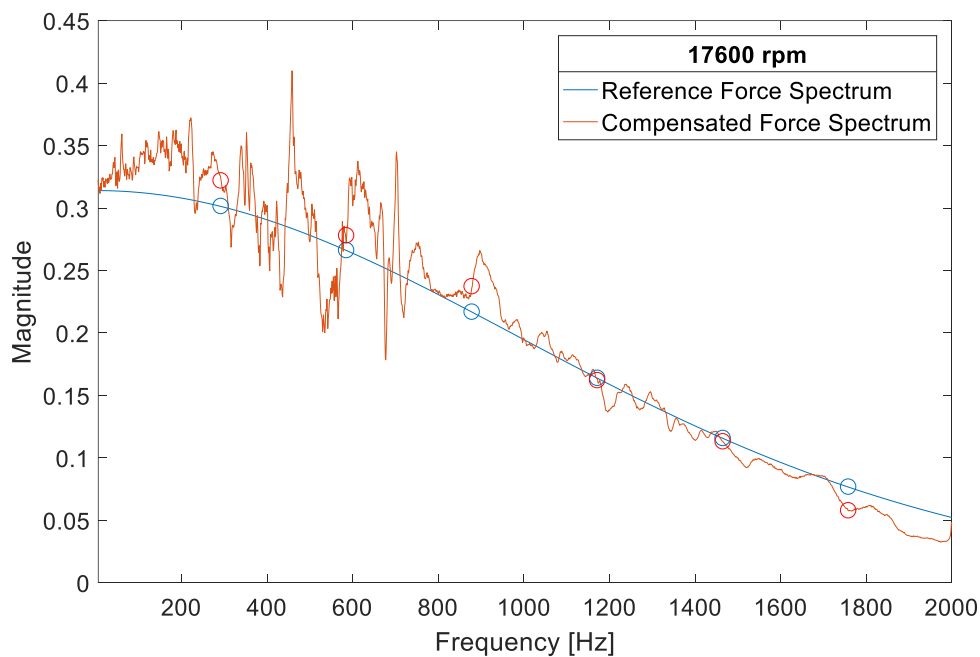


Figure 21 - Comparison between reference force and compensated force spectrums in Tap Test

$$RMSE = \sqrt{\frac{1}{N_{\text{Samples}}} \sum_{k=1}^{N_{\text{Samples}}} (\text{signal spectrum}_1 - \text{signal spectrum}_2)^2}$$

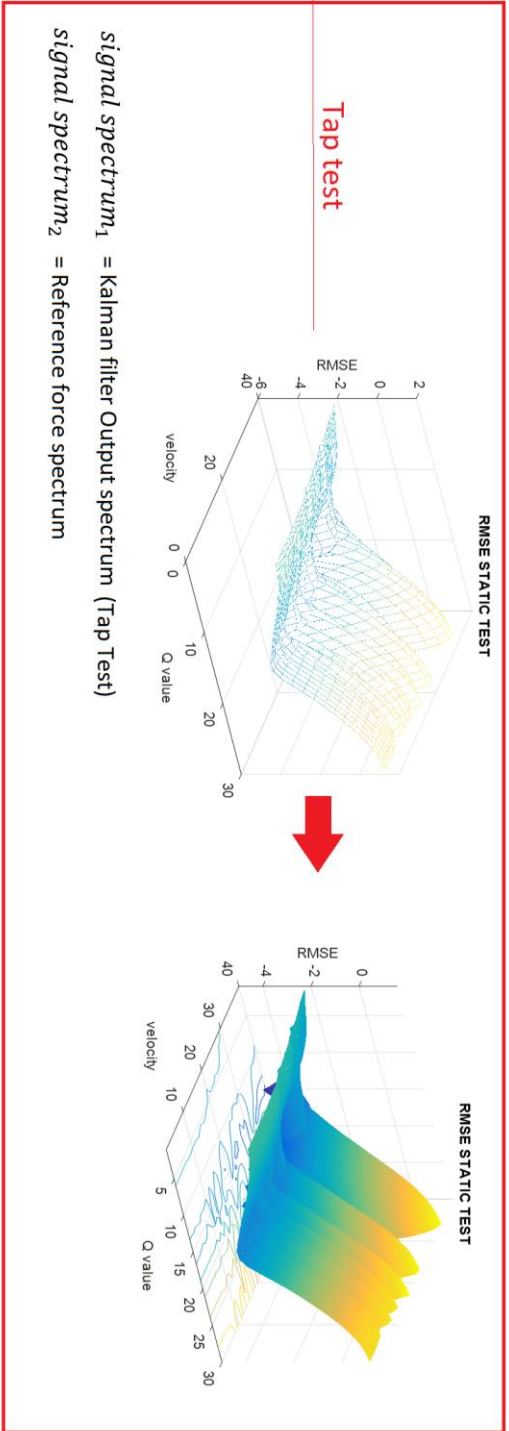
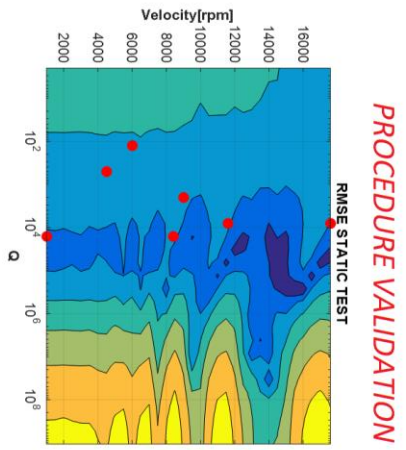
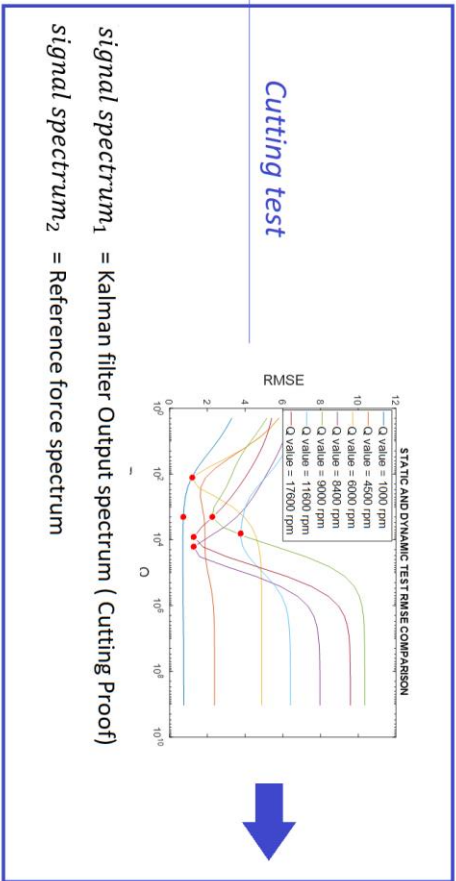


Figure 22 - Flow chart algorithm

## 6.2 Spindle speed oriented observer tuning

Once the analytical model of the system and the  $F$  and  $H$  matrices have been built through the Tap Test, the Kalman's gain evaluation depends only on the  $R$  and  $Q$  matrices choice.

The uncertainty sources of the measure that lead to  $R$  matrix definition are:

- Sensor uncertainty
- Uncertainty due to random and systematic errors in the milling process

The uncertainty sources in the process estimation that lead to  $Q$  matrix definition are caused by a prediction model simplification, e.g:

- Mathematical model simplification (fitting problem)
- Incomplete knowledge of the dynamic system variables that influence the milling process.

If  $Q$  is too small, the filter will be too sure of its forecasting model so will not consider the real measure in any case.

The  $Q$  matrix can never be filled with zeros, because the filter will use the noise-free model to predict the status vector and ignore any measurement data, as the model is considered perfect.

If  $Q$  is too large, the noise could have a bad influence on the estimation leading to a sub-optimal prediction.

In practice, we spend a lot of time performing simulations and evaluating the collected data to select an appropriate  $Q$  value.

The matrices construction is one of the most difficult aspects of Kalman filter design. Firstly, the mathematics requires a good basis in signal theory, and then we are trying to model the noise on the basis of little information.

To create a right connection between static and dynamic proof and set correctly the  $Q$  parameter from the TapTest is necessary to understand how to define the measure uncertainty in static conditions.

Once defined the  $\mathbf{R}$  matrix, the second step is to find the optimal  $Q$  parameter value that permit to obtain the best force prediction as the speed varies.

In Dynamic the  $R$  parameter is computed as the RMS value of the piezoelectric sensor signal during the aircutting phase ( $R=10$ ) so, it depends on a series of random and systematic errors (e. g., spindle rotation noise) that do not occur during the TapTest.

The basic idea is that exist a strong link between these two parameters, so our analysis starts from the formulation of different hypotheses regarding the real value assumed by "R" and "Q parameters".

Each of these theories will be examined in detail and compared with the others to understand the best choice

A first hypothesis, e.g, could be to adopt in the Tap Test the same procedure used in the cutting tests, i. e. to calculate the RMS value of the piezoelectric sensor signal before hammering

In this case we found R value equal to 0.15.

A second idea could be to filter the cutting tests again using  $R = 0.15$ , so considering only the uncertainty of the sensor and ignoring all those random and systematic errors due to spindle rotation.

Below are reported two coloured maps for the main two directions (built using the algorithm developed in chapter (6.1) which summarize all possible combinations.

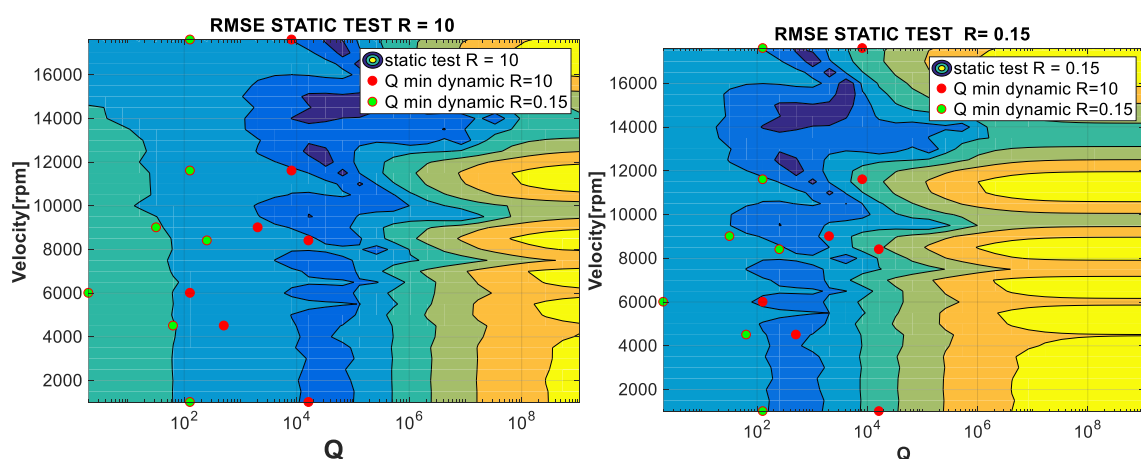


Figure 23 - Relation between Q and R parameters for X axis

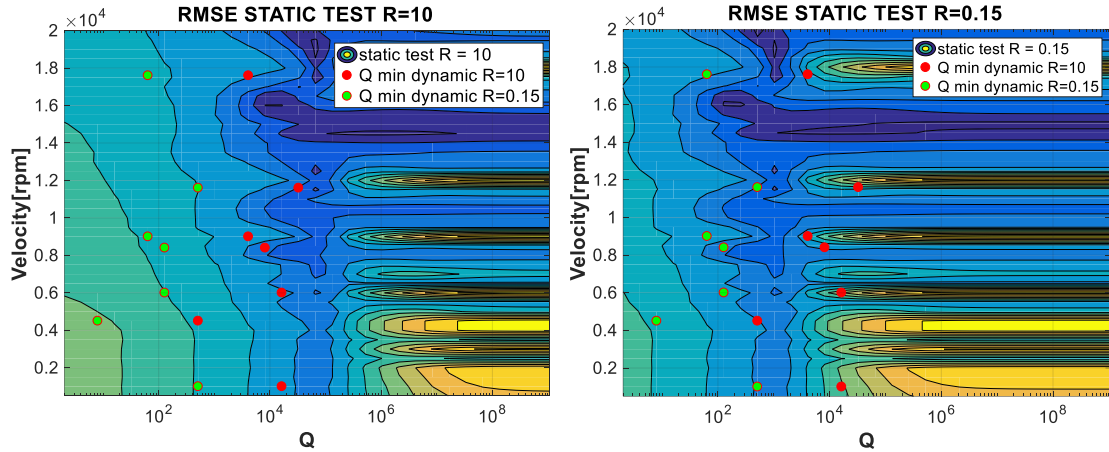


Figure 24 - Relation between Q and R parameters for Y axis

- 1) From the graphs it is possible to observe how the  $\mathbf{R}$  matrix decrement leads to a Q optimal value decrements and vice versa.
- 2) The colored map seems to suggest a Q parameter dependency by the spindle speed variation; although few cutting tests have been carried out, these dependency is still visible.

If we generate a surface starting from only the frequencies related to the cutting test, for sure we get a less precise coloured map, but in this way, we are able to show better the existence of a dependency between the Q parameter and the spindle speed variation. In addition, this dependency is always highlighted whenever any value of the R parameter is used in Tap Test.

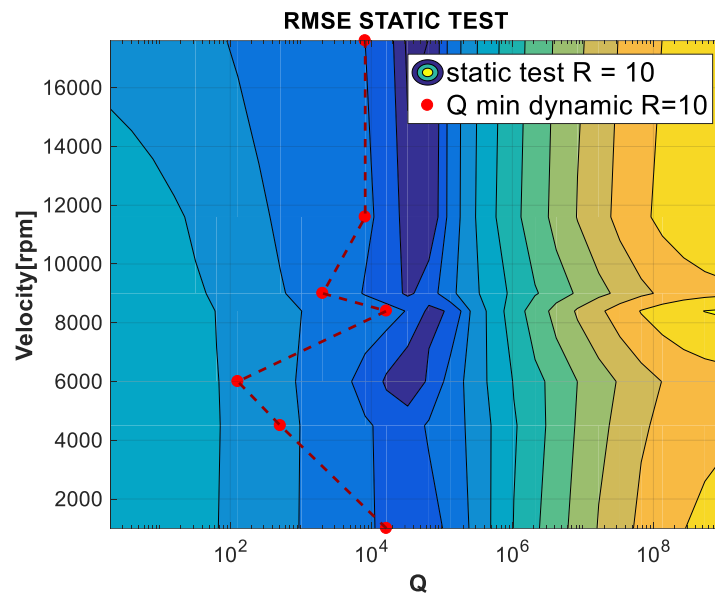


Figure 25 - Dependence of parameter Q on Spindle speed

From a theoretical point of view, assuming to know with extreme precision R matrix both in static and dynamic conditions, we would obtain a result similar to the which one obtained setting  $R = 10$  in the cutting test and  $R = 0.15$  in the Tap Test.

In this case is possible to observe a positioning of the Q optimum points derived from the cutting proofs in a range shifted slightly to the right compared to the optimal area shown by the TapTest.

This phenomenon is due to a process uncertainty increment during the Cutting Tests.

To demonstrate this phenomenon is essential to understand how the filter reacts to an increment of the process uncertainty Q.

Knowing that the mathematical model that generates the Kalman filter is a stochastic model, (i.e. it has been built on the basis an average FRF computed on k different Tap

Tests) we could simulate an imperfect correspondence between the plant and the Kalman filter dynamic model.

Knowing the filter behaviour in front of a slight plant variation (e. g. due to loosening of a screw or machine damage) could be extremely useful to have a greater sensitivity in Q parameter setting

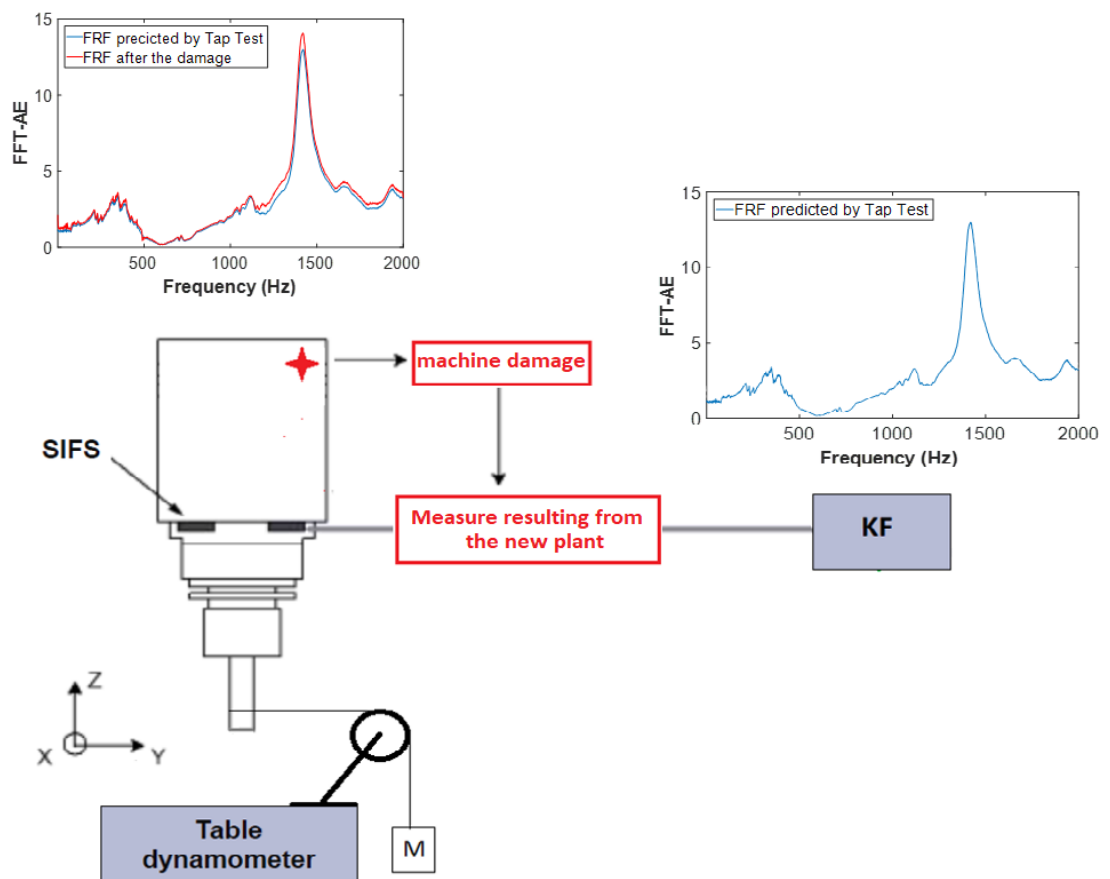


Figure 26 - Plant Variation Overview

## 6.2.1 Study of the effects of model uncertainties and on the tuning procedure

The confidence interval is defined by two confidence limits that indicate the boundaries within which my random variable (X) is distributed according to a probability density function (PDF) that in our case we assume to be Gaussian  $N(\mu, \sigma^2)$ .

In this case, the maximum value of this PDF coincides with the average FRF estimate, with which we have implemented the Kalman filter.

The confidence interval provides information about the accuracy of the values obtained from a sample study.

For example, a (95%) confidence interval (CI) includes a range of values that takes into account the variability of the sample, so you can trust with a reasonable margin of certainty (95%) that this range contains the true value of the entire population that you have not been able to examine. Of course, this is only true if there are no systematic errors in the study.

In this thesis has been used the following CI

CI = 95,5%	$P\{\mu - 2\sigma < X < \mu + 2\sigma\}$
CI = 99,7%	$P\{\mu - 3\sigma < X < \mu + 3\sigma\}$

The first step consists into establish statistical uncertainty bounds on the measured frequency response function (FRF) magnitude and phase.

The analysis presented by Bendat and Piersol leads to the following relations for the

standard deviation,  $\sigma$ , on the magnitude and phase for the FRFs at each frequency value,  $\omega_i$ .

$$\sigma(|H(\omega)|) = \frac{\sqrt{1 - \gamma_{mean}^2(\omega)}}{|\gamma_{mean}(\omega)|\sqrt{2_{nd}}} |H_{mean}(\omega)| \quad (6-3)$$

$$\sigma(\angle H(\omega)) = \frac{\sqrt{1 - \gamma_{mean}^2(\omega)}}{|\gamma_{mean}(\omega)|\sqrt{2_{nd}}} \angle H_{mean}(\omega) \quad (6-4)$$

In Eqs (6-3)  $|H_{mean}(\omega)|$  is the mean value of the FRF magnitude at frequency  $\omega$ , while, in Eq (6.4)  $\angle H_{mean}(\omega)$  is the corresponding mean value of the FRF phase angle,  $\gamma_{mean}^2$  is the mean value of the coherence function and  $nd$  is the number of measurement averages used to form the mean values of the FRF and coherence.

The basic idea of a Monte Carlo analysis is the repeated simulation of random input data, following the probability distribution that is supposed to have the phenomenon to be investigated so the simulation of FRFs with estimated mean and standard deviation values.

For more details see [Charles R. Farrar, Scott W. Doebling<sup>1</sup> Phillip J. Cornwell].

In this thesis for the generation of a new plant, have not been generated a series of points within the confidence intervals as in the Monte Carlo Analysis, but the upper and lower confidence limits are directly used.

The aim is to understand how the filter responds when it must work with a plant that differs from the model with whom it has been implemented.

In the Figure 26 and Figure 27 the CI for the main axes are presented

Once the two new plants have been obtained, a new impulse response is generated for each of them and a new coloured map is built with the same procedure explained in the previous chapter.

The table below shows the results obtained using  $R = 0.15$  in the Tap Test and  $R = 10$  in the cutting test for both axis.

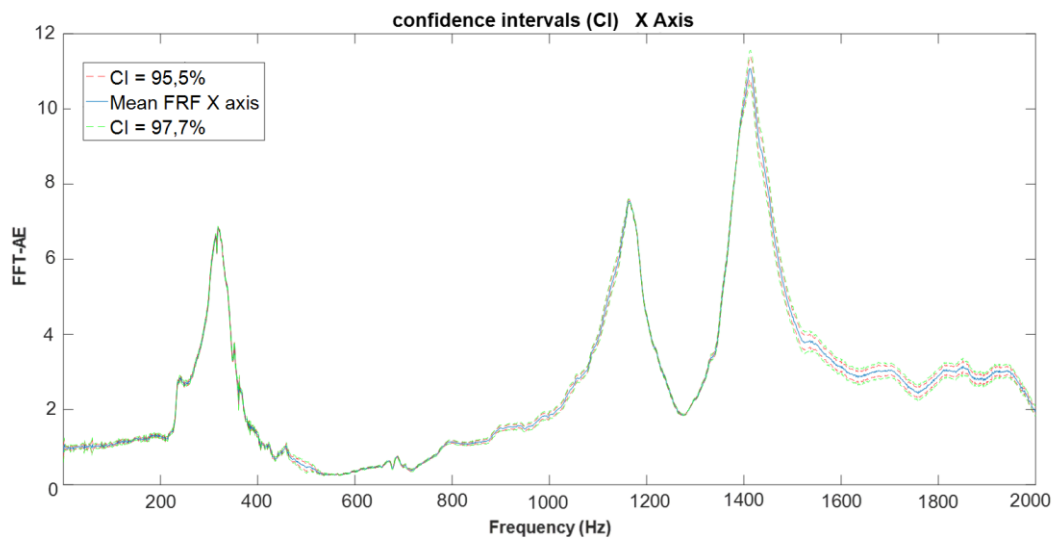


Figure 27 - X-axis Confidence Intervals

The coloured maps graphs below show a slight shift of the optimum region obtained from the Tap Test to the right.

The plant variation introduced according to the confidence interval rule has produced an increment of process uncertainty, this would demonstrate why in cutting test the the Q optimum parameters values are higher.

However, plant changes are not sufficient to justify such a marked shift of red dots on the right; so probably there are others unkown dynamic system variables that

influence the milling process.

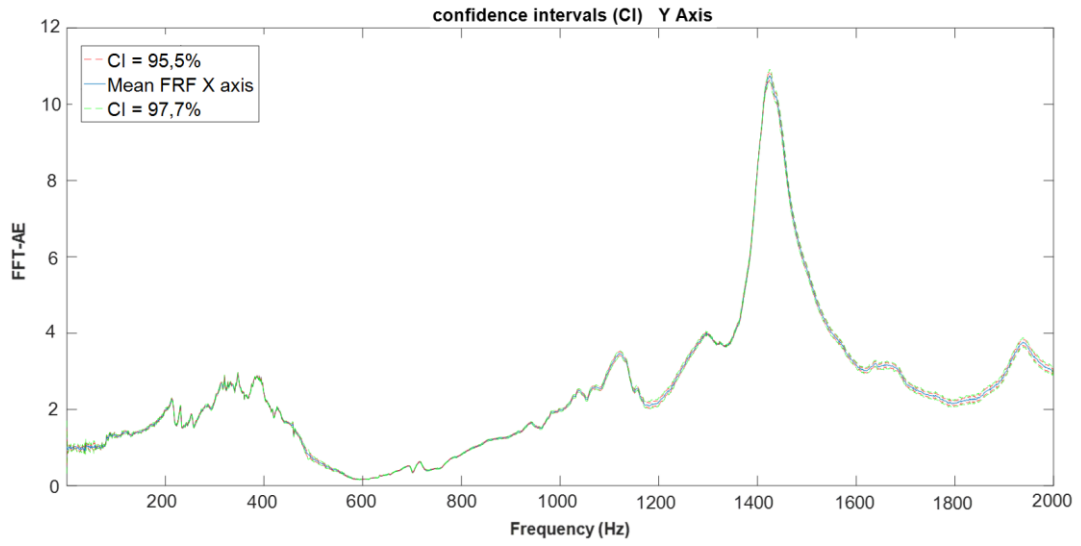


Figure 28 - Y-axis Confidence Intervals

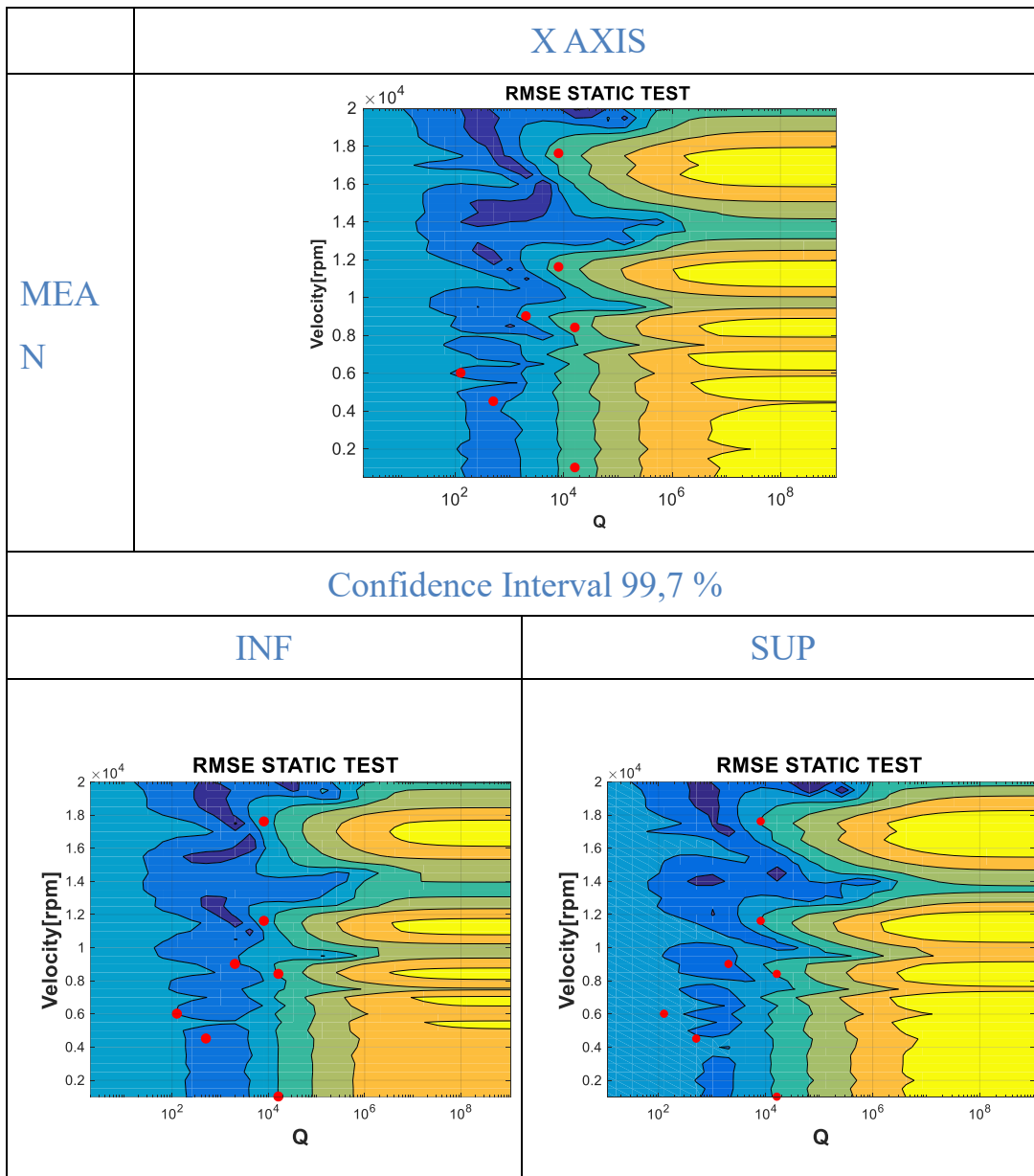


Table 6 - Plant variation effect according to the logic of confidence intervals along the X-axis

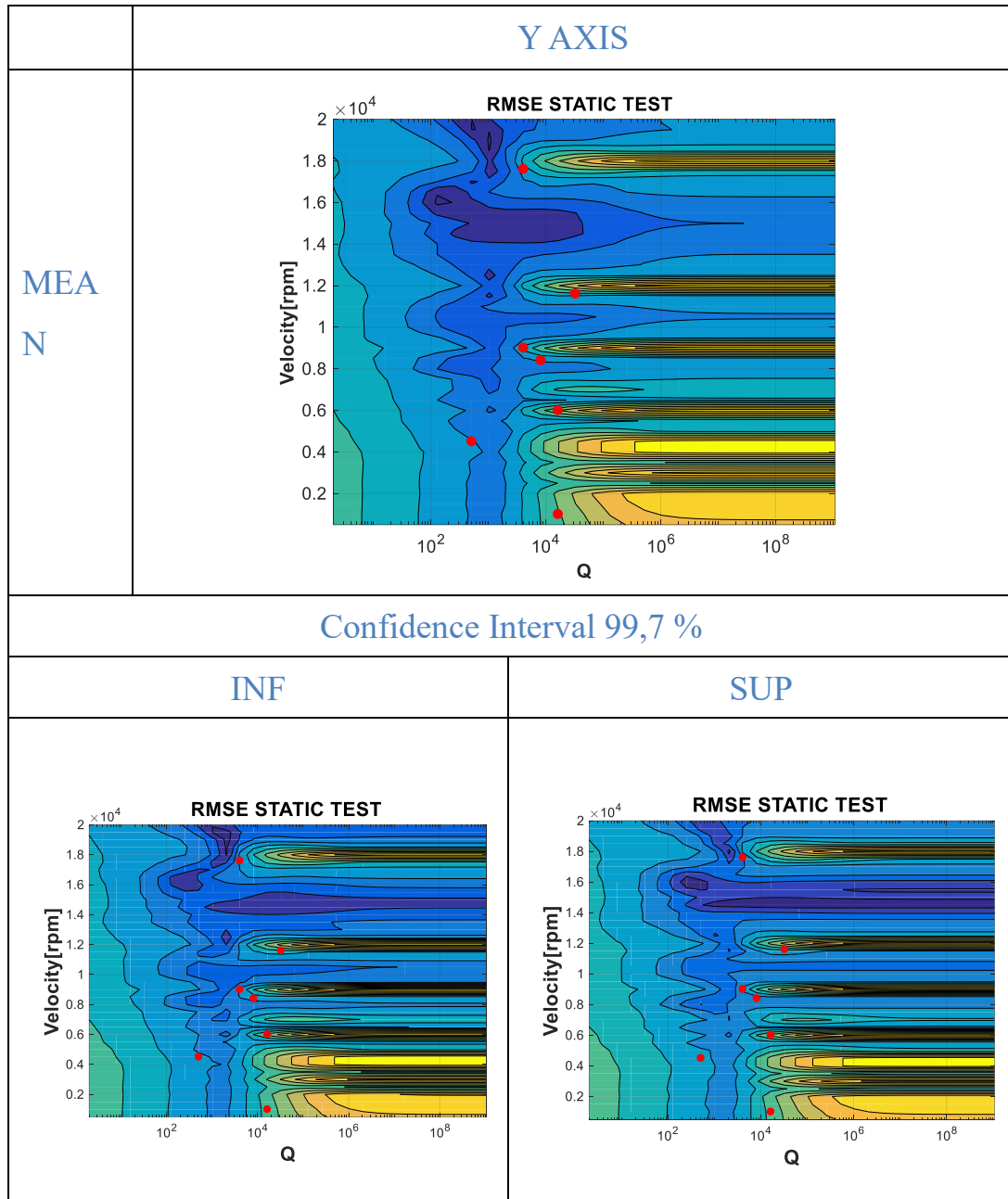


Table 7 - Plant variation effect according to the logic of confidence intervals along the Y-axis

## 6.3 Experimental Equipment and Setting

To conduct those experiments, certain equipment is needed. This section specifies the used equipment and settings and gives an overview of the measurement chain.

### Machine Tool

The experiments described in this section are carried out on a Quaser UX600 Multit Face 5 Axes Machine Center. The machine is equipped with a Heidenhain iTNC 530 control which is connected to an external computer via Ethernet. The spindle of the machine was manufactured by WEISS Spindle Technology GmbH and is capable of spindle speeds up to 24000 *rpm* and a maximum power of 24 *kW*. The spindle is equipped with spindle integrated force sensors as described in Section 3.1.



Figure 29 - a Quaser UX600 Multit Face 5 Axes Machine Center

## Cutting Tools

The verification results for the SIFS compensation are obtained by the use of a four-fluted carbide end mill SH40750 from DATA FLUTE. The tool has a diameter  $D$  of  $\frac{3}{4}$  inch which resembles  $19.05\text{ mm}$ . The helix angle is determined to be  $30^\circ$ .

The tool is used with the shrink fit tool holder H4Y3A0750 by COMMAND Tooling Systems.

This tool holder is chosen because of its capability of being used in high speed machining and its short and rigid structure which ensure a stable cut even for higher axial depth of cut. Figure 29 shows the tool holder with the inserted four flute tool.

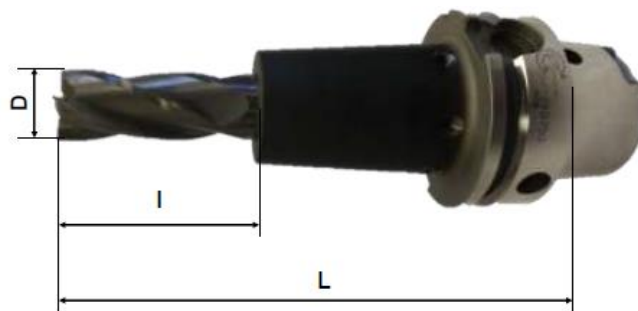


Figure 30 - four-fluted carbide end mill SH40750 from DATA FLUTE

The used tool has a stick out length  $l$  of  $51\text{ mm}$  which lead to a tool length  $L$  of  $138\text{ mm}$ .

## Dynamometer

To compare the measured forces by the SIFS, a table dynamometer of the type KISTLER 9257B is used. The dynamometer is capable of measuring force up to 5 kN. The cross-talk influence on the measurement is thereby smaller than  $\pm 2\%$ .

The dynamometer is calibrated by setting the sensitivities in X-direction to 7.926 pC/N, in Y-direction to 7.943 pC/N and in Z-direction to 3.688 pC/N.

The dynamometer is clamped to the machine table and aligned in machine X and Y-direction to ensure the comparability of the force measurements. Nevertheless, the direction of the dynamometer axis is different to the machine coordinate system. Therefore, a coordinate transformation of the measured values has to be performed to compare the measurements.



Figure 31 - Table dynamometer of the type KISTLER 9257B

### Impact Hammer

In this thesis for the input signal generation an impact hammer of the type Dytran 5800B4 is employed.

It is used with plastic tips to achieve good coherence in low frequency areas.

Its weight is 0.1 *kg* and its sensitivity is 2.248 *mV/N*.

### Charge Amplifiers

The piezoelectric based sensors, like the table dynamometer and the SIFS, have to be connected to a charge amplifier.

Kistler 5010B charge amplifiers are connected to each channel of the SIFS.

The dynamometer itself is connected to a Kistler 5814B1 charge amplifier with three outputs, one for each axis.

For the SIFS, the sensitivity is kept at 3.8 *pc/N* due to its calibration in Matlab after the measurement. The scale value was set to 1000 *N/mV* for the dynamometer and 200 *N/mV* for the SIFS for an optimal use of the voltage spectrum of the input-output-box.

The signal from the charge amplifier is collected by two input-output-boxes (also called data-acquisition-boxes). Both data-acquisition-boxes (DAQ-boxes) are made by National Instruments. The first box, NI USB-4432, has five in- and outputs and an input voltage range of  $\pm 10$  *V*, whereas the second box, NI 9234 included in a NI USB-9162 carrier, has only four in- and outputs and  $\pm 5$  *V* range.

The maximum sampling frequency for both devices is 51200 *Hz* by a resolution of 24-*Bit*.

### *Measurement and Simulation Software*

The collection and analysis of the data provided by the two input-output-boxes is done by the software CUTPRO. The sub-module MALDAQ of CUTPRO is handling the recording of time data during experiments, as they are provided by the DAQ-boxes. The chosen sampling rate for static calibration measurements is 1024 *Hz*. For cutting force measurement, the sampling frequency was increased to 12800 *Hz* since a minimum sampling time of 10000 *Hz* is needed for the compensation approach.

For FRF-measurement, the sub-module MALTF is used. The sensitivity values for the SIFS FRF-measurements are set to one since calibration is conducted in Matlab afterwards.

The subprogram Modal Analysis of CUTPRO is used to fit the measured FRF and generate the modal parameter. Further calculations and compensations as well as the calibration of the SIFS and the coordinate transformation of the dynamometer are done by the use of Matlab.

36 gives an overview over the whole measurement chain.

For further information about the used equipment and setting, please consult the pdf files attached with the thesis.

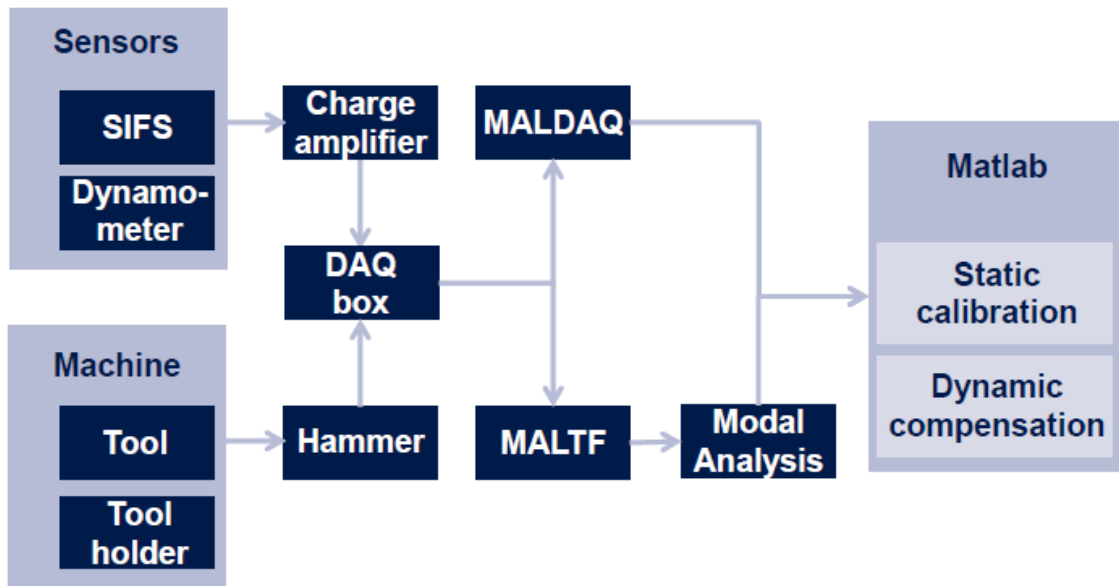


Figure 32 - Measurement Chain Overview

## 6.4 Procedure validation

This Chapter analyses all possible combinations between R and Q parameter formulated in Chapter 6.2 to understand the great setting of the filter and obtain the best force prediction as possible.

### 6.4.1 X Axis

Once setted the R matrix, the optimal Q values obtained from the TapTest are used to initialize the Kalman filter in real cutting tests, then it will be evaluating how far the found solution deviates from the optimal one obtained using the Q optimal value directly derived from cutting tests in terms of committed error (RMSE).

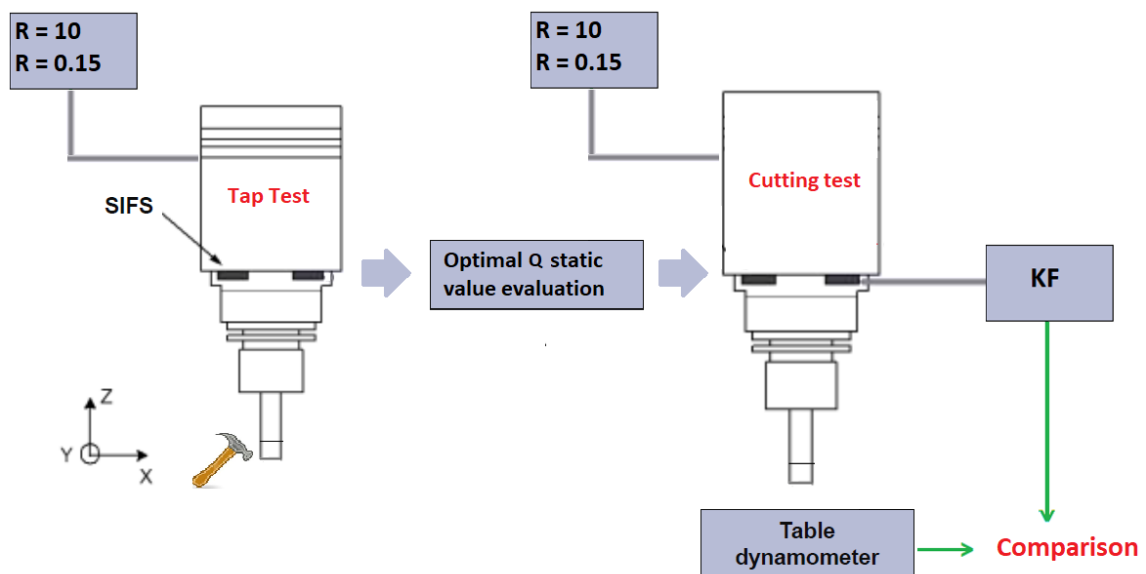


Figure 33 - Experimental Operating logic

We analyze each hypothesis individually

TAP TEST R =0.15			CUTTING TESTS R=10		
1000rpm	$\xrightarrow{Q\ OPT.}$	Q=512	1000rpm	$\xrightarrow{Q\ STATIC\ OPT.}$	RMSE =0.829
4500rpm	$\xrightarrow{Q\ OPT.}$	Q = 512	4500rpm	$\xrightarrow{Q\ STATIC\ OPT.}$	RMSE =1.637
6000rpm	$\xrightarrow{Q\ OPT.}$	Q = 512	6000rpm	$\xrightarrow{Q\ STATIC\ OPT.}$	RMSE =2.499
8400 rpm	$\xrightarrow{Q\ OPT.}$	Q =1024	8400 rpm	$\xrightarrow{Q\ STATIC\ OPT.}$	RMSE =4.033
9000rpm	$\xrightarrow{Q\ OPT.}$	Q = 512	9000rpm	$\xrightarrow{Q\ STATIC\ OPT.}$	RMSE =2.679
11600rpm	$\xrightarrow{Q\ OPT.}$	Q= 1024	11600rpm	$\xrightarrow{Q\ STATIC\ OPT.}$	RMSE =4.010
17600rpm	$\xrightarrow{Q\ OPT.}$	Q = 512	17600rpm	$\xrightarrow{Q\ STATIC\ OPT.}$	RMSE =3.252

Table 8 – Experimental results along X-axis ( $R_{static} = 0.15$   $R_{dynamic} = 10$ )

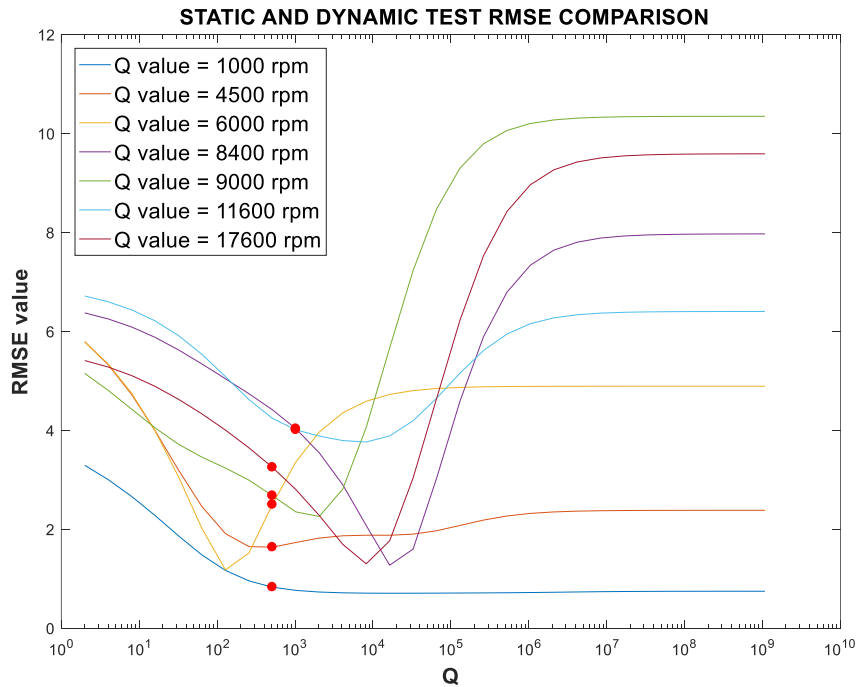


Figure 34 - RMSE comparison between static and dynamic test along X-axis ( $R_{static} = 0.15$   $R_{dynamic} = 10$ )

The coloured curves have been constructed starting from the cutting tests varying the Q parameter.

The red dots represent the errors committed in terms of (RMSE) using the optimal Q values obtained from the static test to implement the filter in the corresponding cutting test.

We carry out some analysis of the most significant tests in time domain to evaluate the actual force estimation.

The time lag introduced by the filter has been eliminated in the following graphs

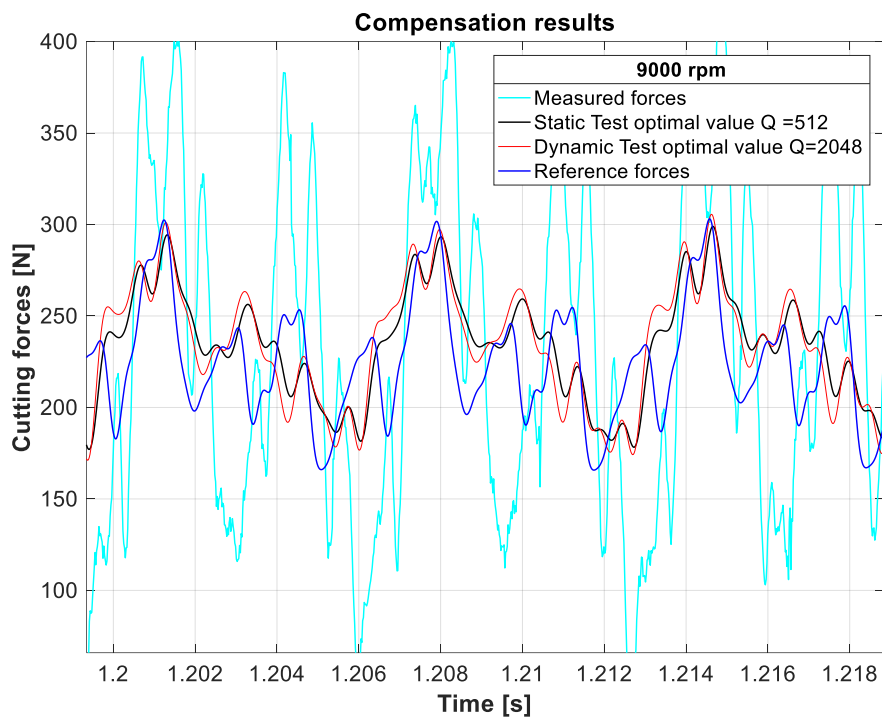


Figure 35 - Compensation results for X-direction measurement with dynamometer of a cutting operation with 9000 rpm spindle speed in time domain ( $R_{static} = 0.15$   $R_{dynamic} = 10$ )

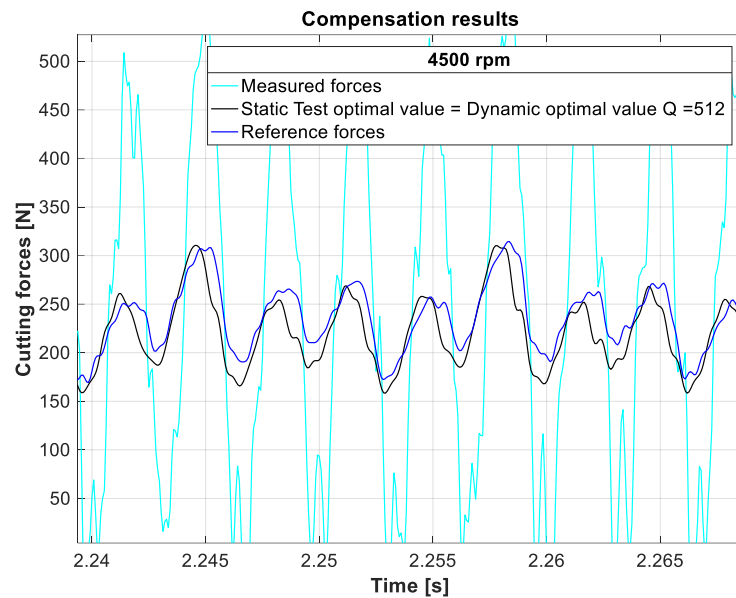


Figure 36 - Compensation results for X-direction measurement with dynamometer of a cutting operation with 4500 rpm spindle speed in time domain ( $R_{static} = 0.15$   $R_{dynamic} = 10$ )

### Critical Speeds

The prediction at 8400 rpm shows an understimation of the Reference force.

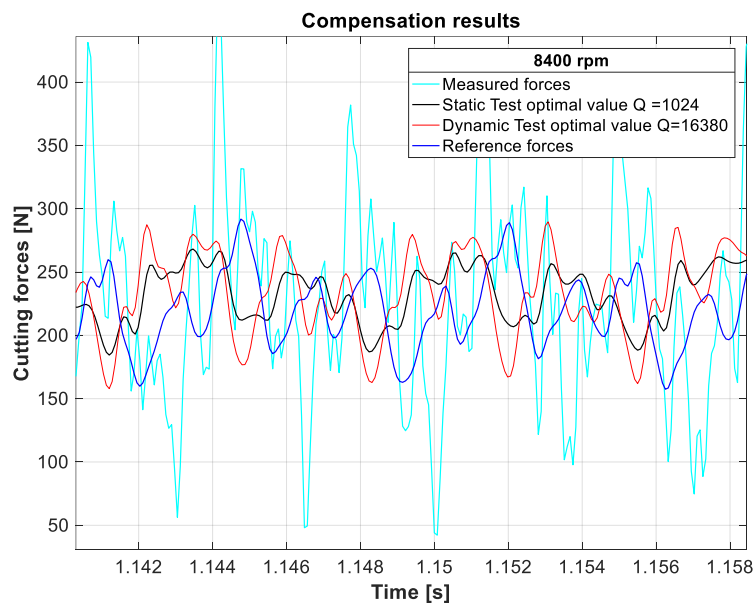


Figure 37 - Compensation results for X-direction measurement with dynamometer of a cutting operation with 8400 rpm spindle speed in time domain ( $R_{static} = 0.15$   $R_{dynamic} = 10$ )

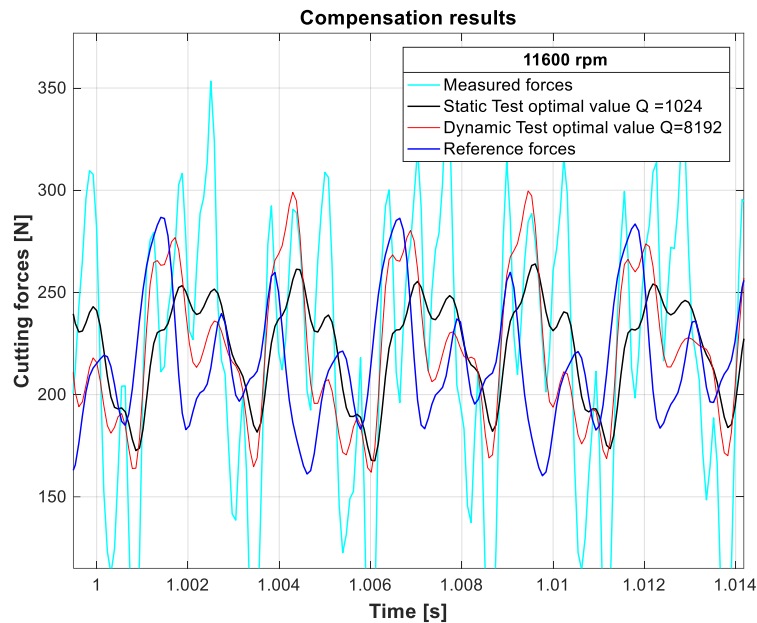


Figure 38 - Compensation results for X-direction measurement with dynamometer of a cutting operation with 11600 rpm spindle speed in time domain ( $R_{static} = 0.15$   $R_{dynamic} = 10$ )

A second idea could be to filter the cutting test again using  $R = 0.15$ , so considering only the uncertainty of the sensor and ignoring all those random and systematic errors due to spindle rotation.

A measurement uncertainty decrement leads to a dynamic curve shift to lower Q parameter values.

The close link between R and Q matrices emerges once again.

In particular is interesting to note as the RMSE values obtained using the two different R values remain almost unchanged for all speeds, so the force estimation depends not so much on R parameter but on the Q value once the first was set.

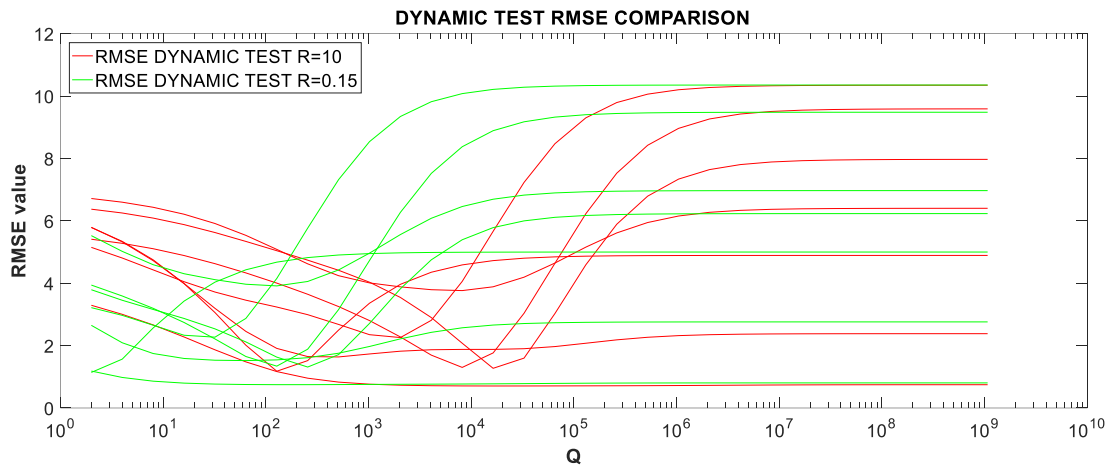


Figure 39 - Dynamic test optimal curves comparisons for X-axis ( $R_{dynamic} = 0.15$   
 $R_{dynamic} = 10$ )

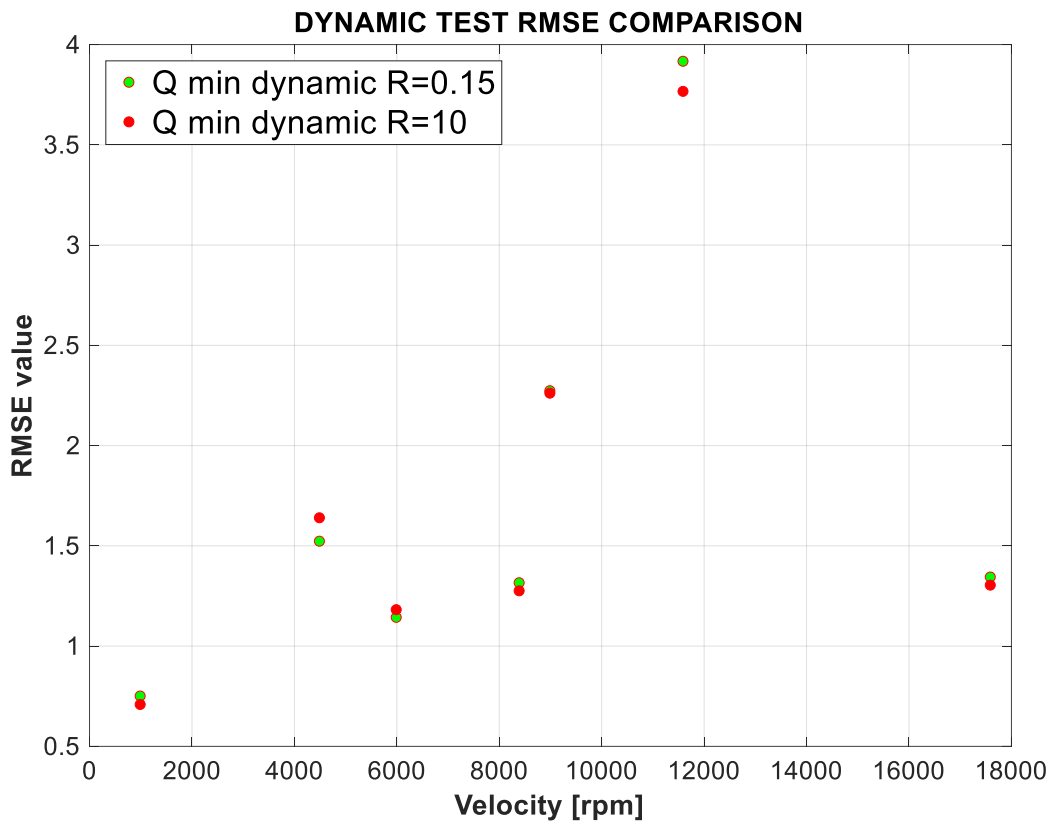


Figure 40 - Comparison between RMSE values calculated using optimal Q values during Cutting test along X-axis ( $R_{dynamic} = 0.15$   $R_{dynamic} = 10$ )

TAP TEST R = 0.15			CUTTING TESTS R=0.15		
1000rpm	$\underline{Q^{OPT.}}$	Q=512	1000rpm	$\underline{Q^{STATIC OPT.}}$	RMSE =0.751
4500rpm	$\underline{Q^{OPT.}}$	Q = 512	4500rpm	$\underline{Q^{STATIC OPT.}}$	RMSE =1.756
6000rpm	$\underline{Q^{OPT.}}$	Q = 512	6000rpm	$\underline{Q^{STATIC OPT.}}$	RMSE =4.905
8400 rpm	$\underline{Q^{OPT.}}$	Q =1024	8400 rpm	$\underline{Q^{STATIC OPT.}}$	RMSE =2.711
9000rpm	$\underline{Q^{OPT.}}$	Q = 512	9000rpm	$\underline{Q^{STATIC OPT.}}$	RMSE =7.321
11600rpm	$\underline{Q^{OPT.}}$	Q= 1024	11600rpm	$\underline{Q^{STATIC OPT.}}$	RMSE =4.965
17600rpm	$\underline{Q^{OPT.}}$	Q = 512	17600rpm	$\underline{Q^{STATIC OPT.}}$	RMSE =3.155

Table 9 - Experimental results along X-axis ( $R_{static} = 0.15$   $R_{dynamic} = 0.15$ )

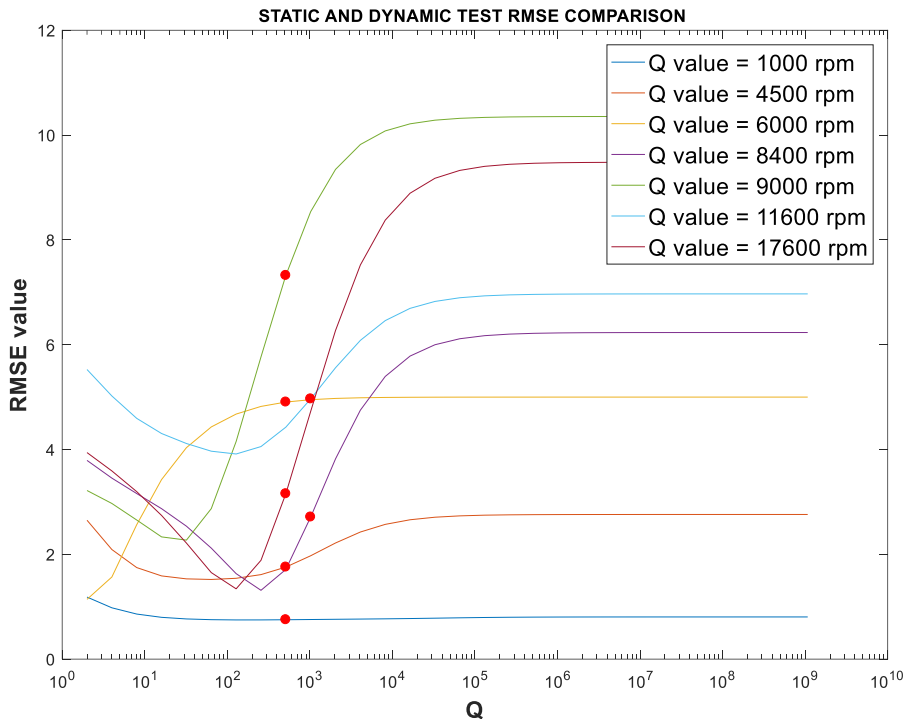


Figure 41 - RMSE comparison between static and dynamic test along X-axis ( $R_{static} = 0.15$   $R_{dynamic} = 0.15$ )

In this case the most critical velocity is 9000 rpm

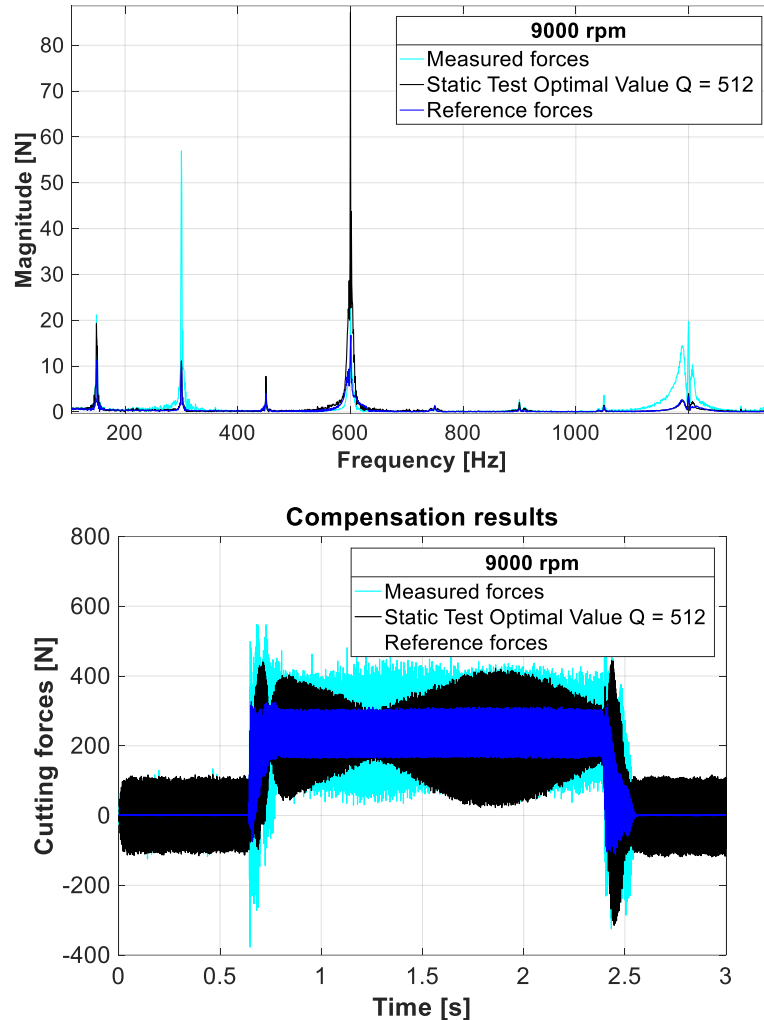


Figure 42 - Compensation results for X-direction measurement with dynamometer of a cutting operation with 9000 rpm spindle speed in time domain (lower graph) and frequency domain (upper plot)

Frequency components within the range [500-700 Hz] are very sensitive to  $Q$  parameter changing because the TF Magnitude close to 0 value determines a very high scale factor therefore, in the filter update phase a small difference between model estimation and actual piezoelectric sensor measure generates very high compensation errors, for further information see [Thomas 2015]. From Figure 22 we can conclude

that the last sensible combination is to set a value of  $R=10$  in both situations.

TAP TEST R = 10			CUTTING TESTS R=10		
1000rpm	$\underline{Q}_{OPT.} \rightarrow$	Q =32770	1000rpm	$\underline{Q}_{STATIC OPT.} \rightarrow$	RMSE=0.706
4500rpm	$\underline{Q}_{OPT.} \rightarrow$	Q= 32770	4500rpm	$\underline{Q}_{STATIC OPT.} \rightarrow$	RMSE =1.901
6000rpm	$\underline{Q}_{OPT.} \rightarrow$	Q =32770	6000rpm	$\underline{Q}_{STATIC OPT.} \rightarrow$	RMSE =4.803
8400 rpm	$\underline{Q}_{OPT.} \rightarrow$	Q =65540	8400 rpm	$\underline{Q}_{STATIC OPT.} \rightarrow$	RMSE =3.029
9000rpm	$\underline{Q}_{OPT.} \rightarrow$	Q = 32770	9000rpm	$\underline{Q}_{STATIC OPT.} \rightarrow$	RMSE =7.232
11600rpm	$\underline{Q}_{OPT.} \rightarrow$	Q= 65540	11600rpm	$\underline{Q}_{STATIC OPT.} \rightarrow$	RMSE =4.648
17600rpm	$\underline{Q}_{OPT.} \rightarrow$	Q = 32770	17600rpm	$\underline{Q}_{STATIC OPT.} \rightarrow$	RMSE =3.036

Table 10 - Experimental results along X-axis ( $R_{static} = 10$   $R_{dynamic} = 10$ )

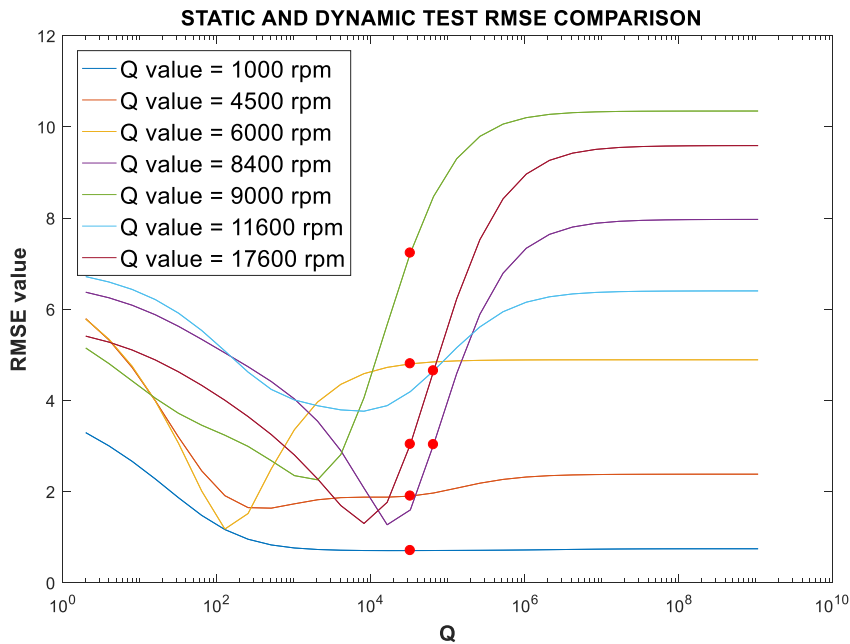


Figure 43 - RMSE comparison between static and dynamic test along x axis ( $R_{static} = 10$   $R_{dynamic} = 10$ )

Once the R matrix value has been set in the cutting test, through a Post process analysis is possible to perform a manually calibration.

For example, assuming R = 10 in cutting test, we get

TAP TEST R = 2			CUTTING TESTS R=10		
1000rpm	$\underline{Q_{OPT.}} \rightarrow$	Q =8192	1000rpm	$\underline{Q_{STATIC OPT.}} \rightarrow$	RMSE=0.714
4500rpm	$\underline{Q_{OPT.}} \rightarrow$	Q= 4096	4500rpm	$\underline{Q_{STATIC OPT.}} \rightarrow$	RMSE =1.879
6000rpm	$\underline{Q_{OPT.}} \rightarrow$	Q =8192	6000rpm	$\underline{Q_{STATIC OPT.}} \rightarrow$	RMSE =4.587
8400 rpm	$\underline{Q_{OPT.}} \rightarrow$	Q =16380	8400 rpm	$\underline{Q_{STATIC OPT.}} \rightarrow$	RMSE =3.029
9000rpm	$\underline{Q_{OPT.}} \rightarrow$	Q = 8192	9000rpm	$\underline{Q_{STATIC OPT.}} \rightarrow$	RMSE =1.273
11600rpm	$\underline{Q_{OPT.}} \rightarrow$	Q= 8192	11600rpm	$\underline{Q_{STATIC OPT.}} \rightarrow$	RMSE =4.058
17600rpm	$\underline{Q_{OPT.}} \rightarrow$	Q = 8192	17600rpm	$\underline{Q_{STATIC OPT.}} \rightarrow$	RMSE =1.301

Table 11 - Experimental results along X-axis ( $R_{static} = 2$   $R_{dynamic} = 10$ )

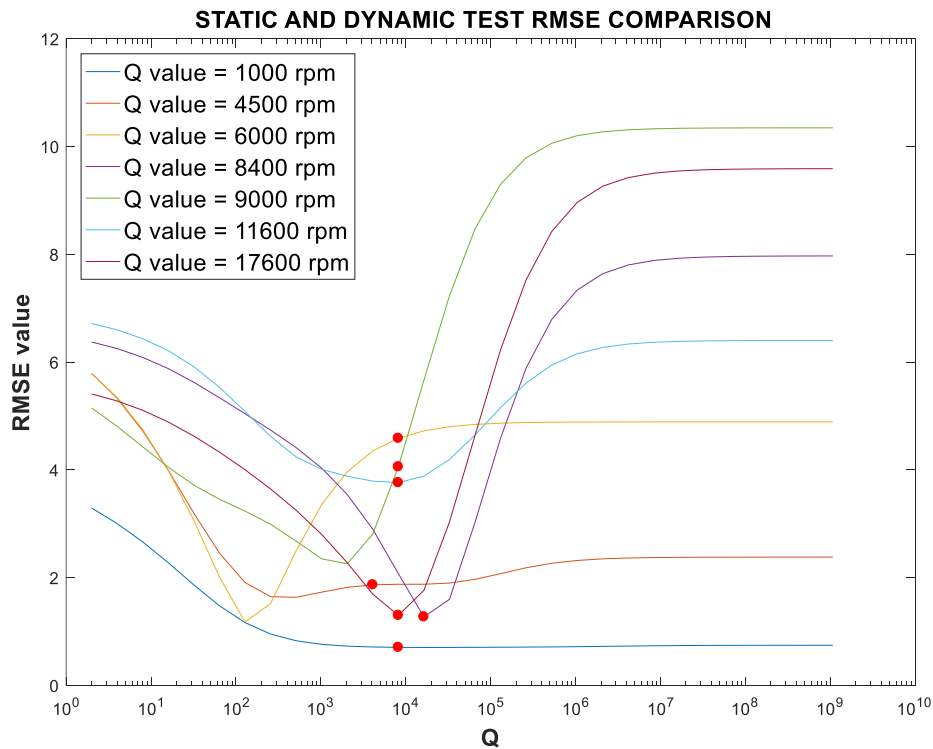


Figure 44 - RMSE comparison between static and dynamic test along X-axis ( $R_{static} = 2$   
 $R_{dynamic} = 10$ )

Summarizing all analyzed cases in Figure 44 where the obtained RMSE values have been compared each other at each spindle speed.

Using the same R-value in static and dynamic proof does not seem to be the optimal solution, because for some speeds the compensation error is high.

Excluding manual calibrations performed in post-process analysis, the use of  $R = 0.15$  in the Tap test and  $R = 10$  in the Cutting test is the choice that allows the operator to get the best prediction for all speeds.

In particular using these noise parameters values so referring to Figure 35 and Figure 37 it is possible to estimate the percentage error committed on the force amplitude estimation, in a case at 4500 where an excellent prediction of the force is obtained

and in the other case at 11600 rpm where instead the value of RMSE is higher.

The obtained results show like for a Spindle Speed of 4500 rpm the percentage error on the amplitude force estimation is about 10%; if we analyse instead the more critical velocity of 11600 rpm the percentage error rise up to 30%

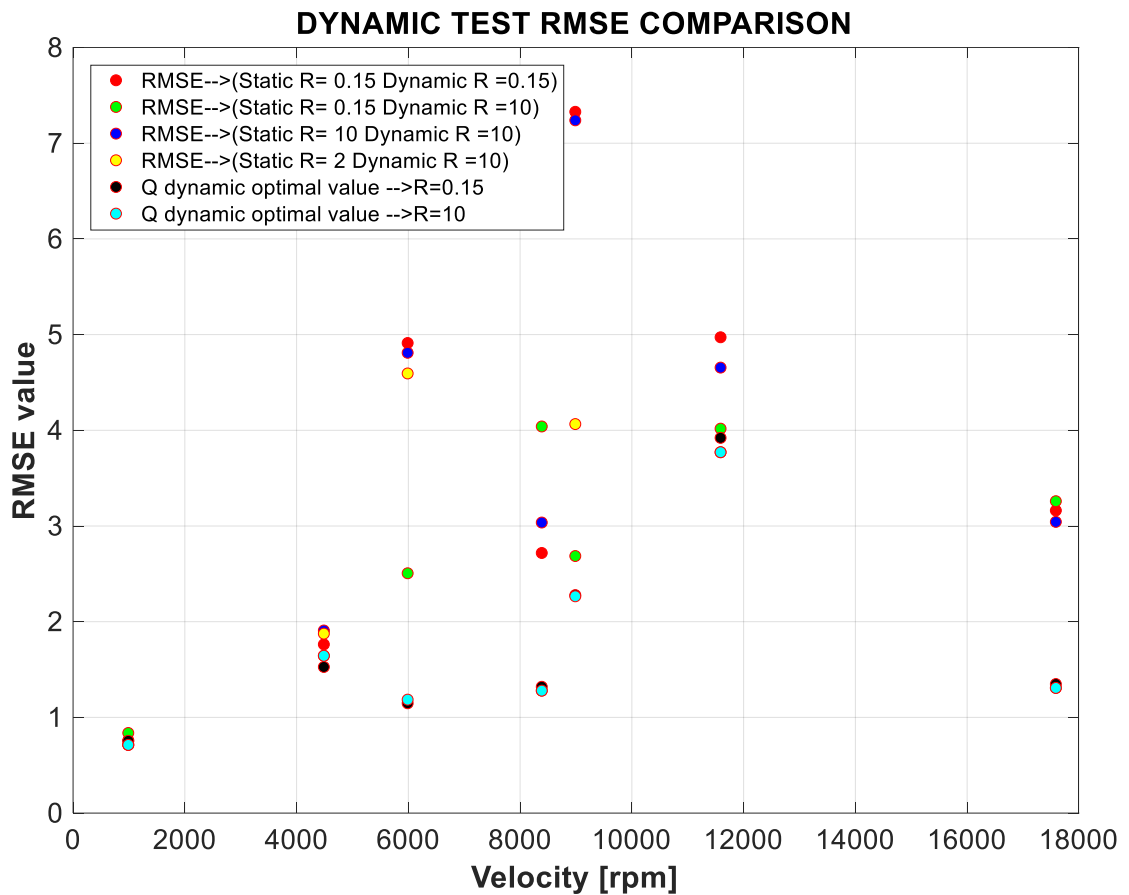


Figure 45 - General Overview of experimental results for X-axis

### 6.4.2 Y Axis

TAP TEST R = 0.15			CUTTING TESTS R=10		
1000rpm	$\underline{Q}_{OPT.} \rightarrow$	Q =1024	1000rpm	$\underline{Q}_{STATIC OPT.} \rightarrow$	RMSE=0.763
4500rpm	$\underline{Q}_{OPT.} \rightarrow$	Q= 1024	4500rpm	$\underline{Q}_{STATIC OPT.} \rightarrow$	RMSE =1.183
6000rpm	$\underline{Q}_{OPT.} \rightarrow$	Q =1024	6000rpm	$\underline{Q}_{STATIC OPT.} \rightarrow$	RMSE =1.818
8400 rpm	$\underline{Q}_{OPT.} \rightarrow$	Q =1024	8400 rpm	$\underline{Q}_{STATIC OPT.} \rightarrow$	RMSE =2.194
9000rpm	$\underline{Q}_{OPT.} \rightarrow$	Q =1024	9000rpm	$\underline{Q}_{STATIC OPT.} \rightarrow$	RMSE =2.025
11600rpm	$\underline{Q}_{OPT.} \rightarrow$	Q= 1024	11600rpm	$\underline{Q}_{STATIC OPT.} \rightarrow$	RMSE =4.486
17600rpm	$\underline{Q}_{OPT.} \rightarrow$	Q = 1024	17600rpm	$\underline{Q}_{STATIC OPT.} \rightarrow$	RMSE =1.296

Table 12 - Experimental results along Y-axis ( $R_{static} = 0.15$   $R_{dynamic} = 10$ )

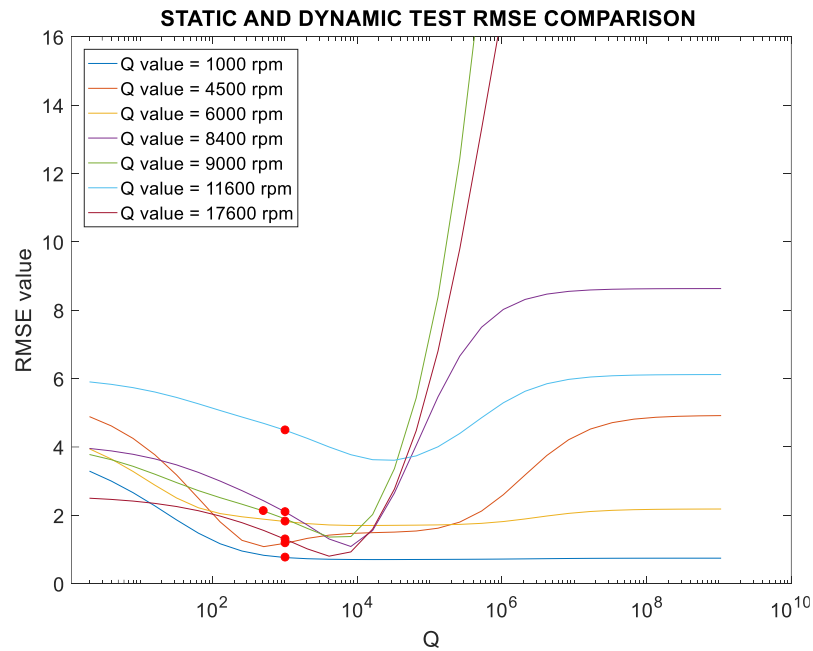


Figure 46 - RMSE comparison between static and dynamic test along Y-axis ( $R_{static} = 0.15$   $R_{dynamic} = 10$ )

Reproposing the same set of hypotheses also for the Y-axis we obtain the following experimental results

TAP TEST R = 0.15			CUTTING TESTS R=0.15		
1000rpm	$\underline{Q_{OPT.}} \rightarrow$	Q =1024	1000rpm	$\underline{Q_{STATIC OPT.}} \rightarrow$	RMSE=0.717
4500rpm	$\underline{Q_{OPT.}} \rightarrow$	Q= 1024	4500rpm	$\underline{Q_{STATIC OPT.}} \rightarrow$	RMSE =1.428
6000rpm	$\underline{Q_{OPT.}} \rightarrow$	Q =1024	6000rpm	$\underline{Q_{STATIC OPT.}} \rightarrow$	RMSE =1.687
8400 rpm	$\underline{Q_{OPT.}} \rightarrow$	Q =1024	8400 rpm	$\underline{Q_{STATIC OPT.}} \rightarrow$	RMSE =4.122
9000rpm	$\underline{Q_{OPT.}} \rightarrow$	Q =512	9000rpm	$\underline{Q_{STATIC OPT.}} \rightarrow$	RMSE =2.701
11600rpm	$\underline{Q_{OPT.}} \rightarrow$	Q= 1024	11600rpm	$\underline{Q_{STATIC OPT.}} \rightarrow$	RMSE =3.174
17600rpm	$\underline{Q_{OPT.}} \rightarrow$	Q = 1024	17600rpm	$\underline{Q_{STATIC OPT.}} \rightarrow$	RMSE =5.021

Table 13 - Experimental results along Y-axis ( $R_{static} = 0.15$   $R_{dynamic} = 0.15$ )

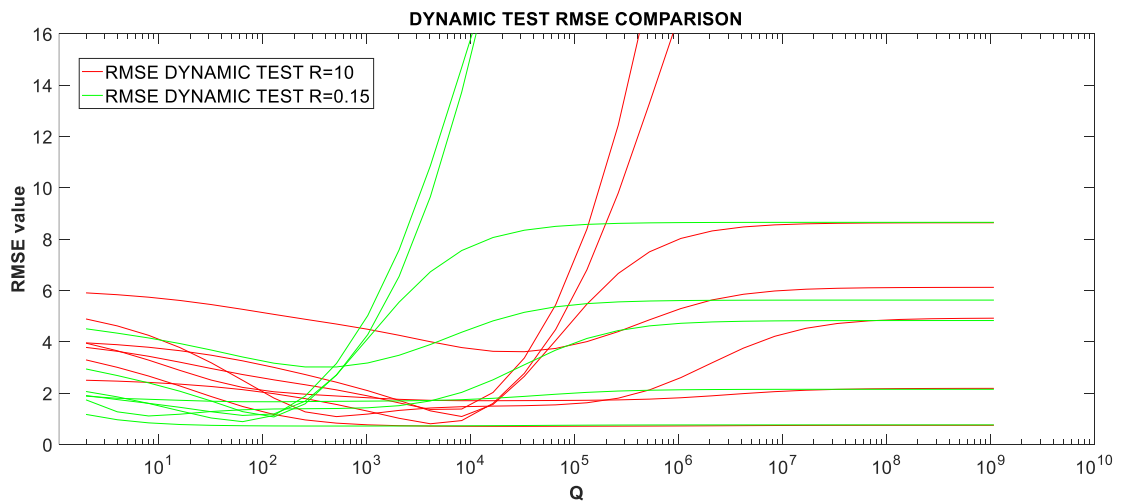


Figure 47 - Dynamic test optimal curves comparisons for Y-axis ( $R_{dynamic} = 0.15$   $R_{dynamic} = 10$ )

For the Y-axis, as already highlighted for the X-axis, a R parameter decrement

produces a shift of the optimum curves built on the cutting tests towards lower values of the Q parameter without, however, significantly changing the minima.

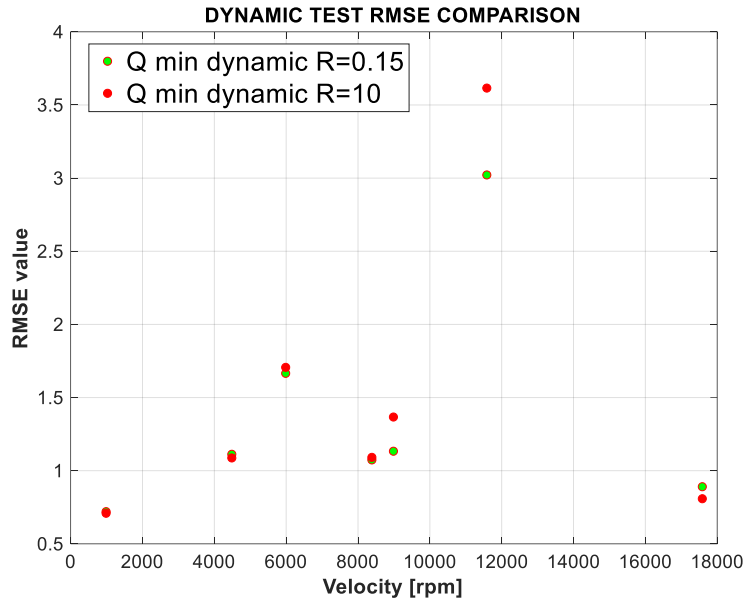


Figure 48 - Comparison between RMSE values calculated using optimal Q values during Cutting test along Y-axis ( $R_{dynamic} = 0.15$   $R_{dynamic} = 10$ )

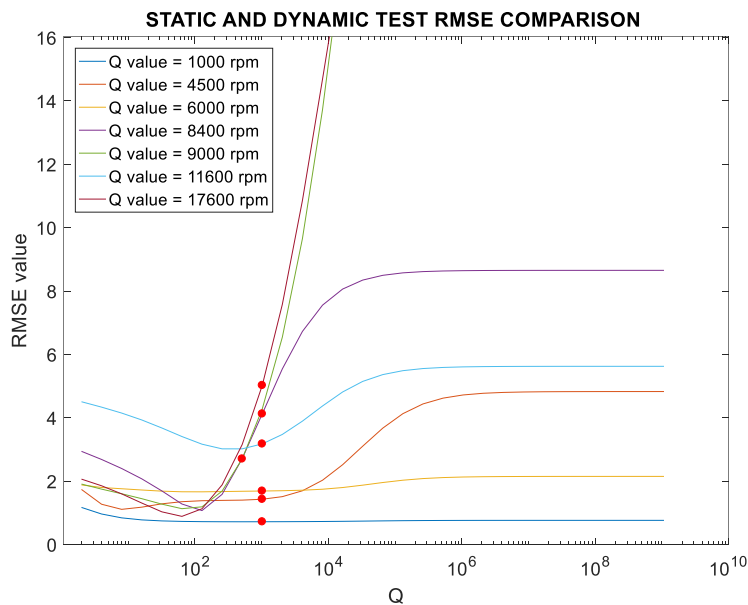


Figure 49 - RMSE comparison between static and dynamic test along Y-axis ( $R_{static} = 0.15$   $R_{dynamic} = 10$ )

TAP TEST R = 10			CUTTING TESTS R=10		
1000rpm	$\underline{Q_{OPT.}}$	Q =65550	1000rpm	$\underline{Q_{STATIC OPT.}}$	RMSE=0.708
4500rpm	$\underline{Q_{OPT.}}$	Q= 65550	4500rpm	$\underline{Q_{STATIC OPT.}}$	RMSE =1.541
6000rpm	$\underline{Q_{OPT.}}$	Q =65550	6000rpm	$\underline{Q_{STATIC OPT.}}$	RMSE =1.712
8400 rpm	$\underline{Q_{OPT.}}$	Q =65550	8400 rpm	$\underline{Q_{STATIC OPT.}}$	RMSE =4.047
9000rpm	$\underline{Q_{OPT.}}$	Q =32770	9000rpm	$\underline{Q_{STATIC OPT.}}$	RMSE =3.365
11600rpm	$\underline{Q_{OPT.}}$	Q= 65550	11600rpm	$\underline{Q_{STATIC OPT.}}$	RMSE =3.739
17600rpm	$\underline{Q_{OPT.}}$	Q = 65550	17600rpm	$\underline{Q_{STATIC OPT.}}$	RMSE =4.475

Table 14 - Experimental results along Y-axis ( $R_{static} = 10$   $R_{dynamic} = 10$ )

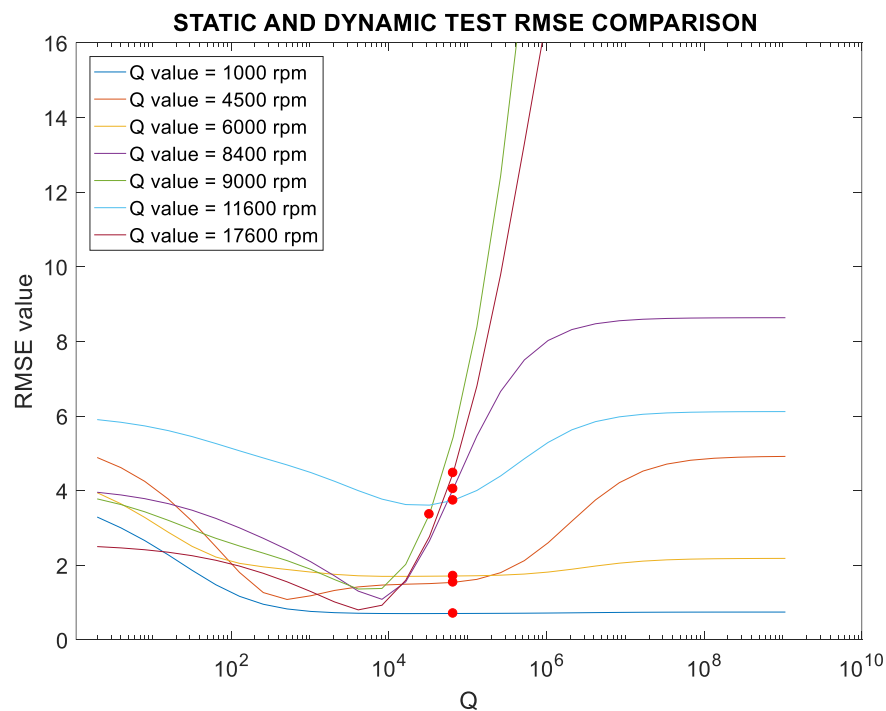


Figure 50 - RMSE comparison between static and dynamic test along Y-axis ( $R_{static} = 10$   $R_{dynamic} = 10$ )

TAP TEST R = 2			CUTTING TESTS R=10		
1000rpm	$\underline{Q}_{OPT.} \rightarrow$	Q =16380	1000rpm	$\underline{Q}_{STATIC OPT.} \rightarrow$	RMSE=0.705
4500rpm	$\underline{Q}_{OPT.} \rightarrow$	Q= 16380	4500rpm	$\underline{Q}_{STATIC OPT.} \rightarrow$	RMSE =1.493
6000rpm	$\underline{Q}_{OPT.} \rightarrow$	Q =16380	6000rpm	$\underline{Q}_{STATIC OPT.} \rightarrow$	RMSE =1.703
8400 rpm	$\underline{Q}_{OPT.} \rightarrow$	Q =16380	8400 rpm	$\underline{Q}_{STATIC OPT.} \rightarrow$	RMSE =1.557
9000rpm	$\underline{Q}_{OPT.} \rightarrow$	Q =4096	9000rpm	$\underline{Q}_{STATIC OPT.} \rightarrow$	RMSE =1.363
11600rpm	$\underline{Q}_{OPT.} \rightarrow$	Q= 16380	11600rpm	$\underline{Q}_{STATIC OPT.} \rightarrow$	RMSE =3.628
17600rpm	$\underline{Q}_{OPT.} \rightarrow$	Q = 16380	17600rpm	$\underline{Q}_{STATIC OPT.} \rightarrow$	RMSE =1.599

Table 15 - Experimental results along X-axis ( $R_{static} = 2$   $R_{dynamic} = 10$ )

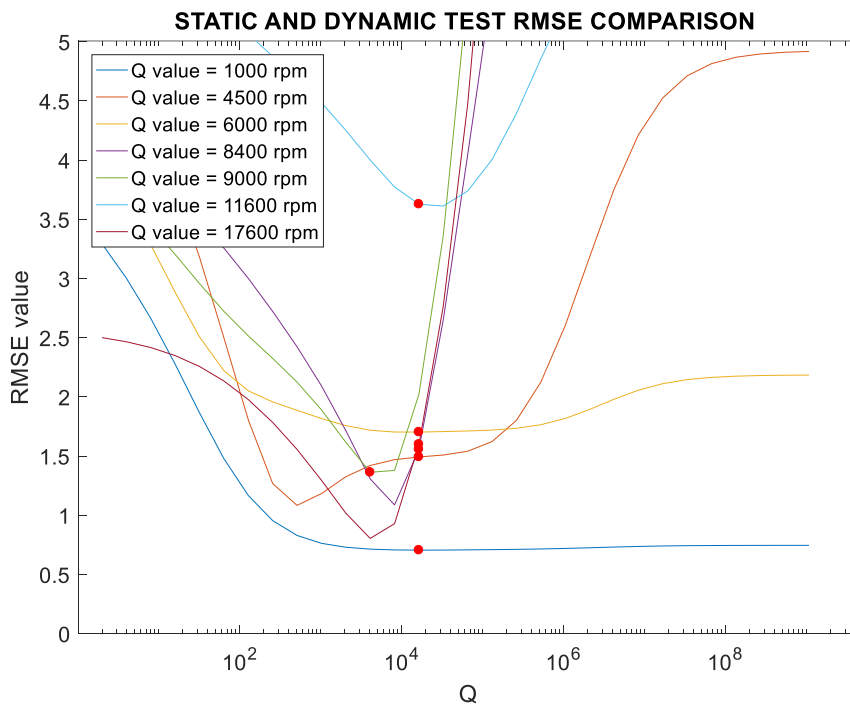


Figure 51 - RMSE comparison between static and dynamic test along y axis ( $R_{static} = 2$   $R_{dynamic} = 10$ )

Summarizing all analyzed cases in a single graph where the obtained RMSE values have been compared each other at each spindle speed, you get

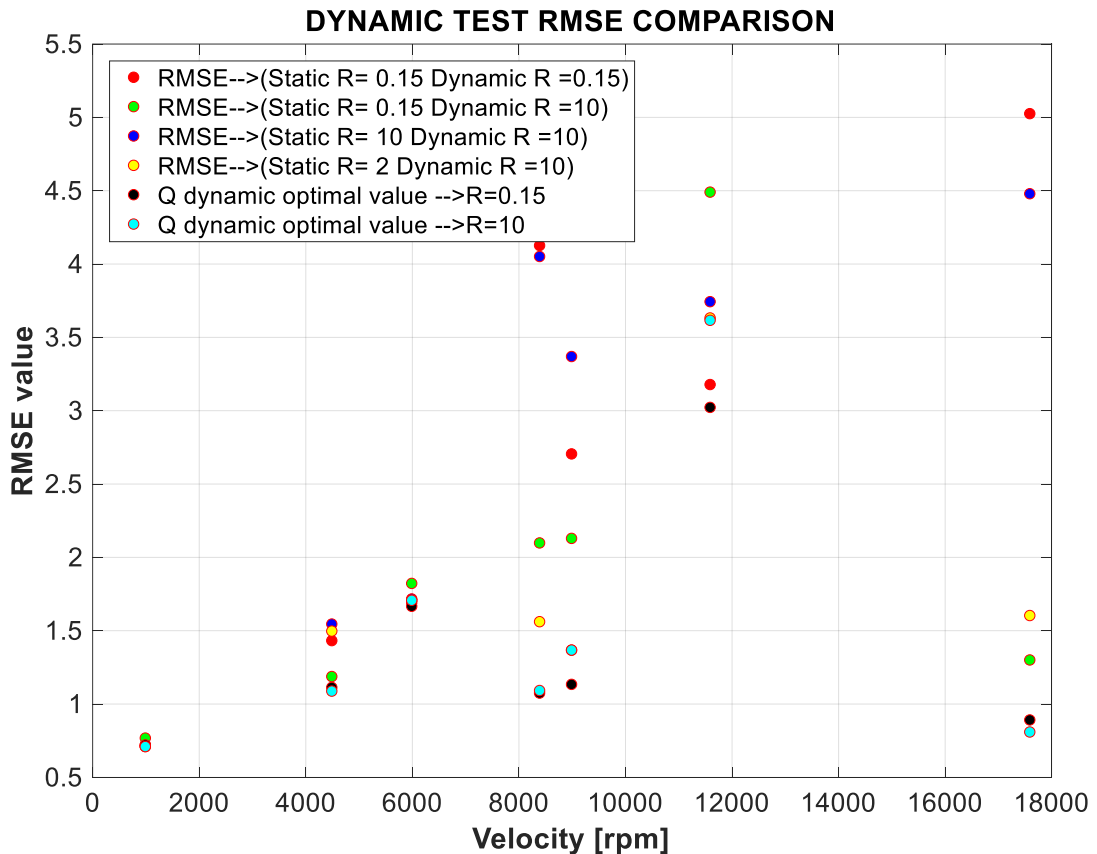


Figure 52 - General Overview of experimental results for Y-axis

The RMSE values recorded for the examined speeds are slightly lower than those obtained for the X axis due to a Smoother trend of the optimum curves calculated from the cutting tests for low Q values.

Experimental results seem to reconfirm the choice of  $R=0.15$  in the TapTest and  $R=10$  in the cutting tests as the best option, except for the speed at 11600 rpm where RMSE remains fairly elevated.

The next figure shows the different prediction in time domain for a cutting test at

17600 rpm using a different R value

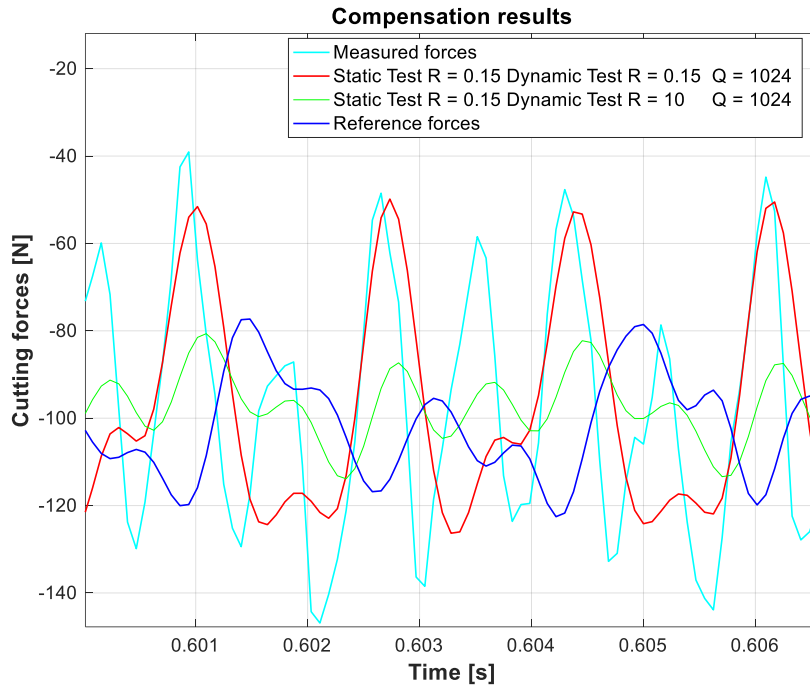


Figure 53 - Comparison between compensation results for Y-direction with different  $R_{dynamic}$  of a cutting operation with 17600 rpm spindle speed in time domain

In particular, the experimental proofs in time domain show how to use Q values to the left of the curve optimum point determines a force underestimation.

On the other hand, a using of a Q values on the right of the curve optimum point determines a force overestimation.

## 7 Final Considerations, conclusions and future developments

In this thesis, guidelines are provided on the use of the SIFS concept as an indirect cutting force measuring instrument for milling applications.

A careful analysis of each individual operation involved in the force compensation process has been proposed.

During compensation, the static and dynamic calibration of the SIFS measurement, the influence of unbalanced forces, the importance of crosstalk components, the precision of the FRF adjustment, the stability of the system and the Kalman filter strategy are discussed.

Particular attention has been paid to the choice of the Kalman filter noise parameters with the aim of understanding whether there can actually be an optimal automatic calibration that guarantees a good force estimation as the spindle speed varies.

The basic idea is that there is a strong link between these two parameters that can be studied during the dynamic identification phase of the model.

The most important element is therefore the elaboration of a new algorithm that, by exploiting the close link between the natural response of the system and cutting test, it is able to predict the real functioning assumed by the Kalman filter during cutting machining through the TapTest.

From a practical point of view, it means that the filter can be calibrated very easily without having to carry out further cutting test, thus achieving considerable savings

not only in terms of costs but also in terms of time.

The study starts from the formulation of different hypotheses about the real value assumed by the parameters "R" and "Q"; through experimental test these theories were then compared, thus understanding which of them is able to provide the best result.

The test shows a maximum percentage error of 30% compared to the optimal calibration carried out in real cutting test.

We are talking about a new filter calibration strategy on which there are wide margins for improvement.

One of the possible developments of this work for example could be to study the causes that generate a different slope of the optimum curves during cutting test as the spindle speed varies.

Another idea could be to study which process variables, beyond the modification of the plant, occur during a cutting operation and how they influence in terms of process uncertainty increment.

Knowing also that the variation of the Q parameter is extremely sensitive in the system's anti-resonance zones due to the high scale factor, one last proposal could be to study the Kalman filter behaviour in these zones and elaborate a new mathematical relation.

The study of all these phenomena could be the starting point for the generation of a new algorithm with better predictive capacities.

---

## Bibliography

[Albertelli 2015]

P. Albertelli, M. Goletti, M. Torta, M. Salehi & M. Monno: Model-based broadband estimation of cutting forces and tool vibration in milling through in-process indirect multiple-sensors measurements

[Altintas 2012]

Altintas, Y.: Manufacturing automation. 2nd ed Aufl. Cambridge, New York: Cambridge University Press 2012. ISBN: 978-0-521-17247-9.

[Altintas et al. 2008]

Altintas, Y.; Stepan, G.; Merdol, D.; Dombovari, Z.: Chatter stability of milling in frequency and discrete time domain. CIRP Journal of Manufacturing Science and Technology 1 (2008) 1, S. 35-44.

[Byrne et al. 1995]

Byrne, G.; Dornfeld, D.; Inasaki, I.; Ketteler, G.; König, W.; Teti, R.: Tool Condition Monitoring (TCM) — The Status of Research and Industrial Application. CIRP Annals - Manufacturing Technology 44 (1995) 2, S. 541-567.

---

[Charles R. Farrar]

Charles R. Farrar, Scott W. Doebling<sup>1</sup> Phillip J. Cornwell: a comparison study of modal parameter confidence intervals computed using the Monte Carlo and bootstrap techniques.

[Chung et al. 1994]

Chung, Y. L.; Spiewak, S. A.: A Model of High Performance Dynamometer.  
Journal of Engineering for Industry 116 (1994) 3, S. 279.

[DeCarlo 1997]

DeCarlo, L.: On the Meaning and Use of Kurtosis. Psychological Methods 2  
(1997) 3, S. 292-307.

[Dunwoody 2010]

Dunwoody, K.: Automated Identification of Cutting Force Coefficients and Tool Dynamics on CNC Machines (Master Thesis) MAL

[Ewins 2000]

Ewins, D. J.: Modal testing. Theory, practice, and application. 2nd ed. Aufl.  
Baldock, Hertfordshire, England, Philadelphia, PA: Research Studies Press  
2000. ISBN: 9780471975182. (Mechanical engineering research studies. Engineering dynamics series 10).

---

[Gauss 2004]

Gauss, C. F.: Theory of the motion of the heavenly bodies moving about the sun in conic sections. Mineola, N.Y.: Dover 2004. ISBN: 9780486439068. (Dover phoenix editions).

[Grewal et al. 2008]

Grewal, M. S.; Andrews, A. P.: Kalman filtering. Theory and practice using MATLAB. 3rd ed Aufl. Hoboken, N.J.: Wiley 2008. ISBN: 978-0-470-17366-4.

[Jun et al. 2002]

Jun, M. B.; Burak Ozdoganlar, O.; DeVor, R. E.; Kapoor, S. G.; Kirchheim, A.; Schaffner, G.: Evaluation of a spindle-based force sensor for monitoring and fault diagnosis of machining operations. International Journal of Machine Tools and Manufacture 42 (2002) 6, S. 741-751.

[Kistler 2009c]

Kistler, I. A.: Data Sheet Multicomponent Dynamometer. - 09.06.2015.

[Kistler 2009a]

Kistler, I. A.: Instruction Manual SlimLine Sensoren(SLS).

[Kistler 2015b]

Kistler, I. A.: Piezoelectric Theory.

<<https://www.kistler.com/fileadmin/files/divisions/automotive-research/test/>

---

engines-research-and-development/20.290e-05.04.pdf> - 09.06.2015.

[Kistler 2009b]

Kistler, I. A.: SlimLine Sensors (SLS)-Data Sheet.

[Kistler 2015a]

Kistler, I. A.: Zerspankraftmessung.

<<http://www.kistler.com/fileadmin/files/divisions/sensor-technology/cuttingforce/960-001d-05.14.pdf>> - 08.06.2015.

[Lasi et al. 2014]

Lasi, H.; Fettke, P.; Kemper, H.-G.; Feld, T.; Hoffmann, M.: Industry 4.0. Business & Information Systems Engineering 6 (2014) 4, S. 239-242.

[Lewis et al. 2007]

Lewis, F. L.; Xie, L.; Popa, D.: Optimal and Robust Estimation. With an Introduction to Stochastic Control Theory, Second Edition. 2nd ed Aufl. Hoboken: CRC Press 2007. ISBN: 978-1-4200-0829-6. (Automation and Control Engineering v.29).

[Lohmann 2012]

Lohmann, B.: Vorlesungsskript Regelungstechnik (Vorlesungsskript TU München) (2012).

---

[Martin Hermann Postel 2015]

Eberhard Abele, Yusuf Altintas: Identification of Dynamics of High Speed Spindles During Machining

[Park 2003]

Park, S. S.: High frequency bandwidth cutting force measurements in milling using the spindle integrated force sensor system (Ph.D. thesis) MAL UBC. Vancouver (2003).

[Park 2006]

Park, S. S.: Identification of Spindle Integrated Force Sensor's Transfer Function for Modular End Mills. *Journal of Manufacturing Science and Engineering* 128 (2006) 1, S. 146.

[Park et al. 2004]

Park, S. S.; Altintas, Y.: Dynamic Compensation of Spindle Integrated Force Sensors With Kalman Filter. *Journal of Dynamic Systems, Measurement, and Control* 126 (2004) 3, S. 443.

[Scippa et al. 2015]

Scippa, A.; Sallese, L.; Grossi, N.; Campatelli, G.: Improved dynamic compensation for accurate cutting force measurements in milling applications. *Mechanical Systems and Signal Processing* 54-55 (2015), S. 314-324.

. [Simon 2006]

---

Simon, D.: Optimal state estimation. Kalman, H [infinity] and nonlinear approaches.  
Hoboken, N.J.: Wiley-Interscience 2006. ISBN: 978-0-471-70858-2.

[Thomas 2015]

Static Calibration and Dynamic Compensation of Force Measurements  
by Spindle Integrated Force Sensors Including Cross Talk Influences

[Westermeier 2010]

Westermeier, M.: Compensation of Cutting Force Measurements in High  
Speed Milling (Master thesis) MAL  
UBC. Vancouver (2017)